Investigating A *Tbx1* And *Pax9* Genetic Interaction During Cardiovascular Development

Jose Alberto Briones Leon

Submitted in accordance with the requirements for the degree of Doctor of Philosophy

Institute of Genetic Medicine
Newcastle University

Supervisors
Dr. Simon D. Bamforth
Dr. Helen M. Phillips
Professor Helen M. Arthur

November 2014

Abstract

Congenital cardiovascular malformations (CCVM) are the most common type of birth defect in humans and can be life threatening for the newborn. 22q11 deletion syndrome (22q11DS) is one of the most common CCVM in humans, with patients presenting a wide variety of abnormalities including craniofacial dysmorphology, immune deficiency, mental retardation and cardiovascular defects, including ventricular septal defects, abnormal right subclavian artery and interrupted aortic arch type B. *TBX1* is considered the main gene underlying the cardiovascular phenotype in 22q11DS patients, however, the great phenotypic variability among 22q11DS patients suggests genetic modifiers define the presentation of the phenotype. The transcription factor *Pax9*, was found significantly down-regulated in Tbx1-null embryos (a mouse model of 22q11DS).

The aim of this project was to determine whether *Pax9* is involved in cardiovascular development and to study a potential genetic interaction between *Pax9* and *Tbx1* during cardiovascular development. The results show that *Pax9* is required for cardiovascular development as all *Pax9*-null embryos have severe cardiovascular abnormalities including IAA, VSD, BAV, DORV, and abnormal or completely absent common carotids. Furthermore, a strong genetic interaction between *Pax9* and *Tbx1* was found, since double heterozygosity leads to lack of formation of the 4th pharyngeal arch arteries consequently leading to a significant increase in the incidence of IAA. The molecular mechanism of this interaction between *Pax9* and *Tbx1* was investigated. The results show that Tbx1 does not bind to any region within the *Pax9* locus *in vitro* and *in vivo*. A physical interaction between Pax9 and Tbx1 proteins was also ruled out by co-immunoprecipitation. qPCR analysis revealed a significant downregulation of *Gbx2* in double heterozygous embryos, and luciferase experiments revealed Pax9 is able to promote luciferase expression of a conserved regulatory region within the *Gbx2* locus, whereas Tbx1 repressed luciferase expression of this Gbx2 cloned regions. The results in this dissertation suggest Pax9 and Tbx1 regulate cardiovascular development, at least in part, through regulating *Gbx2*.

Acknowledgements

First, I would like to thank my supervisors **Dr. Simon Bamforth** and **Dr. Helen Phillips**, for their continuous guidance, help and endless support throughout my PhD.

I would like to also thank **Professor Helen Arthur**, **Professor Deborah Henderson and Professor Kim Spyridopoulos**, for their guidance in the project.

I would like to thank **Rebecca Dodds, Dr. Amy-Leigh Johnson, Kate Bailey and Kath Allison**, for their constant help in the lab, for their friendship and for making the time in the lab more cheerful and enjoyable.

I am thankful to all my friends within the Institute, **Dr. Gavin Richardson** (for the interesting discussions about stem cells), **Vipul Sharma, Paul Chrystal, David Burns, Lorraine Eley, Owen Hughes, Leanne Morrison, Carla Melough, Joe Collins, Kevin Gillinder, Alla Narytnyk** and **Oliver Clewes**, for all the good times.

I would also like to thank **Rachel Challis**, for constantly providing the so-much-needed coffee and cakes during the writing process, as well as her encouragement and nice company.

Finally, I would like to thank my family, for their constant and endless support and encouragement. To my brother **Antonio** for providing me with a coffee maker, this thesis would not have been possible without it. My sister-in-law **Alejandra** for providing with amazing food every Christmas, my beautiful niece and nephew **Adriana** and **Antonio** for providing a nice distraction, and to my parents **Antonio** and **Patricia** who have always been there supporting me, none of this would have been possible without them.

To all of you, **Thank you!**

Abbreviations

22q11DS	22q11 deletion syndrome
Ao	Aorta
AoA	Aortic arch
ARSA	Anomalous right subclavian artery
ASD	Atrial septal defect
AV	Atrioventricular
BAV	Bicuspid aortic valve
BMP	Bone morphogenetic protein
bp	Base pairs
BSA	Bovine serum albumin
cAoA	Cervical aortic arch
CCVM	Congenital cardiovascular malformation
cd	Carotid duct
cDNA	Complementary deoxyribose nucleic acid
ChIP	Chromatin immuniprecipitation
ChIP-WB	Chromatin immunoprecipitation-western blot
co-IP	Co-immunoprecipitation
coRSA	Cervical origin of the right subclavian artery
Ct	Threshold cycle
da	Ductus arteriosus
dAo	Dorsal aorta
DAPI	4',6-diamidino-2-phenylindole
DEPC	Diethyl pyrocarbonate
ddH_2O	Double distilled water
DIG	Digoxygenin
DNA	Deoxyribose nucleic acid
dNTP	Deoxyribonucleotide triphosphate
DORV	Double outlet right ventricle
E	Embryonic day
E. coli	Escherichia coli
EDTA	Ethylenediaminetetraacetic acid

EtBr	Ethidium bromide
FBS	Foetal bovine serum
GAPDH	Glyceraldehyde 3-phosphate dehydrogenase
Gd-DTPA	Gadopentetate dimeglumine
gDNA	Genomic deoxyribose nucleic acid
H_2O_2	Hydrogen peroxide
HCl	Hydrochloric acid
IAA	Interrupted aortic arch
IAA-B	Interrupted aortic arch type B
IVS	Interventricular septum
KCl	Potassium chloride
kDa	Kilo Dalton
LB	Luria Bertani
LCC	Left common carotid
LiCl	Lithium chloride
LSA	Left subclavian artery
LV	Left ventricle
MEFs	Mouse embryonic fibroblasts
$MgCl_2$	Magnesium chloride
MRI	Magnetic resonance imaging
NaCl	Sodium chloride
NaOH	Sodium hydroxide
NC	Neural crest
NCC	Neural crest cells
OFT	Outflow tract
P	Postnatal day
PA	Pharyngeal arch
PAA	Pharyngeal arch artery
PAGE	Polyacrylamide gel electrophoresis
PBS	Phosphate-buffered saline
PBT	Phosphate-buffered saline with Tween-20
PCR	Polymerase chain reaction
PFA	Paraformaldehyde
PHF	Primary heart field
PT	Pulmonary trunk

PTA	Persistent truncus arteriosus
PVDF	Polyvinyl difluoride
qPCR	Quantitative polymerase chain reaction
RCC	Right common carotid
RIPA	Radioimmunoprecipitation assay buffer
RNA	Ribose nucleic acid
RSA	Right subclavian artery
RT-PCR	Reverse-transcription polymerase chain reaction
RV	Right ventricle
S.E.M	Standard error of the mean
SDS	Sodium dodecyl sulphate
SHF	Secondary heart field
TAE	Tris-acetic acid-EDTA
TBST	Tris-buffered saline with Tween-20
TBS-TX	Tris-buffered saline with Triton-X 100
TE	Tris-EDTA
Thy	Thymus
Tm	Melting temperature
V	Volts
VSD	Ventricular septal defect
v/v	Volume per volume
WB	Western blot
w/v	Weight per volume
WISH	Whole mount in situ hybridisation

Table of Contents

List of Figures

List of Tables

Chapter 1. Introduction

1.1. Heart Development

The heart is the first organ to form and function during embryonic development as it is essential to maintain a sufficient blood supply to support the growing embryo, while a vascular network is necessary to efficiently circulate the blood throughout the body.

The development of the heart occurs in a similar pattern in all vertebrates (Figure 1.1) (Reviewed in Anderson et al, 2003; Buckingham et al, 2005), starting around embryonic day 15 in humans equivalent to embryonic day (E) 6.5 in the mouse with the specification of the cardiogenic fields (Figure 1.1a) (Reviewed in Brade et al, 2013).

In embryonic development the three germ layers (endoderm, mesoderm and ectoderm) are specified during gastrulation. The mesoderm, lying between the endoderm and ectoderm layers migrates laterally forming the paraxial, intermediate and lateral plate mesoderm. The latter is further divided into somatic and splanchnic mesoderm. From this bilateral splanchnic mesoderm the first cardiogenic precursors are derived, namely the primary heart fields (Rawles, 1943; Rosenquist, 1970; Garcia-Martinez and Schoenwolf, 1993; Tam et al, 1997).

The primary heart fields migrate from the lateral plates and fuse together in the midline of the embryo at E7.5 (about 18 days in human) forming a crescent-shaped epithelium known as the cardiac crescent (Figure 1.1b; Rosenquist, 1970; Garcia-Martinez and Schoenwolf, 1993). The cardiac crescent then forms a linear tube (Christoffels et al, 2000; Meilhac et al, 2004; Figure 1.1c) composed of an inner lining of endocardial cells attached to an intermediate thick layer of extracellular matrix known as the cardiac jelly and surrounded by a single layer of myocardial cells.

At this point, the myocardial cells have the ability to depolarize spontaneously which allows peristaltic contractions to appear along the tube, while differences between the cardiac chambers become apparent with the presumptive atrial and ventricular regions beating at different rates.

The tube further elongates by proliferation of the primary heart field-derived cells and by addition of cells from a second population of heart progenitors derived from the pharyngeal mesoderm known as the secondary heart field (Mjaatvedt et al, 2001; Waldo et al, 2001; Kelly et al, 2001), of which cells incorporate to the anterior and posterior poles of the tube and will later contribute to the outflow and inflow tracts, the right ventricle, and both atrial chambers (Zaffran et al, 2004; Meilhac et al, 2004).

The anterior (arterial) pole of the tube, the truncus arteriosus, is the primitive outflow tract that will later septate into the aorta and pulmonary trunk. The posterior (venous) pole namely sinus venosus connects the tube with the vitelline veins from which blood is drained from the yolk sac and will later form the sinus node and part of the right atrium.

As the tube elongates it loops rightward (Figure 1.1d), moving the venous pole (presumptive atrial) anteriorly and dorsal to the arterial pole (Christoffels et al, 2000). As the tube is looping, the presumptive ventricular regions begin to balloon outwards to shape the future ventricles, and switching from incorporation of extracardiac cells to intramyocardial proliferation (Moorman and Christoffels, 2003).

Within the looped tube the four chambers of the heart are then specified by initially forming the atrioventricular (AV) canal, which creates a boundary between the atrial and ventricular regions (Habets et al, 2002; Harrelson et al, 2004). Soon after, following signals from the myocardium some endocardial cells undergo epithelial-to-mesenchymal transition to migrate through the cardiac jelly and form the endocardial cushions (outflow tract and AV cushions) which will then define the four chambers (Figure 1.1e) and later become the four major valves of the heart (Eisenberg and Markwald, 1995; Timmerman et al, 2004).

The outflow tract cushions will form the aortic and pulmonary valves while the AV cushions will form the tricuspid and mitral valves. By E10.5 (about 32 days in human) the four chambers of the heart are completely defined (Figure 1.1e) and connected to the aorta and pulmonary trunk.

The myocardium then differentiates into two layers: an outer compact region and an inner trabeculated sheet protruding within the lumen of both ventricles (Wang et al, 1998; Grego-Bessa et al, 2007). Trabeculation starts around E10.5 (about 32 days in human) with cells of the inner myocardium proliferating and migrating into the lumen of the ventricle, forming inward-protruding sheets of organised cardiomyocytes to increase the surface area of the heart for oxygenation in the absence of coronary circulation (Sedmera et al, 2000; Wagner and Siddiui, 2007).

A subpopulation of cells derived from the pharyngeal endoderm, known as epicardial cells, migrate and form a monolayer surrounding the heart covering the ventricles and atria forming the epicardium (Komiyama et al, 1987). Furthermore, a subset of epicardial cells undergo epithelial-to-mesenchymal transformation, delaminate from the epicardium and populate the myocardium, where they differentiate into smooth muscle and endothelial cells to contribute to the formation of the coronary vessels, as well as differentiating into interstitial and adventitial fibroblast (Mikawa and Gourdie, 1996; Perez-Pomares et al, 2002).

By this stage, the cardiac outflow tract (OFT) is septated into the ascending aorta and pulmonary trunk, which arise from the left and right ventricles, respectively (Sedmera et al, 2000; Nemer et al, 2007).

The remodelling of the outflow tract is a complex process that is disrupted in a significant number of CCVM accounting for about 30% of all cardiovascular malformations.

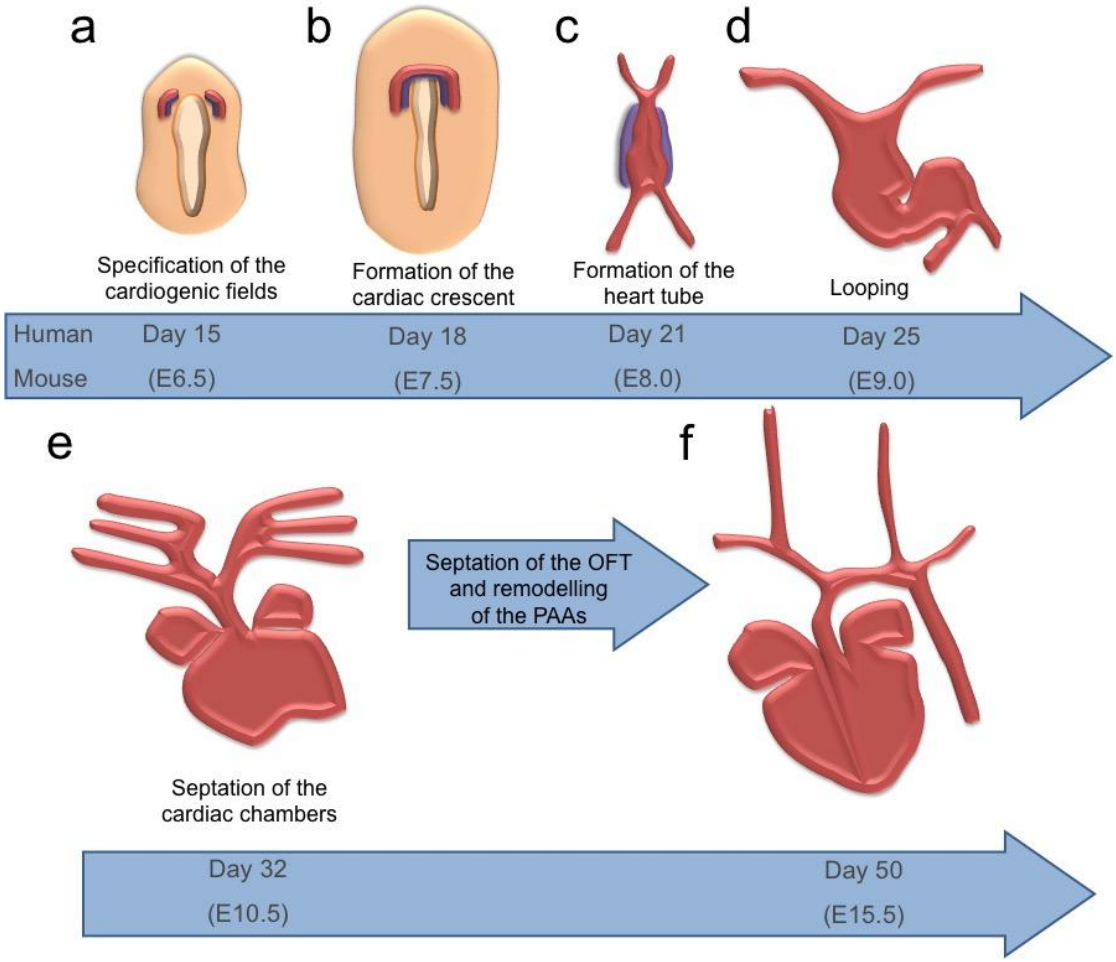

Figure 1.1. Overview of heart development in human and mouse.
The development of the mammalian heart starts with the specification of the cardiogenic fields **(a)** around embryonic day (E) 6.5 in mouse (day 15 in humans). The primary heart fields fuse in the midline of the embryo forming the cardiac crescent **(b)**. Cells from the cardiac crescent proliferate forming a linear tube along the embryo **(c)**; the tube elongates by proliferation of primary heart field cells (red) and by incorporation of cells from the secondary heart field (blue). As the tube grows it loops rightwards **(d)**, moving the venous pole (presumptive atrial) anteriorly and dorsal to the arterial pole. The four chambers of the heart are then specified and completely septated **(e)** by E10.5 (32 days in humans). By E11.5 the outflow tract (OFT) is completely septated into the aorta and pulmonary trunk, and from E11.5 the symmetrical pharyngeal arch arteries undergo a complex remodelling process to form the assymetrical great arteries. The remodelling of the PAAs and the formation of the heart is finished **(f)** by E15.5 (50 days in humans).

1.1.1. Extracardiac Contributions

1.1.1.1. Secondary Heart Field

The secondary heart field is a population of progenitor cells derived from the pharyngeal mesoderm located posterior to the dorsal surface of the developing heart tube (Figure 1.1a) (Mjaatvedt et al, 2001; Waldo et al, 2001; Kelly et al, 2001). Secondary heart field cells start to migrate and incorporate to the arterial pole of the heart tube around E8.0 in the mouse embryo (about 21 days in humans) contributing to the elongation and then the looping of the heart tube. Later on, the secondary heart field cells form the outflow tract, the right ventricle and both atria (Zaffran et al, 2004; Meilhac et al, 2004).

1.1.1.2. Cardiac Neural Crest Cells

Neural crest cells are a multipotent population of highly migratory cells originating from the dorsal neural tube at the early gastrula stage of vertebrate embryo development. Neural crest cells migrate and colonize the embryo to finally settle in different locations and generate a wide array of cell types and tissues (Le Douarin and Kalcheim, 1999).

A subpopulation of neural crest cells, namely cardiac neural crest cells, originate from the level of the otic placode and the third somite, and migrate through the pharyngeal arches (described in section 1.2.1) to the outflow tract of the heart (Figure 1.1c) around E9.0 in the mouse embryo (around 21 days in humans) to help with the septation of the outflow tract (Phillips et al, 1987; Jiang et al, 2000). The role of neural crest cells in the pharyngeal arches and for the formation of the great arteries will be discussed in more detail in section 1.2.1.

1.1.2. Outflow Tract Septation

The septation of the outflow tract involves three main elements (reviewed in Webb et al, 2003): the formation of the aorticopulmonary septum, distinct histological identity of the truncus arteriosus and the outflow tract, and hemodynamics.

After looping of the heart tube four ridges are formed along the OFT and the truncus arteriosus by proliferation of pharyngeal mesenchymal cells. One opposing pair of ridges are formed over the endocardial cushions (which will later form the semilunar valves) at the near end of the truncus arteriosus, while another pair of opposing ridges are formed at the end of the outflow tract between the 4^{th} and 6^{th} pharyngeal arch arteries (discussed in detail in section 1.2.2).

As neural crest cells migrate through the outflow tract they colonize these ridges inducing their condensation and proliferation (Kramer, 1942; Pexieder, 1978; van Mierop, 1979).

The four ridges grow towards each other in a 180^{o} angle with the OFT ridges joining the conotruncal ridges of their opposite side and fusing all in the middle of the outflow tract forming a spiral septum.

The outflow tract is histologically different from the truncus arteriosus and the junction between them is not symmetrical, with the outflow tract region being longer anteriorly than posteriorly and longer towards the left side.

After the formation of the aorticopulmonary septum blood flows in a spiral clockwise way through the outflow tract which pushes the OFT towards the left side as it lengthens (Kramer, 1942; Pexieder, 1978; van Mierop, 1979).

Finally, the force of blood flowing in a spiral pattern and the myocardialization (where mesenchymal cells are replaced with cardiomyocytes) of the aorticopulmonary septum causes the complete septation into the aorta and the pulmonary trunk (van den Hoff et al, 1999). The asymmetrical spiral flow of blood also contributes to the asymmetrical remodelling of the pharyngeal arch arteries during the formation of the great vessels as described below.

1.2. Development Of The Great Arteries And Pharyngeal Arch-Derived Tissues

1.2.1. The Pharyngeal Arches

The pharyngeal arches (Figure 1.2) in mammals appear as a transient series of bulges formed on the lateral surface of the developing embryo below the forming head around E9.0 in the mouse and about 21 days in humans (Graham and Smith, 2001). In mammals, the 5th pharyngeal arch is not formed, with the most caudal arch consequently being the sixth (Bamforth et al, 2013).

The pharyngeal arches develop sequentially in a cranio-caudal direction formed by a mesenchymal core derived from cardiac neural crest cells and pharyngeal mesoderm, surrounded by an outer layer of pharyngeal ectoderm and an inner lining of pharyngeal endodermal cells (Figure 1.2b) (Noden, 1988).

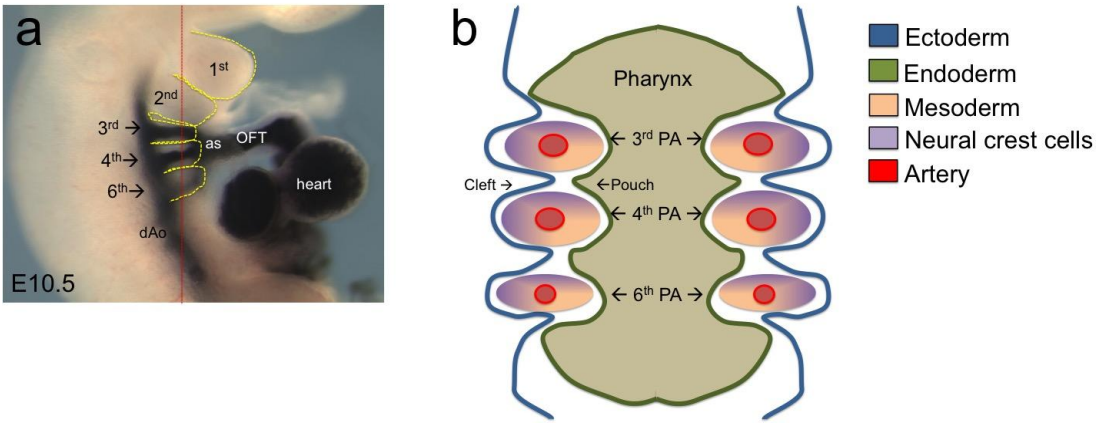

Figure 1.2. Anatomy of the pharyngeal arches.
(a) Wild-type E10.5 embryo injected with India ink to visualise the pharyngeal arch arteries; the dotted yellow line underlies each pharyngeal arch. **(b)** Drawing illustrating the cellular components within the pharyngeal arches from a coronal view (red dotted line in Figure a). Five pairs (1-4 and 6) of arches are sequentially formed below the developing head and surrounding the developing pharynx. **(b)** Each arch is formed by an external layer of pharyngeal ectoderm (blue), an internal lining of pharyngeal endoderm (green), and a mesenchymal core composed of pharyngeal mesoderm (pink) and neural crest cells (purple); within each arch, a pharyngeal arch artery (red) is formed, **(a)** connecting the cardiac outflow tract (OFT) with the paired dorsal aortas (dAo). PA, pharyngeal arch; OFT, outflow tract; as, aortic sac; dAo, dorsal aorta.

As development continues, the endodermal and ectodermal walls invaginate towards each other to be in direct contact forming a closing membrane in between the arches. The grooves formed externally by the ectoderm are known as the pharyngeal clefts while the internal invaginations of the endoderm form the pharyngeal pouches.

The physical arrangement of the pharyngeal arches contributes to the segmentation of the pharynx but also all different regions and components of the arches give rise to distinct tissues around the pharynx (reviewed in Grevellec and Tucker, 2010), including the great arteries.

1.2.1.1. Derivatives of the First and Second Pharyngeal Arches

The first pharyngeal arches expand ventrally to form the upper and lower jaw while the second arches form the hyoid apparatus, a group of bones that hold the larynx and support the pharynx and tongue. The first and second arches are separated by the first cleft and pouch, which in turn contributes greatly to the external and middle ear (Mallo, 2001). In this context, the first pouch elongates and distally forms the epithelium of the tympanic cavity and proximally the Eustachian tube, whereas the first cleft forms the external auditory canal, which later elongates and joins the tympanic cavity where the joining forms the tympanic membrane and connects with the Eustachian tube (Mallo, 2001; Lazaridis and Saunders, 2008). Although the second cleft appears to not have derivatives, the second pouch forms the tonsil epithelium (Rogers, 1929; Wilson et al, 2005) a lymphoid organ that provides antigenic response to foreign microbes entering orally.

1.2.1.2. The Caudal Pharyngeal Arches and the Pharyngeal Glands

The third and fourth pouches form the thymus, parathyroid glands and ultimobranchial bodies (Cordier and Haumont, 1980). The cranial region of the third pouch forms the inferior parathyroid and the caudal part forms the thymus epithelium while the anterior part of the fourth pouch forms a second pair of parathyroid glands known as the superior parathyroids (Cordier and Haumont, 1980; Hilfer and Brown, 1984; Gordon et al, 2001).

The caudal ventral fourth pouch forms the ultimobranchial bodies, a transient tissue which forms calcitonin-producing cells known as C-cells after its fusion with the thyroid gland (Hilfer and Brown, 1984).

After specification and differentiation of the different pouch derivatives, the thymus, parathyroids and ultimobrachial bodies move along the midline of the embryo to reach their final position (Manley and Capecchi, 1998; Kameda et al, 2004).

The thymus and parathyroid primordium detach from the pharynx and move together caudal-ventrally towards the anterior thoracic cavity. As they move, they reach the thyroid gland to which the parathyroid connects consequently separating it from the thymus. The parathyroids then stay connected to the thyroid lobe whereas the thymus descends further caudally along the midline to finally settle above the heart behind the sternum (Manley and Capecchi, 1998; Kameda et al, 2004).

The ultimobranchial bodies detach from the pharynx as well, moving caudally and ventrally along the midline to reach the anterior thyroid lobe. Cells of the ultimobranchial bodies then spread around the lobe and fuse with the thyroid follicular tissue to finally differentiate into C-cells (Rogers, 1927).

1.2.1.3. Cellular Components of Pharyngeal Arch-Derived Tissues

Within the pharyngeal arches the different cellular components (endoderm, mesoderm, ectoderm and neural crest cells) contribute to different parts of the tissues described above (pharynx, thymus, parathyroids, ultimobranchial bodies).

The epidermis and sensory neurons of the epibranchial ganglia and pharynx are derived from the ectoderm (Couly and Le Douarin, 1990; D'Amico-Martel and Noden, 1983), while the endoderm generates the epithelial cells covering the pharynx and the thyroid, parathyroid and thymus glands (Le Douarin and Jotereau, 1975; Cordier and Haumont, 1980).

Mesoderm cells differentiate into endothelium and musculature of the pharyngeal arch arteries (Couly et al, 1992; Trainor et al, 1994) and neural crest cells form connective and skeletal tissue of pharyngeal arch-derived glands (Noden, 1983; Couly et al, 1992) and form the latter musculature surrounding the aortic arch. Although neural crest cells are not necessary for the formation of the pharyngeal arch arteries, they are required after the remodelling into the great arteries where they form the vascular smooth muscle cells covering the aortic arch and the proximal region of the descending aorta before the left subclavian artery (Waldo et al, 1996).

The endoderm in particular plays a key role in both patterning of the pharyngeal arches as well as for the specification of the different pharyngeal arch-derived tissues. Such specification is driven by differential expression of signalling molecules within the pharyngeal endoderm.

1.2.1.4. Signalling Within The Pharyngeal Arches

Although the specific signalling pathways by which the pharyngeal arches are initially formed are still not completely clear, numerous evidence has originated from knockout mice displaying abnormal formation of the pharyngeal arches. For instance, retinoic acid signalling is required for correct formation of the pharyngeal arches and subsequent derived tissues as shown by deletion of *Raldh2*, the enzyme that catalyses the synthesis of retinoic acid. Homozygous deletion of *Raldh2* in mice leads to failure in the formation of the caudal pharyngeal arches, with only the first arch forming (Niederreither et al, 1999; Begemann et al, 2001); further pharmacological perturbation of retinoic acid signalling by blocking the three retinoic acid receptors (RAR α, β, γ) with the BMS493 antagonist confirmed retinoic acid signalling requirement for the formation of the pharyngeal arches (Wendling et al, 2000).

Deletion of other genes such as *Tbx1* has shown their requirement for the initial formation of the pharyngeal arches, as homozygous deletion of *Tbx1* in mice shows complete failure in the formation of the caudal arches with only the first pharyngeal arch forming (Jerome and Papaioannou, 2001; Lindsay et al., 2001).

Tbx1 haploinsufficiency in mice does not affect the formation of the pharyngeal arches or patterning of the pouches, however, *TBX1* haploinsuficiency in humans is considered to be responsible for underlying the phenotype in 22q11 deletion syndrome, where patients present a variety of abnormalities mainly affecting pharyngeal arch-derived tissues including the jaw, ears, thymus and the great arteries. The role of *Tbx1* in the development of the great arteries and in 22q11 deletion syndrome will be discussed in detail in section 1.4.

Within the pharyngeal endoderm, differential expression of homeobox genes (Hox), particularly *Hoxa2* and *Hoxa3* specify regions of the second and third pharyngeal pouches and their derivatives (Hunt et al, 1991; Rijli et al, 1993; Pasqualetti et al, 2000; Grammatopoulos et al, 2000).

Moreover, *Pax1*, *Pax9*, *Six1*, *Eya1* are all required within the pharyngeal pouch endoderm, where they act within the same genetic network to promote Fgf8 signalling and subsequently inducing *Gcm2* and *Foxn1* expression to induce thymus and parathyroids organogenesis (Manley and Capecchi, 1995; Wallin et al, 1996; Su et al, 2001; Abu-Issa et al, 2002; Xu et al, 2002).

Gcm2 is essential for parathyroid proliferation and survival (Gunther et al, 2000; Liu et al, 2007), while *Foxn1* is then required for differentiation and proliferation of thymus epithelial cells. (Manley and Capecchi, 1995; Hetzer-Egger et al, 2002; Wallin et al, 1996; Xu et al, 2002). Disruption of retinoic acid signalling (Mulder et al, 1998; Quinlan et al, 2002; Wendling et al, 2000) or deletion of *Tbx1* (Ivins et al, 2005; Vitelli et al., 2002; Guo et al., 2011) affects *Pax1*, *Pax9*, *Six1* and *Eya1* expression, consequently disrupting thymus development.

Defects of some pharyngeal arch-derived tissues are often found in patients with congenital cardiovascular malformations (CCVM). For instance, patients with 22q11 deletion syndrome (discussed in detail in section 1.4.2.1.1), present thymus hypoplasia, jaw and ears malformations along with cardiovascular abnormalities mainly affecting the great arteries; such defects in the great arteries are derived from abnormal development of the pharyngeal arch arteries as described below.

1.2.2 Formation and Remodelling of the Pharyngeal Arch Arteries

The pharyngeal arch arteries (PAAs) are formed sequentially within the core of each of the pharyngeal arches (Figure 1.2b) and connect the heart (through the aortic sac) with the systemic circulation (paired dorsal aorta; Figure 1.2a).

Although it was initially suggested the pharyngeal arch arteries are formed by angiogenesis (Noden, 1989), where new vessels are formed from pre-existing ones, mounting evidence suggests they are formed by vasculogenesis (DeRuiter et al, 1993; Hiruma and Hirakow, 1995; Waldo et al, 1996), where vessels are formed *de novo* by differentiation of mesoderm cells into endothelium. Recent evidence shows mesodermal cells differentiate into endothelium forming threads that join the dorsal aorta and the aortic sac, which then grow towards each other to form a single vessel (Anderson et al, 2008; Li et al, 2012).

Initially, the pharyngeal arch arteries are formed symmetrically on both sides of the embryo but then undergo a remodelling process (Hiruma et al, 2002; Bamforth et al, 2013) to form the final asymmetrical structure of the great arteries as described below (Figure 1.3)

The 1st PAAs become evident as early as E8.5 in the mouse embryo, with the 2nd PAAs appearing by E9.5; however these PAAs persist only for a short period before regressing almost completely, with their remnants contributing to parts of the maxillary and stapedial arteries.

Around E9.5 (28-32 days in humans) the 3rd PAAs are visible connecting the aortic sac with the dorsal aorta, while the 4th PAAs appear as thin vessels and the 6th PAAs are just forming. By E10.5 (31-35 days) the 4th and 6th PAAs are completely formed and can be seen connecting the aortic sac with the dorsal aorta with the 3 pairs showing a similar diameter (Figure 1.3a). At this stage the pulmonary arteries start to sprout from the proximal region of the 6th PAAs where they incorporate endothelial cells derived from the pharyngeal mesoderm to grow caudally and parallel to the dorsal aorta.

By E11.5 (37-42 days in humans) the outflow tract is fully septated into the aortic and pulmonary outflows, with the 3rd and 4th PAAs connecting to the aortic end and the 6th PAAs connecting to the pulmonary outflow (Figure 1.3b).

As described above, the clockwise spiral flow of blood pushes the aortic and pulmonary outflows towards the left side. This rotation causes the right 6th PAA to lengthen reducing its diameter and restricting the flow of blood from this side (Hiruma et al, 2002; Anderson et al, 2008). This reduction in blood flow on the right side causes the right dorsal aorta to also start regressing. By E12.5 (42-44 days in humans) the right 6th PAA has completely regressed along with the portion of the right dorsal aorta below the 4th PAA (Figure 1.3c).

The left 6th PAA forms the ductus arteriosus (Figure 1.3f, da), a connection between the pulmonary trunk and the descending aorta that persists during foetal life to allow blood to bypass the non-functional lungs and then closes after birth.

The portion of the paired dorsal aortas between the 3rd and 4th PAAs is called the carotid duct and this also regresses completely by E12.5 (Figure 1.3c). The complete regression of the right dorsal aorta by E13.5 forces the flow of blood towards the left side, causing the left dorsal aorta to further enlarge. The left 4th PAA that is connecting the aortic sac with the left dorsal aorta now forms the central part of the aortic arch. As the flow of blood increases, the aortic sac enlarges forming a “Y” shape, with the left end connecting to the aortic arch and the right end forming the trunk of the brachiocephalic artery.

The brachiocephalic artery further branches, connecting on the right side with the right 4th PAA and cranially with the right 3rd PAA. The right 4th PAA persists as the central part of the right subclavian artery (RSA), and with the regression of the right dorsal aorta, the right 7th intersegmental artery (ISA) is now connected with the right 4th PAA forming the right subclavian artery (Figure 1.3e). As the dorsal aorta enlarges, the left 7th ISA moves cranially closer to the aortic arch where it forms the left subclavian artery (Figure 1.3d).

At the same time as the embryo grows the 3rd right and left PAAs are pulled up cranially, lengthening them and forming the right and left common carotid arteries (Figure 1.3d); both common carotids further branch cranially into the internal and external carotids (Figure 1.3e).

Thus, the 3rd PAAs form the common carotids; the right 4th PAA forms the proximal part of the right subclavian artery while the left 4th forms the aortic arch. The left 6th forms the ductus arteriosus, and the 7th ISAs form the subclavian arteries.

Evidence suggests that the 5th pair of PAAs exist only briefly, although their contribution to the final structure of the great arteries is still unclear (Bamforth et al., 2013).

The formation of the PAAs is evolutionarily conserved among vertebrates (Reviewed in Kardong, 2008), although some differences are observed among different species. For example, in the zebrafish, only two of the initial six PAAs are remodelled and the other four persist. Another example is the remodelling of the PAAs in chick embryos where the right 4th PAA forms the aortic arch instead of the left as in humans and mice. However, the formation of a set of bilaterally symmetrical arteries connecting the primitive heart with the paired dorsal aorta, which are then remodelled into the great vessels to correctly bring blood in and out of the heart, occurs overall in the same fashion in all mammals. Imaging studies have revealed that the formation and patterning of the PAAs in mouse (Bamforth et al., 2013; Hiruma et al., 2002) closely resembles the process that occurs in humans (Bamforth et al., 2013; Congdon, 1922) as both present with 5 pairs of pharyngeal arches in the developing embryo and form a similar structure of the great arteries in adults. Although the timing slightly differs due to the short pregnancy in mice, the remodelling process occurs in the same way. Additionally, the genetics underlying this process in mice also appears to be similar to humans, making the mouse a good model for the study of PAA development in congenital heart disease.

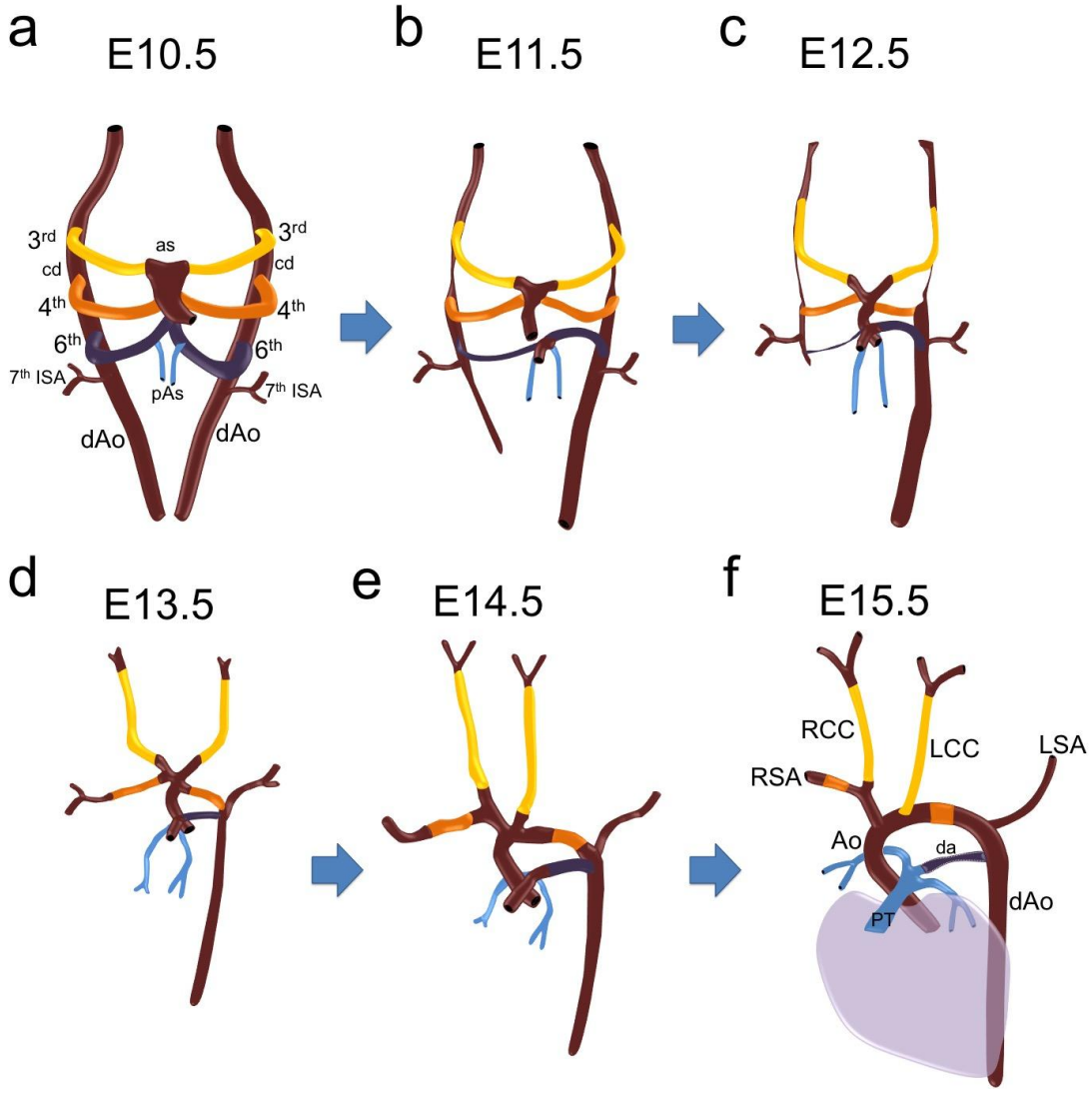

Figure 1.3. Remodelling of the pharyngeal arch arteries.
The pharyngeal arch arteries start as symmetrical pairs on both sides of the developing embryo. **(a)** at E10.5, the 3rd, 4th and 6th pairs of arteries are patent connecting the heart through the aortic sac (as) with the paired dorsal aortas (dAo). (**b**) by E11.5, the aortic sac is fully septated into the aorta and pulmonary trunk, whereas the carotid duct (cd) and the right dorsal aorta start to regress, whilst the left dorsal aorta begins to enlarge; the right 6th PAA degenerate due to regression of the right dorsal aorta. (**c**) by E12.5 the carotid duct, the right dorsal aorta and the right 6th PAAs have almost completely disappeared, and the 7th intersegmental arteries (7th ISA) move up opposite to the 4th PAAs. (**d**) by E13.5, the remodelling is almost completed. (**f**) the 3rd PAAs (yellow) form the common carotids (RCC, LCC), while the right 4th PAA forms the central part of the right subclavian artery, and the left 4th PAA forms the central region of the aortic arch. The right 6th PAA regresses completely, whereas the left 6th PAA forms the ductus arteriosus (da). The 7th intersegmental arteries (ISA) form the distal part of the subclavian arteries. Ao, aorta; dAo, dorsal aorta; RSA, right subclavian artery; RCC, right common carotid artery; LSA, left subclavian artery; LCC, left common carotid artery; da, ductus arteriosus; pAs, pulmonary arteries; PT, pulmonary trunk; as, aortic sac.

1.3. The Mouse As A Model To Study Cardiovascular Development

Mice are commonly used in research to study different aspects of physiology or disease as they share with humans many important genetic and physiological features. Although mice also have physiological differences, more than 99% of human genes are conserved in mice (Pennacchio, 2003), and their low maintenance cost and ease to breed make them a good tool for research.

In particular, the development of the heart (Reviewed in Anderson et al, 2003; Buckingham et al, 2005) and the great arteries (Reviewed in Kardong, 2008; Bamforth et al, 2013) is highly conserved including the genetics underlying their development.

Although the chicken and zebrafish have proved invaluable models in cardiovascular development research, key differences in the formation of the great arteries as mentioned before, with the chicken having a right-sided aortic arch and the zebrafish PAAs remaining symmetrical, the mouse is a superior model for the study of PAAs development.

Furthermore, the ability to modify the mouse genome by genetic engineering allows researchers to generate models to study a specific gene or disease.

There are two ways to generate a genetically modified mouse: by pronuclei microinjection (transgenesis; Gordon et al, 1980), and by gene targeting (knock-out; Thomas and Capecchi, 1987).

In the first approach (transgenesis), an exogenous gene or piece of artificial DNA (transgene) is injected into the egg directly after fertilization (Gordon et al, 1980), where the transgene will incorporate randomly into the genome. Transgenes are typically used to over-express a gene, interfere with its function as dominant-negative isoforms, or simply as reporters.

Although this approach is easier as it does not require to know the specific genomic sequence of the target gene, this means the integration of the transgene into the genome cannot be controlled, and the integration site may

interfere with other gene's function. Additionally, multiple copies of the transgene may integrate into the genome, making it difficult to control for copy numbers and levels of expression of the transgene.

In the second approach (knock-out), the artificial DNA is designed containing identical or homologous sequence to the target gene both up- and down-stream of the gene location in the chromosome; the homologous DNA sequence is then inserted into embryonic stem (ES) cells, where during DNA replication for cell division the cell's machinery will recognize the exogenous DNA as its own, and will interchange it with the endogenous sequence by homologous recombination, therefore knocking out the endogenous gene typically by replacing it with a reporter gene cassette (i.e. neomycin).

Although this approach allows for a controlled modification as it is specifically targeted, it requires knowing the specific sequence of the target gene and a more complex genomic integration, thus making it more technically difficult.

Newer genetic engineering techniques allow the conditional inactivation of a gene spatially and/or temporally using site-directed recombination, such as the Cre/LoxP recombination system, in which a target gene is flanked by LoxP sites, which are recognized by the Cre complex and recombined.

The LoxP (locus of X-over P1) is a 34bp site on the bacteriophage P1 DNA that includes a core asymmetric 8bp sequence in between two sets of 13bp palindromic inverted repeats (ATAACTTCGTATA-NNNTANNN-TATACGAAGTTAT); the central senquence, where the recombination takes place is variable (-NNNTANNN-) and specifies the direction of recombination.

Upon Cre induction, the Cre complex binds to the 13bp flanking repeats of a LoxP site forming a dimer, which in turn binds to another dimer of a second LoxP site to form a tetramer. The adjacent double stranded DNA is cut at both LoxP sites at the central 8bp sequence by the Cre protein, and the strands are then re-joined by the DNA ligase. The result of recombination depends on the orientation of the central sequence, where parallel sequences will cause a deletion, whereas inverted sequences will cause an inversion.

Cre can be driven by a specific promoter, thus when the promoter of the gene of interest is expressed, Cre is expressed targeting a specific cell type at a specific time. The system can be used in the opposite way to activate a gene, where LoxP sites flank a “stop” codon or a “stop” sequence that prevents gene transcription, therefore upon Cre activation, the “stop” sequence is excised allowing gene transcription.

Cre can also be pharmacologically induced, to selectively promote recombination at a specific time. To achieve this, a Cre chimeric protein fused to a mutated estrogen receptor-binding domains (ER) is used, where ubiquitously expressed but inactive chimeric Cre is localised within the cytoplasm, and upon ER agonist administration (i.e. Tamoxifen), Cre is translocated into the nucleous to be able to mediate DNA recombination (Danielian et al, 1998).

The ability to specifically target a gene has helped to expand knowledge in genetics; regarding cardiovascular development, the use of mouse models has revealed more than 500 genes potentially related to cardiovascular development (reviewed in Andersen et al, 2013), some of which have already been directly associated with human congenital cardiovascular malformations.

1.4 Congenital Cardiovascular Malformations

Abnormalities in the formation of the heart or the main vessels that bring blood in and out of it (great arteries) can lead to defects in the newborn that can be life threatening. Such defects commonly denominated congenital cardiovascular malformations (CCVM) are the most common type of birth defect occurring about 10-12 in every 1000 live births (Hoffman, 2013).

The main defects found in patients with CCVM involve abnormal blood flow between the cardiac chambers (ventricles and atria) or between the chambers and cardiac outflows (aortic and pulmonary arteries) (Figure 1.4).

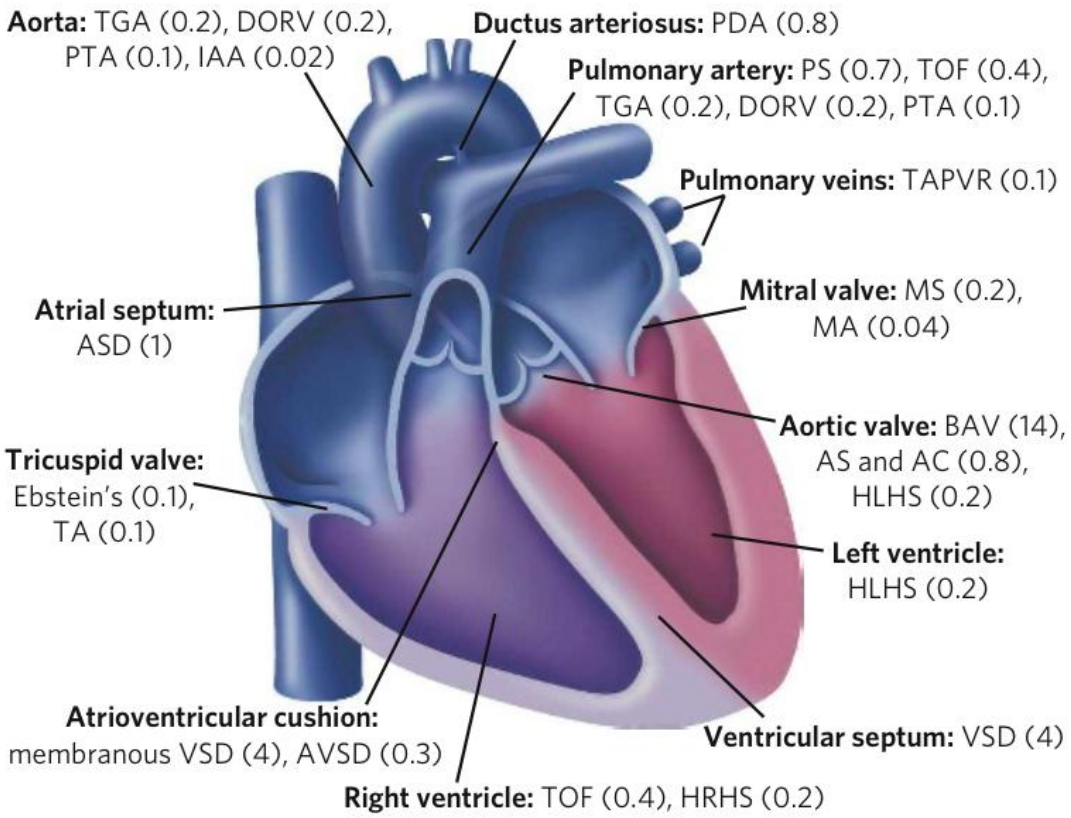

Figure 1.4. Congenital cardiovascular malformations.
Diagram illustrating the structures affecting in CCVM with their estimated incidence per 1000 live births indicated in parentheses AC, aortic coarctation; AS, aortic stenosis; ASD, atrial septal defect; AVSD, atrioventricular septal defect; BAV, bicuspid aortic valve; DORV, double outlet right ventricle; Ebstein's, Ebstein's anomaly of the tricuspid valve; HLHS, hypoplastic left heart syndrome; HRHS, hypoplastic right heart; IAA, interrupted aortic arch; MA, mitral atresia; MS, mitral stenosis; PDA, patent ductus arteriosus; PS, pulmonary artery stenosis; PTA, persistent truncus arteriosus; TA, tricuspid atresia; TAPVR, total anomalous pulmonary venous return; TGA, transposition of the great arteries; TOF, tetralogy of Fallot; VSD, ventricular septal defect. (from Bruneau, 2008).

For instance, ventricular septal defects (VSD) are one of the most common defects (4 in every 1000 live births; Hoffman et al, 2004) that cause abnormal flow of blood between the ventricles, since the interventricular septum fails to fully close allowing blood to flow between the right and left ventricles mixing oxygenated and deoxygenated blood. VSD can be asymptomatic (which means the incidence could be higher) and patients can survive with no complications without the need for treatment, with more than 70% of VSD closing in the first year after birth (Hoffman et al, 2004).

Cardiovascular abnormalities that affect the flow of blood between the cardiac chambers and the cardiac outflows are usually the result of abnormal formation of the valves, which control a unidirectional flow in or out of the cardiac chambers. For instance, bicuspid aortic valve (BAV) is the most common CCVM occurring in about 14 per 1000 live births (Bruneau, 2008). BAV is caused when two leaflets of the aortic valve fuse during embryonic development resulting in a valve with only two leaflets instead of three which later causes regurgitation of blood back from the aorta into the left ventricle. Although patients may be asymptomatic, BAV has been associated with a tendency to develop ascending aorta aneurisms in adulthood due to the stress caused by the regurgitation of blood (Tadros et al, 2009).

Double outlet right ventricle (DORV) affects 1-3% of patients with CCVM (Obler et al, 2008), and occurs when both the aorta and pulmonary trunk arise from the right ventricle; DORV is typically accompanied by a VSD to allow oxygenated blood from the left ventricle to reach the aorta. Patients with DORV require surgery, and the severity of the symptoms varies depending on the presentation of the DORV and other cardiovascular malformations.

A more rare but severe malformation affecting the flood of blood in and out of the heart is a persistent truncus arteriosus (PTA, also known as common arterial trunk, CAT), in which the primitive outflow tract (truncus arteriosus) fails to properly septate into the aorta and pulmonary trunk, resulting in a single arterial tube arising from the heart, providing mixed blood to the pulmonary and systemic circulation.

Other abnormalities affecting the flow of blood in or out of the cardiac chambers are directly caused by malformation of the great arteries (aortic and pulmonary arteries), which are the result of abnormal development of the pharyngeal arch arteries.

1.4.1 Pharyngeal Arch Artery Defects

Anomalies specifically affecting the formation of the great arteries account together for about 30% of all CCVM (Thom et al, 2006) and are derived from failure during the formation or remodelling of the pharyngeal arch arteries in the developing embryo.

One of the most common pharyngeal arch artery-derived defect is the anomalous right subclavian artery (ARSA) which is the most common aortic branching abnormality occurring in about 1% of the population and 3% of patients with CCVM (Zapata et al, 1993). ARSA occurs when the right 4th PAA abnormally regresses or is not formed (Figure 1.5a), causing the right dorsal aorta to persist as a connection with the right 7th intersegmental artery (future right subclavian artery). The abnormal right dorsal aorta travels cranially along the thoracic aorta reaching the aortic arch proximal to the left subclavian artery, where it travels behind the oesophagus towards the right side (Figure 1.5c) (Bergwerff et al, 1999).

Although ARSA is not lethal *per se*, it can cause complications when the artery presses against the oesophagous causing difficulty swallowing, and the continuous compression of the artery against the oesophagous frequently causes aneurisms or complete rupture of the artery with a 50% mortality rate (Leong et al, 2012).

If the right 4th PAA is absent and the right carotid duct fails to regress, the 7th ISA joins the carotid duct forming a right subclavian artery that originates from the right common carotid at a higher cervical position known as cervical right subclavian artery (coRSA; Figure 1.5d) (Kellenberger, 2010).

When the left 4th PAA is affected either by abnormal regression or a complete lack of its formation (Figure 1.5b), the result is a cervical aortic arch (coAA) or an interrupted aortic arch (IAA). A cervical aortic arch is formed when the left 4th PAA is absent and the left carotid duct persists forming an arch that connects the thoracic aorta to the left common carotid (Figure 1.5e) (Kellenberger, 2010).

If the left 4th PAA is absent and the carotid duct normally regresses, the result is an interrupted aortic arch (IAA, Figure 1.5f), which is a complete disruption in the connection between the ascending and descending aorta that disrupts the flow of oxygenated blood.

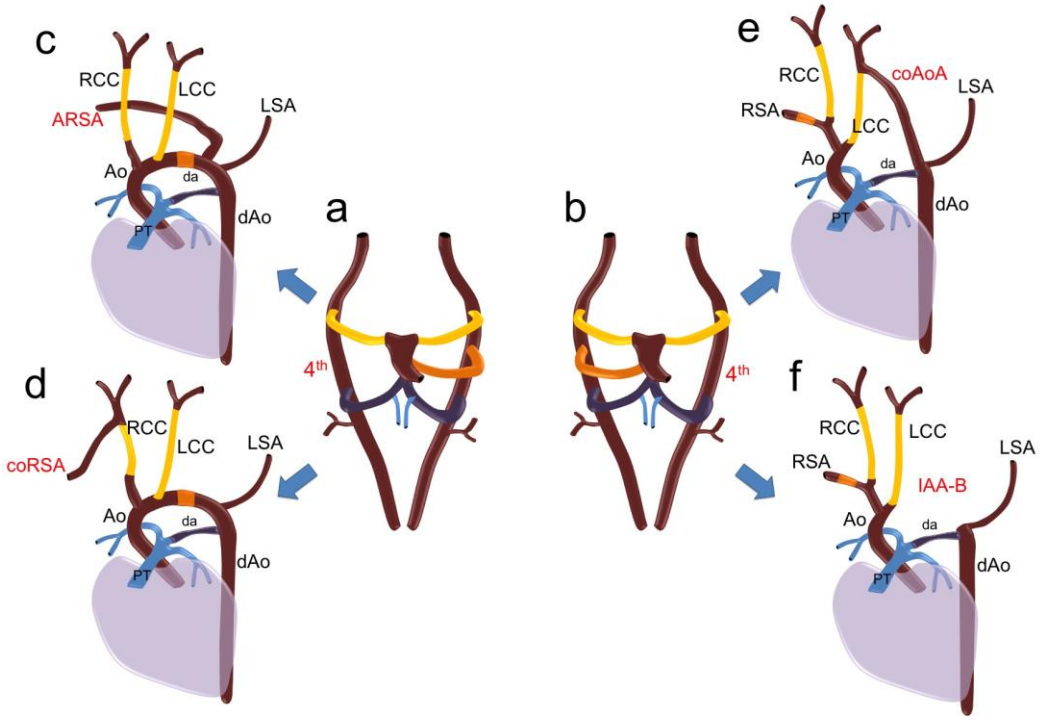

Figure 1.5. Pharyngeal arch artery defects.
(a) When the right 4th PAA abnormally regresses or is not formed, the right dorsal aorta may persist as a connection with the right 7th intersegmental artery, thus the right dorsal aorta travels cranially along the thoracic aorta proximal to the left subclavian artery, where it travels behind the oesophagus towards the right side forming an anomalous retro-esophageal right subclavian artery (ARSA) **(c)**. If the right 4th PAA is absent and the right carotid duct fails to regress, the 7th ISA joins the carotid duct forming a right subclavian artery that originates from the right common carotid with a cervical origin (coRSA) **(d)**. **(b)** When the left 4th PAA abnormally regresses or is not formed, a cervical aortic arch (coAoA) may be formed if the left carotid duct persists **(e)**, whereas if the carotid duct regresses normally, the result is an interrupted aortic arch (IAA) **(f)**. Ao, aorta; dAo, dorsal aorta; RSA, right subclavian artery; RCC, right common carotid artery; LSA, left subclavian artery; LCC, left common carotid artery; da, ductus arteriosus; PT, pulmonary trunk.

There are 3 types of IAA: type A (IAA-A) occurs when the interruption is just beyond the left subclavian artery (distal); in type B (IAA-B) the interruption occurs between the left common carotid and the left subclavian artery (Figure 1.5f), whereas in type C the interruption is between the brachiocephalic artery and the left common carotid (proximal). IAA type C is the least common case accounting for less than 5% of cases, whereas type B is the most common occurring in more than 55% of patients with IAA.

In utero the embryo is not affected by this disruption since oxygenated blood flows to the descending aorta through the ductus arteriosus. However, the ductus arteriosus closes after birth cutting down the flow of oxygenated blood to the rest of the body. Patients born with IAA need to be treated immediately by administering prostaglandins to maintain the ductus arteriosus open to preserve the flow of blood, followed by open heart surgery to graft an arterial connection between the ascending and descending aorta to prevent lethality, which occurs within 4 days in 90% of patients with IAA if left untreated.

Although IAA is not common as an isolated defect (2 per million live births), it is usually found in association with other CCVM. Interestingly, about 50% of patients with IAA-B have 22q11 deletion syndrome.

1.4.2 Genetics of Congenital Cardiovascular Malformations

The aetiology of congenital cardiovascular malformations is complex typically involving environmental and genetic causes. In the context of genetics, more than 55 genes have been associated with human CCVM (reviewed in Andersen et al, 2013), either in isolated CCVM or as part of the phenotype in genomic syndromes (syndromic CCVM).

1.4.2.1 Chromosomal aberrations associated with CCVM

About 8-18% of CCVM are due to chromosomal aberrations (Meberg et al, 2007; Schellberg et al, 2004), including aneuploidy, micro-deletions and micro-duplications.

Within typical aneuploidy syndromes presenting cardiovascular malformations are Down syndrome (trisomy 21; Freeman et al, 2008), Turner syndrome (monosomy X; Mazzanti and Cacciari, 1998) and Edward syndrome (trisomy 18; Embleton et al, 1996).

About 40% of patients with Down's syndrome present cardiovascular abnormalities including atrial/ventricular septal defects, valve defects, persistent ductus arteriosus and tetralogy of Fallot (Freeman et al, 2008). Cardiovascular defects are the main cause of mortality in patients with monosomy X (Turner syndrome; Price et al, 1986), typically presenting coarctation of the aorta and biscupid aortic valves (Mazzanti and Cacciari, 1998). Edward syndrome patients typically present atrial/ventricular septal defects and persistent ductus arteriosus. Cardiovascular defects in patients with trisomy 18 are the second main cause of mortality (Embleton et al, 1996).

Among micro-deletion syndromes presenting cardiovascular malformations are Williams-Beuren syndrome, Wolf-Hirschhorn syndrome and 22q11 deletion syndrome.

Williams-Beuren syndrome is caused by a 1.5-1.8 Mb deletion in 7q11.23 encompassing about 28 genes (Ewart et al, 1993; Perez Jurado et al, 1996); About 75% of patients present cardiovascular malformations mainly aortic and pulmonary arterial stenosis (del Pasqua et al, 2009). Wolf-Hirschhorn syndrome is caused by a micro-deletion in 4p16.3, and patients may present atrial (ASD) and ventricular septal defects (VSD) (Maas et al, 2008).

1.4.2.1.1 22q11 Deletion Syndrome

22q11 deletion syndrome (22q11DS) is the common term for patients carrying a micro-deletion on the long arm of chromosome 22 that includes DiGeorge Syndrome, velo-cardio-facial syndrome and conotruncal anomaly face syndrome patients.

22q11DS is the most common micro-deletion syndrome occurring in humans, affecting 1 in every 4000 live births (Wilson et al, 1994; Devriendt et al, 1998) where affected individuals present with a wide variety of abnormalities (reviewed in Shprintzen, 2008) including craniofacial dysmorphology, cleft palate, immune deficiency, mental retardation and cardiovascular defects.

Although the craniofacial dysmorphology along with immunodeficiency and hypothyroidism are the classical features of 22q11DS, the main cause of morbidity and mortality are cardiovascular defects (Ryan et al, 1997). About 80% of patients with 22q11DS have cardiovascular abnormalities including ventricular septum defects (VSD), persistent truncus arteriosis (PTA), tetralogy of Fallot, anomalous right subclavian artery (ARSA) and interrupted aortic arch type B (IAA-B).

The cardiovascular abnormalities seen in patients with 22q11 deletion seem to particularly affect the outflow tract and the great arteries. Along with craniofacial abnormalities and immune deficiency due to thymus hypoplasia, 22q11DS seem to predominantly affect the development of the pharyngeal arch-derived tissues.

About 90% of 22q11DS patients harbour a 3Mb deletion known as the typical deleted region (TDR) while most of the remaining patients have a smaller 1.5Mb deletion (known as the critical region) on band 11.2 on the long arm (q) of chromosome 22 (Figure 1.6).

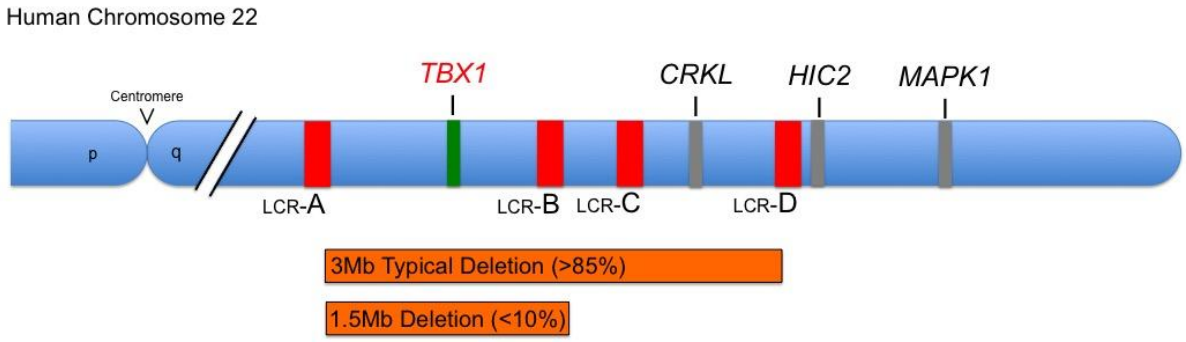

Figure 1.6. 22q11 deletion.
Schematic of human 22q11 chromosomal region, illustrating the typical and critical deletions. 22q11 deletions are caused by recombination between four low copy repeats (LCR-A-D, red boxes); LCR-A and D producing the typical 3Mb deletion, and LCR-A and B generating the critical 1.5Mb deletion. More than 85% of 22q11DS patients harbour the 3Mb typical deletion, while less than 10% of patients have a smaller 1.5Mb deletion. Within the typical region several genes are deleted, including *TBX1* (green box) and *CRKL*. (Adapted from Lindsay, 2001 and Dykes et al, 2014).

The 22q11 chromosomal region presents a high frequency of *de novo* rearrangements, attributed to the presence of 8 highly homologous low copy repeats (LCRs) (Shaikh et al, 2000); these LCR present a high sequence identity (<98%) and are known to typically mediate interchromosomal exchanges during meiosis (Saitta et al, 2004).

Recombination of the four most proximal LCRs (LCR-A through -D), mediate the typical and critical 22q11 deletions (Figure 1.6), with LCR-A and D producing the typical 3Mb deletion and LCR-A and B generating the critical 1.5Mb deletion (Shaikh et al, 2000; Shaikh et al, 2001; Spiteri et al, 2003). Due to the high conservation of the LCRs among eukaryotic genomes these 22q11 deletions are highly homogeneous.

In this context, the 22q11-deleted region is highly conserved in mouse within chromosome 16 (Galili et al, 1997; Botta et al, 1997; Puech et al, 1997; Sutherland et al, 1998), which has allowed the generation of different mouse models to dissect the genetic aetiology of 22q11DS.

Heterozygous deletion of the mouse homologue of the 22q11 region (*Df1*) can recapitulate most of the cardiovascular defects seen in human patients (Lindsay et al, 1999); however, 22q11 deletions result in heterozygosity for more than 30 genes deleted within the typical region, suggesting the 22q11DS phenotype may result from complex genetic interactions.

Targeted specific deletions of genes within the 22q11 typical region revealed *Tbx1* as the main determinant gene underlying the 22q11DS phenotype (Yagi et al, 2010), as *Tbx1* haploinsufficiency in mice resembled the typical cardiovascular phenotypes seen in 22q11DS patients, including 4th PAA-derived defects such as IAA-B (Jerome and Papaioannou, 2001; Lindsay et al., 2001; Merscher et al., 2001).

Another deleted gene within the typical 22q11 regions is *CRKL,* which encodes an adaptor protein required for normal FGF8 signalling. Although *Crkl*-null mice present cardiovascular defects including VSD, the incidence of 4th PAA-derived defects (a hallmark of 22q11DS) is low in *Crkl*-null mice (Guris et al, 2001), and

such penetrance only increases with *Fgf8* heterozygosity (Moon et al, 2006); Crlk haploinsufficiency does not affect cardiovascular development, rather it seems to modify the *Tbx1* heterozygous phenotype by affecting FGF and retinoic acid signalling (Guris et al, 2006).

Moreover, sole transgenic expression of *TBX1* can rescue the 22q11DS-like defects seen in haploinsufficient mice (Merscher et al, 2001). Additionally, point mutations in *TBX1* have been reported in patients without 22q11 deletion but presenting cardiovascular phenotypes similar to those of 22q11DS patients (Zweier et al, 2007), further identifying *TBX1* as the gene underlying the 22q11DS phenotype.

1.5 *TBX1* In Cardiovascular Development

TBX1 belongs to a family of T-box genes, which encode transcription factors that play key roles during embryonic development for the formation of many tissues (Bollag et al, 1994).

There are 17 T-box genes grouped in 5 sub-families based on amino acid homology, although the T-box binding domain is highly conserved (Muller et al, 1997). The T-box binding domain (also known as T-box binding element, TBE) consists of about 180 residues (17-26 kDa) which recognize a characteristic palindromic DNA sequence known as the T-half site (5'-AGGTGTGAAATT-3') however, T-box proteins bind to this sequence in different orientations and spacing which could determine gene specificity for each particular T-box gene (Bollag et al, 1994; Sinha et al, 2000; Conlon et al, 2001). In this context, it was recently reported that *Tbx1* binds preferentially to tandem repeats of the T-half site on a 5'-3' orientation unlike other T-box family members that typically recognize palindromic sequences of the T-half site (Castellanos et al, 2014).

Tbx1 is initially expressed exclusively in the embryonic mesoderm at E7.5 and its expression remains restricted to the pharyngeal region and the otic vesicle by E9.5 (Chapman et al, 1996). Within the pharyngeal arches *Tbx1* is expressed in the ectoderm, mesoderm and endoderm but not in neural crest cells (Chapman et al., 1996; Zhang et al., 2005).

Tbx1 expression is induced and sustained by Sonic hedgehog (*Shh*) expression in the pharyngeal endoderm (Garg et al., 2001), which in turn promotes mesodermal expression of the Forkhead transcription factors *Foxa2*, *Foxc1* and *Foxc2*, which directly promote *Tbx1* expression (Hu et al., 2004; Yamagishi et al., 2003). *Foxa2* is also a direct target of Tbx1, which in turn generates a positive feedback loop (Hu et al., 2004; Yamagishi et al., 2003).

The significant role of *Tbx1* during embryonic development has been extensively described using transgenic mice, in which deletion of *Tbx1* leads to severe cardiovascular defects (Jerome and Papaioannou, 2001; Lindsay et al., 2001; Merscher et al., 2001). *Tbx1* knockout mice die soon after birth due to severe cardiovascular anomalies and present various craniofacial abnormalities such as shorter neck, abnormally folded or absent external ears and they all lack the thymus glands (Jerome and Papaioannou, 2001). The majority of *Tbx1*-null pups or late-stage embryos present a persistent truncus arteriosus (also known as common arterial trunk) where the truncus arteriosus fails to septate into the aorta and pulmonary trunk, delivering mixed oxygenated and deoxygenated blood into the systemic circulation.

The origin of the persistent truncus arteriosus in *Tbx1* knockout mice is due to abnormal development of the pharyngeal arches at earlier stages of embryonic development. By E9.5 the 1st, 2nd and 3rd arches should be completely formed however, in *Tbx1*-null embryos only the 1st pair of arches is developed while the caudal pharyngeal arches are not formed, consequently causing the pharyngeal arch arteries to be absent with a single artery connecting the aortic sac with the dorsal aorta that gives rise to a common arterial trunk in the later embryo.

The majority of *Tbx1* heterozygous (*Tbx1*$^{+/-}$) mice are viable with only about 5% of perinatal lethality due to interrupted aortic arch (Vitelli et al, 2002; Guris et al, 2006; Zhang et al, 2008; Calmont et al, 2009; Randall et al, 2009; Ryckebusch et al, 2010). These defects are caused by abnormal development of the pharyngeal arch arteries by E10.5 in mouse embryos, where a proportion of *Tbx1*$^{+/-}$ display abnormal 4th PAAs, which can be hypoplastic or completely absent either unilaterally or bilaterally (Lindsay and Baldini, 2001; Calmont et al, 2009; Randall et al, 2009; Ryckebusch et al, 2010).

Complete absence of the left 4th PAA by E10.5 is the cause of an interrupted aortic arch seen later in development, while absence of the right 4th may cause an aberrant right subclavian artery (ARSA).

The frequency of abnormal 4th PAAs (hypoplastic and/or aplastic PAA) seen around mid-embryogenesis (E10.5) in *Tbx1*$^{+/-}$ embryos is much higher compared to the incidence of 4th PAA-derived defects (IAA, ARSA) seen in older embryos (Vitelli et al, 2002; Guris et al, 2006; Zhang et al, 2008; Calmont et al, 2009; Randall et al, 2009; Ryckebusch et al, 2010), indicating that some form of recovery occurs during the remodelling of the PAAs in Tbx1 haploinsufficient embryos (Lindsay and Baldini, 2001; Calmont et al, 2009; Papangeli and Scambler, 2012).

Tbx1 mRNA levels are critical for correct PAAs development as shown using hypomorphic alleles of *Tbx1* (Zhang and Baldini, 2007). Reduced levels of *Tbx1* mRNA mainly affects the development of the 4th PAAs and the septation of the outflow tract, and the severity of the cardiovascular defects observed increases with further reductions in the levels of *Tbx1* expression. Whereas over-expression of *Tbx1* in mice with extra copies of the gene, leads to cardiovascular abnormalities similar to those seen in *Tbx1* heterozygous mice (Liao et al., 2004).

Furthermore, timed conditional inactivation of *Tbx1* revealed its requirement at a precise time frame between E7.5 and E8.5 for correct PAAs development, whereas septation of the outflow tract requires *Tbx1* expression between E8.5 and E9.5 (Xu et al., 2005). Later deletion of *Tbx1* at E11.5 or E12.5 affects only the formation of other tissues such as the thymus and secondary palate but not the outflow tract or the pharyngeal arch arteries.

Tbx1 is known to be required for correct development of the pharyngeal arches and their derived tissues, including the jaw, ears, thymus and the pharyngeal arch arteries (Arnold et al, 2006; Reviewed in Scambler, 2010, and Gao et al, 2013).

The required expression of *Tbx1* within the different compartments of the pharyngeal arches has been shown using conditional-knockout models to delete *Tbx1* specifically from the mesoderm (Zhang et al., 2006), endoderm (Arnold et al., 2006) and ectoderm (Calmont et al., 2009; Randall et al., 2009).

In this context, conditional deletion of *Tbx1* from the mesoderm using *MesP1cre* (Zhang et al, 2006), or the endoderm using *Foxg1cre* (Zhang et al, 2006) results in abnormal patterning of the pharyngeal arches resembling the *Tbx1*-null phenotype, where the caudal pharyngeal arches are not developed and only the first arch is formed, consequently the PAAs are not formed and embryos present with persistent truncus arteriosus (Arnold et al., 2006; Zhang et al., 2006).

Conditional deletion of *Tbx1* from the pharyngeal surface ectoderm does not affect the patterning of the pharyngeal arches but affects the formation of the 4th PAAs, presenting defects similar to the heterozygous (*Tbx1*$^{+/-}$) embryos (Calmont et al., 2009; Randall et al., 2009). Additionally, *Tbx1* expression in the pharyngeal ectoderm was shown to be required to control cardiac neural crest cell migration (Zhang Z et al, 2006; Calmont et al., 2009). In this context, Tbx1 regulates ectodermal *Gbx2* expression, which in turn controls neural crest cell migration through Slit/Robo signalling (Calmont et al, 2009).

The requirement of *Tbx1* for correct pharyngeal arch development and their related arteries is highly conserved as shown by using zebrafish. Mutation of *tbx1* (*vgo*) in zebrafish results in abnormal patterning of the caudal pharyngeal arches and a reduction in the number of pharyngeal arch arteries (Piotrowski and Nusslein-Voldhard, 2000; Piotrowski et al, 2003), similar to the phenotypes seen in mice. Additionally, *tbx1* mutation in zebrafish also affects neural crest cells (Piotrowski and Nusslein-Voldhard, 2000) similar to that seen in mouse models (Zhang Z et al, 2006; Calmont et al., 2009).

The cardiovascular defects seen in *Tbx1*-null mice are largely due to a significant reduction in proliferation of secondary heart field cells. Such reduction in proliferation is caused mainly by down-regulation of *Fgf8*, a direct target of *Tbx1* (Vitelli et al., 2002).

Further studies have found that Tbx1 interacts with Six1-Eya1 transcription factors which in turn regulate *Fgf8* expression, and loss of either Six1, Eya1 or both lead to cardiovascular defects similar to those in *Tbx1* mutant mice and 22q11DS patients (Guo et al., 2011). Moreover, proliferation of secondary heart field cells is also affected by down-regulation of *Wnt5a* in *Tbx1*-null embryos, as Tbx1 is required to interact with Baf60a/Smarcd1 chromatin remodelling factors to promote *Wnt5a* expression (Chen et al., 2012).

It has also been suggested that Tbx1 may promote proliferation of secondary heart field cells by directly interacting with Smad1, which inhibits Bmp4 signalling (Fulcoli et al., 2009).

It was recently reported that proliferation of secondary heart field cells are negatively regulated by p53 through repressing *Gbx2* expression (Caprio and Baldini, 2014). In this context, Tbx1 regulates expression of *Gbx2* by binding to a conserved T-box binding element within the *Gbx2* locus, however, p53 is able to bind a close genomic element within the same region and recruit the polycomb repressive complex to methylate and silence *Gbx2* expression (Caprio and Baldini, 2014).

Gbx2 is a downstream target of Tbx1 required for correct NCC migration and 4th PAA development; in this context, *Gbx2*-null embryos present with 4th PAA-derived cardiovascular defects including IAA-B and ARSA (Byrd and Meyers, 2005), due to defective migration of NCC towards the PAs as a consequence of Slit/Robo signalling lose in NCC (Calmont et al, 2009). Consequently, heterozygous deletion of p53 ameliorates the Tbx1 heterozygous phenotype by rescuing *Gbx2* expression and promoting SHF cells proliferation (Caprio and Baldini, 2014).

However, *Tbx1* does not only regulate heart and PAA development by promoting proliferation of progenitor cells, but also by regulating their differentiation. Tbx1 has been found to regulate *Smad7* expression by binding directly to T-box elements within the *Smad7* gene and further regulating *Tgfβ* signalling to control vascular smooth muscle differentiation, which is essential for PAAs remodelling (Papangeli and Scambler, 2012).

Although *Tbx1* haploinsufficiency resembles most of the 22q11DS cardiovascular defects, 22q11DS patients present with a high phenotypic variability in terms of penetrance and severity, suggesting the presence of genetic modifiers that influence the presentation of the phenotype.

The possibility of stochastic events causing the great phenotypic variability in 22q11DS has been shown less likely, with evidence sustaining the existence of genetic modifiers influencing the 22q11 phenotype; the evidence shows that genetic background strongly affects the presentation of cardiovascular and thymic defects in a mouse model of 22q11DS (*Df1*) (Taddei et al, 2001); similarly, genetic background strongly influences the incidence of 4th PAA defects in *Tbx1* heterozygous embryos (Zhang et al, 2005).

Moreover, analysis of genes within the 22q11 deletion region showed no variations among these genes related to changes in the genetic background, suggesting genes elsewhere in the genome are capable of influencing the phenotype supporting the existence of genetic modifiers, which may potentially be in epistasis (the interaction between two or more genes to define a phenotype) with *TBX1* to define the phenotype.

In this context, various genes have been shown to genetically interact with *Tbx1* (reviewed in Aggarwal and Morrow, 2008) including *Vegf* (Stalmans et al, 2003), *Crkl* (Guris et al, 2006), *Pitx2* (Nowotschin et al, 2006), *Gbx2* (Calmont et al, 2009), and *Aldh1a2* (Ryckebusch et al, 2010), typically by increasing the incidence of 4th PAA-derived defects and modifying the Tbx1 heterozygous phenotype penetrance.

However, more than 200 genes are affected by homozygous loss of *Tbx1* in mouse embryos (Ivins et al, 2005; Liao et al, 2008) that could potentially be in epistasis with *TBX1* and be genetic modifiers of the 22q11 deletion syndrome.

Among those genes, the transcription factor *Pax9* was found significantly down-regulated by microarray of *Tbx1*-null embryos and further validated by quantitative PCR and *in situ* hybridisation (Figure 1.7) (Ivins et al, 2005).

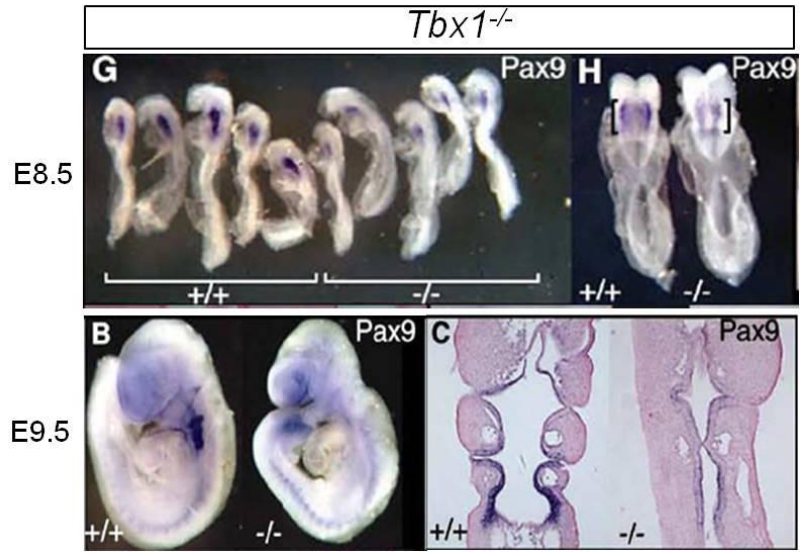

Figure 1.7. *Pax9* mRNA is down-regulated in *Tbx1*-null embryos.
Whole-mount *in situ* hybridisation using a riboprobe for *Pax9* showing *Pax9* down-regulation in *Tbx1*-null embryos at E8.5 and E9.5, further validating results from a microarray analysis and qPCR. (modified from Ivins et al, 2005).

1.6 Paired Box 9, *PAX9*

PAX9 belongs to a family of 9 transcription factors characterized by a common motif, the DNA-binding paired domain (Chi and Epstein, 2002), all of which play essential functions during mammalian embryogenesis.

The paired domain is a highly conserved 128 amino acid motif found in the N-terminal that binds to specific sequences within the DNA (Goulding et al, 1991; Chalepakis et al, 1991; Czerny et al, 1993; Epstein et al, 1994). Pax genes are classified into four subfamilies according to their genomic organization and expression patterns (Chalepakis and Gruss, 1995).

The chromosomal location of *PAX9* in humans is 14q13.3, and mutations in *PAX9* and deletions within this chromosomal region are commonly associated with syndromic and non-syndromic oligo-/hypodontia (Reviewed in Cudney and Vieira, 2012; and De Coster et al, 2009) and holoprosencephaly (HPE) (Chen et al, 1997; Kamnasaran et al, 2005).

The critical role of *Pax9* for tooth development has been described by deletion of *Pax9* in mouse models (Kist et al, 2005), which has also revealed the requirement of *Pax9* for correct development of some pharyngeal arch- derived tissues including the thymus, parathyroids and ultimobrachial bodies (Peters et al, 1998).

During mouse embryogenesis *Pax9* expression starts around E8.5, and becomes more evident within the pharyngeal arches by E9.5 (Figure 1.8a) (Neubüser et al, 1995; Peters et al, 1998), and its expression is restricted to the pharyngeal endoderm. Later on, *Pax9* is also expressed in the axial skeleton and in neural crest-derived mesenchyme involved in craniofacial, tooth and limb development (Figure 1.8b; Peters et al, 1998).

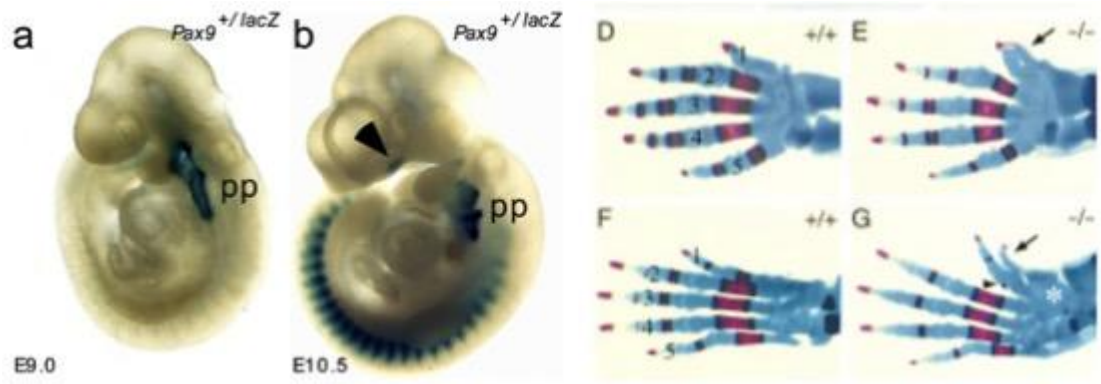

Figure 1.8. *Pax9* expression and skeletal defects in *Pax9*-null embryos
Pax9 expression starts around E8.5 exclusively within the pharyngeal arches (**a**); by E10.5 *Pax9* expression extends along the body axis and facial mesenchyme (**b**). *Pax9*-null mice present with preaxial duplication of the 1st digit of the fore- (**e**) and hindlimbs (**f**).
(adapted from Peters et al, 1998)

Pax9 knockout embryos lack most derivatives of the caudal pharyngeal arches such as the thymus, parathyroid glands and ultimobranchial bodies. Additionally, they present craniofacial and skeletal defects including a supernumerary digit on the limbs (Figure 1.8e, g), absent teeth and cleft palate (Peters et al, 1998). Although most pharyngeal arch-derivatives are absent in *Pax9*-null mice, the pharyngeal arches are actually formed, however development of the 3rd and 4th arches stops at E11.5 (Peters et al, 1998). *Pax9*-null mice die shortly after birth because of respiratory insufficiency due to the cleft palate (Peters et al, 1998).

Pax9 expression is induced and sustained by ectodermal *Fgf8*, whereas *Bmp2* and 4 signalling repress *Pax9* expression (Neubüser et al, 1995). Moreover, expression of *Pax9* is affected by loss of *Tbx1*, as shown by microarray analysis, quantitative PCR and *in situ* hybridisation of *Tbx1* knockout embryos. *Pax9* expression is down-regulated in *Tbx1*-null embryos prior to the formation of the caudal pharyngeal arches (around E8.5), therefore before any anatomical abnormalities appear (Figure 1.7; Ivins et al, 2005). Additionally, expression of Pax9 and Tbx1 co-localizes within the pharyngeal endoderm at E9.5 and 10.5 mouse embryos (Okubo et al, 2011).

Although there is no published evidence to date indicating *Pax9* involvement in cardiovascular development, there is some evidence in humans that potentially links *PAX9* with cardiovascular development.

In a study screening for deletions within chromosome 14q13 (the chromosomal location of *PAX9*), a patient was identified that had been born with several cardiovascular malformations including interrupted aortic arch type B (IAA-B), bicuspid aortic valve, ventricular septal defect and hypoplastic aorta. This patient was carrying a 14q13 deletion including *PAX9*, however no other cardiovascular-related mutations were found such as 22q11 deletion (Santen et al, 2012). Two other cases of 14q chromosomal deletions that include PAX9 in patients with cardiovascular abnormalities have been reported: a male patient with persistent ductus arteriosus and pulmonary stenosis (Schuffenhauer et al, 1999), and a female patient with persistent ductus arteriosus (Kamnasaran et al, 2001).

There is therefore some evidence potentially linking *PAX9* to cardiovascular development: The requirement of both *Tbx1* and *Pax9* for the development of the pharyngeal arches and their derived tissues as well as the overlap between some defects found in both *Tbx1* and *Pax9* knockout embryos including the cleft palate, abnormal teeth, craniofacial abnormalities and abnormal development of the pharyngeal arch-derived tissues; and together with *Pax9* down-regulation in *Tbx1*-null embryos and their co-localization within the pharyngeal endoderm, the role of *Pax9* during cardiovascular development as well as a potential genetic interaction with *Tbx1* were investigated in this project.

1.7 Aims

1. To determine whether *Pax9* is involved in cardiovascular development
2. To study a potential genetic interaction between *Pax9* and *Tbx1*
3. To determine the molecular mechanism of *Pax9* and *Tbx1* interaction

1.7.1. To determine whether Pax9 is involved in cardiovascular development

Previous reports have shown *Pax9* expression is down-regulated in *Tbx1*-null embryos, suggesting *Pax9* could potentially be a downstream target of Tbx1. Additionally, preliminary results from our group shows *Pax9*-null embryos present some cardiovascular defects at E14.5

Therefore, the first aim of this project was to determine whether homozygous deletion of *Pax9* affects cardiovascular development.

1.7.2. To study a potential genetic interaction between Pax9 and Tbx1

Given that homozygous deletion of *Pax9* leads to severe cardiovascular defects, most of them phenocopying the *Tbx1* heterozygous phenotype, the second aim of this project was to study a potential genetic interaction between *Tbx1* and *Pax9*, determining whether double haploinsufficiency affects cardiovascular development.

1.7.3. To determine the molecular mechanism of Pax9 and Tbx1 interaction

With the results showing a strong genetic interaction between *Tbx1* and *Pax9* during cardiovascular development, the third aim of this project was to determine the molecular mechanism of this interaction.

Chapter 2. Materials and Methods

2.1. Mouse Lines And Crosses

All animals used in this project were maintained and euthanized according to the requirements of the Animals (Scientific Procedures) Act 1986 of the UK government. All mice were kept in individual ventilated cages with food and water *ad libitum* under a 12-hour light/dark cycle.

Pax9$^{LacZ/+}$ mice (Peters et al, 1998), referred as Pax9$^{+/-}$ throughout the thesis, were obtained from Dr. Heiko Peters (Newcastle University, UK), and *Tbx1*$^{+/-}$ mice (Jerome and Papaioannou, 2001) were obtained from Dr. Robert Kelly (Aix Marseille University, France). Both *Pax9*$^{+/-}$ and *Tbx1*$^{+/-}$ mouse lines were maintained on a C57Bl/6J genetic background.

Pax9-null embryos were generated by intercrossing *Pax9* heterozygous mice, and double heterozygous (*Tbx1*$^{+/-}$;*Pax9*$^{+/-}$) embryos were generated by crossing *Pax9*$^{+/-}$ mice with *Tbx1*$^{+/-}$ mice.

Embryos were collected at the specified stages for each experiment considering embryonic day (E) 0.5 the day of detection of a vaginal plug in the female. Pregnant females were euthanized by dislocation of the neck and the uterus was dissected and collected in phosphate-buffered solution (PBS, pH 7.0) or pre-warmed balanced Hank's solution with EDTA for MRI.

Embryos for MRI and histology were then fixed in 4% (w/v) paraformaldehyde (PFA, in PBS) for at least 2 days, whereas embryos for whole-mount *in situ* hybridisation (WISH) were fixed in DEPC-treated 4% PFA overnight, followed by dehydration in methanol as described below (section 2.6.2).

For E9.5 and E10.5 embryos the somites were counted to properly stage match the embryos. For E15.5 embryos the stage was confirmed by the presence of hair follicles in the trunk but its absence in the head region and closed eyelids according to the Theiler staging criteria (The House Mouse: Atlas of Mouse Development; 1989).

Newborn pups were collected to analyze the survival of double heterozygotes. Pups were euthanized by intraperitoneal injection of anaesthetic and dissected under a stereomicroscope (Leica, Stemi 2000) to visualize the heart and the great vessels.

2.2. Genotyping

2.2.1 DNA Extraction

DNA for genoyping was extracted from tissue samples using 600µg/mL of proteinase K in lysis buffer (50 mM KCl, 1.5 mM $MgCl_2$, 10 mM Tris, 0.45% NP40, 0.45% Tween-20) incubating the samples for 2 hours at 56^{o}C followed by a final 10 minutes incubation at 95^{o}C to inactivate proteinase K.

Ear notches (150µl of lysis buffer) were used to genotype and identify adult mice. For E9.5 (50µl) and E10.5 (100µl) embryos the yolk sacs were collected, whereas a limb or a piece of tail (400µl) was used for genotyping older embryos and newborn pups. 2µl of the lysate was used for PCR. The primers used in PCR reactions for each gene are described in Table 2.1.

Table 2.1. List of primers used for genotyping

Gene	Primer	Sequence	TM	Product size
Tbx1	Tbx1.1	TGCATGCCAAATGTTTCCCTG	58°C	WT 196 bp
	Tbx1.2	GATAGTCTAGGCTCCAGTCCA		Mutant 450 bp
	Tbx1.3	AGGGCCAGCTCATTCCTCCCAC		
Pax9	P9-gen2-F1	ACTCACCGGCCTGCACCAATTAC	58°C	WT 268 bp
	P9-gen2-R1	TTGTTCTCACTGAGCCGGCCTGT		Mutant 350 bp + 480 bp
	P9-gen2-R2	GGATGTGCTGCAAGGCGATTAAG		

2.2.2. Polymerase Chain Reaction And Electrophoresis

PCR reactions were performed using 1 unit of GoTaq polymerase (Promega) in 1x GoTaq reaction buffer containing 1.5 mM $MgCl_2$, 0.25mM of each deoxyribonucleotide triphosphate (dATP, dCTP, dGTP and dTTP), 0.5 µM of each primer and 2µl of DNA sample as mentioned above in a final volume of 20µl.

Samples were then incubated in a thermocycler with an initial denaturation step of 94^{o}C for 2 minutes, followed by 35 cycles of denaturation at 98^{o}C for 30 seconds, followed by 30 seconds at the specific annealing temperature (Table 2.1) and extension at 72^{o}C for 30 seconds, followed by a single final elongation incubation at 72^{o}C for 10 minutes.

PCR samples were then analysed by electrophoresis in a 1.5% (w/v) agarose gel in 1x TAE buffer (40mM tris, 20mM acetic acid, 1mM EDTA) containing 0.5µg/ml ethidium bromide (EtBr). Gels were run at 100 volts for 30-45 minutes and photographed under a UV light transilluminator. DNA ladders (100bp or 1Kb, Promega) were run along with samples in gels to analyse the band size of the PCR products.

2.3 Magnetic Resonance Imaging

Magnetic resonance imaging (MRI) was performed as described (Bamforth et al, 2011). Pregnant female mice were euthanized by cervical dislocation and the uterus was dissected and collected in pre-warmed (37°C) Hank's balanced salt solution with 5mM EDTA. Embryos were dissected out of the uterus and carefully from the yolk sacs to expose the umbilical vessels, which were subsequently cut firmly with Vannas scissors and the embryos were allowed to bleed out for no more than 20 minutes removing blood clots.

Bleeding is critical in order to remove as much blood as possible, since blood can give a high contrast signal and interfere with the MRI, therefore embryos are dissected in pre-warmed Hank's solution plus EDTA on a heating mat to maintain the hearts beating to help the bleeding.

Embryos were subsequently washed twice in PBS and photographed to record any external phenotype. The left forelimb was cut and used for genotyping. Embryos were then fixed in 4% paraformaldehyde (PFA) and kept at 4°C until used. Slits were cut on each side of the trunk of the embryos to help penetration of the fixative.

Four days before sending the embryos for MRI, Gd-DTPA (Magnevist), was added (6µl/mL) as contrast agent. Fixed embryos were then embedded in 1% agarose plus Gd-DTPA in a 28mm diameter glass tube, stacking the embryos in 8 layers of 4 embryos each. To identify embryos in each layer, a different limb or the tail was removed, and this was recorded on a data sheet with the ID of each embryo for subsequent analysis. The loaded tube was sent to the British Heart Foundation MRI unit in Oxford (University of Oxford, UK) for imaging. The embryos and MRI datasets were later returned and embryos were subsequently processed for histology as described below, and the data sets were used to analyse the phenotype and reconstruct 3D models using Amira software (Visage Imaging).

2.4. Histology

2.4.1. Embedding And Sectioning

Fixed embryos (4% PFA) were dehydrated through a series of ethanol dilutions (Table 2.2) and then cleared with Histoclear (National Diagnostics) to completely remove ethanol. Embryos were then incubated in wax to allow the paraffin to penetrate the tissue, and embryos were finally embedded in paraffin blocks. The incubation times depending on the age are shown in Table 2.2.

Embedded embryos were sectioned transversally using a microtome (Leica, RM 2235) to obtain 8µm slices. Sections were placed on glass microscope slides (VWR) pre-coated with warm water (37^{o}C) to allow the sections to stretch. Excess water was then removed and slides were allowed to dry overnight in an oven at 37^{o}C to completely dry the slides.

Table 2.2. Dehydration of embryos for histology

		E9.5	**E10.5**	**E15.5**
Room temperature	50% Ethanol	30 minutes	30 minutes	3 hours
	70% Ethanol	30 minutes	30 minutes	3 hours
		30 minutes	30 minutes	3 hours
	95% Ethanol	30 minutes	30 minutes	3 hours
	100% Ethanol	30 minutes	30 minutes	3 hours
		30 minutes	1 hour	Overnight
	Histoclear	10 minutes	15 minutes	30 minutes
		10 minutes	15 minutes	30 minutes
60°C	Histoclear/wax	15 minutes	20 minutes	1 hour
	Wax	20 minutes 20 minutes 20 minutes	30 minutes 30 minutes 30 minutes	1 hour 1 hour 1 hour 1 hour

2.4.2. Hematoxylin And Eosin Staining

To analyse the morphology in detail, sections were stained with haematoxylin, which stains cell nuclei in purple, and eosin to counterstain the cytoplasm in pink.

Slides were dewaxed by incubating them in Histoclear for 10 minutes twice; Sections were then washed for 3 minutes twice in 100% ethanol and rehydrated through ethanol dilutions (90%, 70% and 50%) immersing the slides on each solution for 2 minutes each with a final wash in distilled water for 2 minutes. Sections were then stained in Harris' hematoxylin solution for 10 minutes and then washed under running tap water for 5 minutes. Slides were then dipped twice in an acid ethanol solution (1% v/v hydrochloric acid (HCl) in 70% ethanol) for differentiation to remove background staining of hematoxylin. Slides were washed again under running tap water for 5 minutes and then immersed in Eosin for 5 minutes followed by a final wash under running tap water until water was clear. Slides were rehydrated through 50%, 70% and 90% ethanol solutions dipping them twice on each solution.

Slides were then incubated 3 minutes twice in 100% ethanol and finally cleared for 10 minutes twice in Histoclear to remove all ethanol. Stained slides were mounted in Histomount (National Diagnostics) with a coverslip and left to dry overnight.

Mounted sections were photographed under bright-field using a transmitted light microscope (Zeiss, Axioplan) with its corresponding AxioVision software (Zeiss).

2.5. Ink Injections

India ink was used to visualize the patterning of the pharyngeal arch arteries at mid embryogenesis. Embryos were collected at E10.5 in 1x PBS at room temperature and the yolk sacs were kept for genotyping. Diluted India ink (1:1 in water v/v) was injected into the left ventricle of the beating heart using a pulled glass pipette and a mouthpiece to slowly inject the ink into the heart. The pipette was removed to allow the heart to pump ink through the arteries and embryos were immediately photographed from both sides under a stereomicroscope (Leica, Stemi 2000).

2.6. Whole-Mount *In Situ* Hybridisation

For whole-mount *in situ* hybridisation all solutions (water, PBS and stock solutions) were pre-treated with 0.1% Diethylpyrocarbonate (DEPC), and all material and tools (dissection tools, flask, sieves) were washed with RNAse Away (Fisher) to remove any traces of RNAses prior to commencing the procedure.

2.6.1 Probe Dig-Labelling

The *Pax9* plasmid probe was donated by Dr. Ralf Kist (Newcastle University, UK), and *Gbx2* plasmid probe was donated by Dr. Alexandra Joyner (Sloan Kettering Institute, USA). To generate each probe, plasmids were linearized with the respective restriction enzyme (Table 2.3). Linearized plasmids were purified using a PCR purification kit (Qiagen) according to manufacturer's protocol and quantified using a Nanodrop spectrophotometer (Thermofisher).

Table 2.3. Restriction enzymes and RNA polymerases used for probe preparation.

Probe		Restriction enzyme	RNA polymerase
Pax9	Antisense	Eco RI	T7
	Sense	Hind III	T3
Gbx2	Antisense	Hind III	T7
	Sense	Kpn I	T3

Probes were then generated from each linearized plasmid using the respective RNA polymerase (Table 2.3) and labelled with Digoxygenin (DIG) using a DIG labelling kit (Roche) according to manufacturer's protocol, in a mix containing 1µg of linearized plasmid, 40 units of the respective RNA polymerase (Table 2.3) 1x NTP labelling mixture, 1x transcription buffer and 20 units of RNAse inhibitor; each sample mix was incubated at 37^{o}C for 2 hours, and subsequently treated with DNAse I to remove template DNA.

DIG-labelled RNA probes were purified by precipitation with ethanol, adding two volumes of tris-EDTA buffer (TE pH 8.0), 5 volumes of ice-cold ethanol (100%) with 0.1M lithium chloride (LiCl), and left overnight at -20^{o}C. The following day, samples were centrifuged at 13,000g for 30 minutes at 4^{o}C, the supernatants were discarded and pellets were air-dried for 5 minutes before re-dissolving in 100µl of TE buffer containing 80 units of RNAse inhibitor.

Probes were quantified using the Nanodrop spectrophotometer, and tested by electrophoresis in a 1% agarose gel ran quickly for 10 minutes at 200V to minimise RNA degradation.

Probes were aliquoted in single use aliquots (final concentration of 1µg/mL) to avoid multiple thawing/freezing, and stored at -80^{o}C, and prior to hybridisation, probes were denatured at 100^{o}C for 5 minutes in hybridisation solution.

2.6.2. Hybridisation

Embryos were collected and dissected in cold 1x PBS. The yolk sacs were kept for genotyping and embryos were fixed overnight at 4^{o}C in 4% PFA (in PBS).

Embryos were then washed for 5 minutes twice with PBS and then dehydrated through a series of methanol dilutions (25, 50, 75%) in PBS for 10 minutes each at room temperature, followed by two 10 minutes washes in 100% methanol. Embryos were then stored in 100% methanol at -20^{o}C until used.

Embryos of the same genotype were pooled and processed in 12-well plates using 15mm Netwell inserts (Corning) pre-washed with RNAse-away.

Embryos were re-hydrated through methanol dilutions (75, 50, 25%) in PBT (0.1% Tween-20 in PBS) for 5 minutes each at room temperature, and then washed twice for 5 minutes in PBT. Embryos were then bleached in 6% hydrogen peroxide (in PBT) for 1 hour at room temperature, followed by three 5 minutes washes in PBT. Embryos were then permeabilized with 10µg/mL Proteinase K (in PBT) for 15 minutes at room temperature. Proteinase K activity was quenched by incubating embryos in 2mg/mL glycine (in PBT) for 5 minutes at room temperature, followed by two 5 minutes washes with PBT. Embryos were then re-fixed in 0.2% glutaraldehyde/4% PFA (in PBS) for 20 minutes at room temperature, followed by two 5 minutes washes with PBT.

Embryos were then transferred to cryovials and incubated in pre-hybridisation solution (50% Formamide, 5x saline-sodium citrate buffer (SSC) pH 4.5, 0.1% Tween-20, 50µg/mL heparin in DEPC-treated ddH_2O) for 1 hour at 70^{o}C in a hybridisation oven with gentle rocking.

Embryos were then incubated with hybridisation solution (50% Formamide, 5x SSC pH 4.5, 0.1% Tween-20, 50µg/mL heparin, 50µg/mL yeast tRNA, 100µg/mL salmon sperm DNA and 1µg/mL of denatured probe in DEPC-treated water) at 70^{o}C overnight in a hybridisation oven with gentle rocking.

The following day embryos were washed twice in pre-warmed (70^{o}C) solution I (50% formamide, 4x SSC, 1% Sodium dodecyl sulphate (SDS, w/v) in DEPC-treated water) for 30 minutes at 70^{o}C, followed by a 10 minute wash in pre-warmed (70^{o}C) solution I/solution II mix (1:1 v/v; solution II: 0.5M sodium chloride, 0.01M Tris pH 7.5, 0.1% Tween-20) in the hybridisation oven with gentle agitation.

Embryos were further washed three times for 5 minutes at room temperature in solution II, and then treated with 100µg/mL RNAse A (in solution II) for 30 minutes at 37^{o}C, twice. Embryos were then washed for 5 minutes with solution II at room temperature, followed by a 5 minutes wash in solution III (50% formamide, 4x SSC, 0.2% SDS in DEPC-treated water) at room temperature; embryos were then incubated in solution III for 30 minutes at 65^{o}C, twice.

Embryos were then transferred into glass vials, and washed three times with TBST (0.05M Tris pH7.5, 0.15M NaCl, 0.05% Tween-20) for 5 minutes at room temperature.

Prior to antibody incubation, embryos were blocked with 10% fetal bovine serum (FBS; in TBST) for 2.5 hours at room temperature with gentle agitation; embryos were then incubated with 0.5µl/mL anti-Digoxigenin-alkaline phosphatase Fab fragments (Roche) in 1% FBS (in TBST) overnight at 4^{o}C with gentle rocking.
The following day, the antibody was removed and embryos were washed five times for 1 hour each in TBST at room temperature with gentle rocking, followed by a final overnight wash in TBST at 4^{o}C.

Embryos were then washed twice for 10 minutes at room temperature, in NTMT (100M NaCl, 0.1M Tris pH 9.5, 0.1% Tween-20) and then incubated with 20µl/mL of NBT/BCIP (nitro blue tetrazolium chloride/ 5-Bromo-4-chloro-3-indolyl phosphate; Roche) developing solution (in NTMT) in the dark. Developing of staining was monitored every 10 minutes and the reaction stopped at the same time for all embryos.

To stop the developing reaction, embryos were washed for 10 minutes at room temperature twice with NTMT followed by a 10 minute wash with PBT pH 5.5 at room temperature.

Embryos were then fixed in 0.1% glutaraldehyde/4% PFA for 1 hour at room temperature and then rinsed with PBS. Embryos were photographed from both sides using a stereomicroscope (Leica, Stemi 2000).

2.7. Tissue Culture

2.7.1 JEG3 Cells Culture

Human placental choriocarcionoma cells (JEG3; ATCC) were used for all *in vitro* experiments since they have shown to be efficient for Tbx1 expression and activation of the 2xTtkGL2 reporter (Zweier et al, 2007).

JEG3 cells were cultured in high glucose Dulbecco's modified eagle medium (Life Technologies) supplemented with 10% (v/v) fetal bovine serum (FBS, Life Technologies) and 100units/mL of Penicillin and 100µg/mL of Streptomycin (Life Technologies); cells were kept at 37^{o}C in a humidified incubator with 5% CO_2.

Cells were passaged every two days before reaching confluency by dissociation with 0.05% Trypsin in EDTA (Life Technologies); culture media was removed and cells were washed once with 1x PBS followed by incubation with trypsin for 5 minutes at 37^{o}C. Two volumes of complete culture media were then added to stop trypsin activity; cell suspensions were transferred to sterile 50mL centrifuge tubes and centrifuged for 5 minutes at 1000g. The supernatant was removed and cell pellets were homogeneously resuspended in 10 mL of complete culture media; cells were counted using a hemocytometer and resuspended in the appropriate volume of media to achieve the final cell density required. Cells were plated at the desired density in T75 flask, 100mm dishes or multiwell plates according to each experiment.

2.7.2. Mouse Embryonic Fibroblasts

Mouse embryonic fibroblasts were obtained from wild-type E14.5 embryos; pregnant females were euthanized by cervical dislocation and the uterus was collected in PBS. Embryos were dissected in PBS removing all membranes and the head; carcasses were washed twice with PBS and then minced in 2mL of trypsin/EDTA, the liver was removed and an extra 3mL of trypsin/EDTA added. Minced tissue was transferred into a 15mL centrifuge tube and incubated at 37^{o}C for 30 minutes, mixing the tube vigorously every 10 minutes to dissociate clumps.

One volume (5mL) of FBS was added to the minced tissue and incubated for 5 minutes to allow larger clumps to settle; supernatant was then transferred into a fresh centrifuge tube and centrifuged at 1000g for 5 minutes.

The supernatant was discarded and cells were resuspended in complete medium (1x DMEM, 10% FBS, 100units/mL of Penicillin and 100µg/mL of Streptomycin); cells were resuspended, pipetting up and down vigorously to further dissociate into single cells.

Cells were counted using a hemocytometer, resuspended in the appropriate volume of media and seeded in T75 flasks. MEFs were passaged before reaching confluency using trypsin/EDTA as described above for JEG3 cells.

2.8. Molecular Cloning

2.8.1. Cloning

Human and mouse Tbx1 and Pax9 cDNAs sub-cloned into pcDNA3.1 had been previously generated in the lab.

For the luciferase constructs, DNA fragments containing the conserved TBEs, the *Pax9* promoter and introns, and the conserved Gbx2 enhancer region were obtained by PCR from mouse genomic DNA using the primers described in Table 2.4, resolved in a 1.5% agarose gel to confirm the size and specific amplification, and purified using a gel extraction purification kit (Qiagen).

PCR fragments were subcloned into the respective pGL3 plasmid (Table 2.4) by enzymatic digestion with the corresponding restriction enzyme (Table 2.5), followed by ligation with T4 DNA ligase (Promega).

Ligated constructs were subsequently transformed into DH5α competent cells (as described in section 2.8.2); plasmid DNA was purified by mini-prep (section 2.8.3) and the cloned fragments were verified by sequencing. The verified constructs were further transformed and midi-prepped (section 2.8.3).

The Pax9 intron 3 was produced from two fragments (intron 3.1 and 3.2), which were initially generated by PCR as mentioned above, and then ligated together into one fragment by digestion with Bgl II (Table 2.4) and T4 DNA ligase before ligation into the pGL3 vector.

Table 2.4. List of primers and restriction enzymes used for cloning

Target	Oligo	Sequence	Enzyme	pGL3 vector
Pax9 locus				
TBE-1	F	ggggcTAGCCTGGCTAGGAAGACTTG	Nhe I	Promoter
	R	AGATCTCGAGGGCTGGGGAAAG	Xho I	
TBE-2	F	ggggctAGCCAGGAGTATTGCTCCTTG	Nhe I	Promoter
	R	ccccctCGAGTCTATAAGCAAATCTTCCC	Xho I	
TBE-3	F	ggggctAGCCAGGAGTATTGCTCCTTG	Nhe I	Basic
	R	cccctCGAGCGCTTAGCCCGGCTC	Xho I	
TBE-4	F	ggggctAGCCTGGGTCGTTGGAGGCAG	Nhe I	Promoter
	R	ccccctcGAGGTCATGGGGGAATCAGGAG	Xho I	
TBE-5	F	cccgagCTCCAAGGGTCAGTGGCGG	Sac I	Promoter
	R	cccagaTCTCAAAACAAGCTGCGGCCAG	Bgl II	
TBE-6+7	F	CGCGCTGCCCTACAACCACA	Sac I	Promoter
	R	TCAAGTCGCCCGGGAAAGCC	Bgl II	
TBE-8+9+10	F	cccgaGCTCTGTCCTGGACGTCTGTTGTG	Sac I	Promoter
	R	cccagaTCTGGTTGCAGGATTCCCCAGAGG	Bgl II	
Intron 2	F	ccccggatccGTGAGTGGCTGATGGGGGAC	Bam HI	Promoter
	R	ccccgtcgacCTGCAAAAGGAGCACAGAGC	Sal I	
Intron 3.1	F	cccggatcCTCAGAGGCAGTGTGCAGAG	Bam HI	Promoter
	R	CCGAGATCTTTCTGAACAATCACAACAGACGTC	Bgl II	
Intron 3.2	F	GTCCTGGACGTCTGTTGTGA	Bgl II	
	R	GTCGCTCACTCCTGAGAAGG	Sal I	
5kb promoter	F	ggggctAGCGAGGTCTCCTCTGGACAAT	Nhe I	Basic
	R	cccgctagCGCACTCCCAGAAAGAAACT	Nhe I	
Gbx2 conserved region				
Gbx2 enhancer	F	TCCTGGAACCCCAGAGC	Kpn I	Promoter (upstream)
	R	TTCTGATCATAATTATTTGATCTGC	Bgl II	
	F	TCCTGGAACCCCAGAGC	Bam HI	Promoter (enhancer)
	R	TTCTGATCATAATTATTTGATCTGC	Sal I	

2.8.2. Transformations

For plasmid subcloning, DH5α chemically competent E. coli cells (Invitrogen) were transformed according to manufacturer's instructions; DH5α cells were aliquoted and stored at -80^{o}C.

For transformation, 1-5ng of plasmid DNA was added to an aliquot of competent cells with gently mixing followed by a 30 minutes incubation on ice. Competent cells were then heat-shocked for 20 seconds in a 42^{o}C water bath and then returned to ice for 2 minutes; pre-warmed sterile LB broth (170mM NaCl, 1% tryptone, 0.5% yeast extract) was then added to the cells to a final volume of 1mL and incubated at 37^{o}C for 60 minutes with gentle agitation (250rpm) to allow cells to recover. Cells were then centrifuged for 5 minutes at 3000g, the supernatant discarded and cells resuspended in 100µl of LB broth; cell suspension was then spread onto pre-warmed agar plates (170mM NaCl, 1% tryptone, 0.5% yeast extract, 1.5% agar, 50µg/mL ampicillin), and incubated overnight (12-18 hours) at 37^{o}C.

2.8.3. DNA Plasmid Preps

For plasmid miniprep, 5mL of LB broth with ampicillin (50µg/mL) were inoculated with an individual colony picked from the agar plate. Inoculated LB broth was the incubated overnight (12-18 hours) at 37^{o}C with agitation (250rpm). Miniprep was performed using the Qiaprep spin miniprep kit (Qiagen), according to the manufacturer's protocol. Plasmid DNA from minipreps was eluted in 30µl of ddH_2O and quantified with a Nanodrop spectrophotometer.

For plasmid midiprep, a starter culture was set up by inoculating 5mL of LB broth with ampicillin (50µg/mL) with a single colony picked from an agar plate and incubated for 8 hours at 37^{o}C with constant agitation (250rpm). After 8 hours, 50mL of LB broth with ampicillin (50µg/mL) were inoculated with 100µl of the starter culture and incubated overnight (12-18 hours) at 37^{o}C with agitation (250rpm).

Midiprep was performed using the plasmid midi kit (Qiagen), according to the manufacturer's protocol. Plasmid DNA from midipreps was eluted in 100µl of ddH_2O and quantified with a Nanodrop spectrophotometer.

2.8.4. Site-directed mutagenesis

Mutation of the TBE-9 site was performed using the QuickChange II XL site-directed mutagenesis kit (Agilent).

Primers introducing the multiple nucleotide changes into TBE-9 (Table 2.5) were designed using the QuickChange Primer Design tool (www.genomics.agilent.com). Three nucleotides were changed (lowercase underlined, Table 2.5) to modify the core sequence of TBE-9.

The mutated sequence was generated by PCR using proof-reading high-fidelity DNA polymerase (Agilent) with the designed primers (Table 2.5) and TBE-8+9+10 construct as template. The parental DNA was digested with Dpn I restriction enzyme, and the mutated DNA was transformed into XL10-gold ultracompetent cells (Agilent) according to manufacturer's protocol. Plasmid DNA from transformed colonies was purified by mini prep and verified by sequencing.

To delete the VP motif from Pax9, primers flanking the VP motif were designed (Table 2.5) with the forward primer binding the 3' end of the motif and the reverse primer binding to the 5' region of the motif, in order to amplify the rest of the Pax9 cDNA except for the flanked region (VP motif).

The mutated DNA was generated by PCR using proof-reading phusion DNA polymerase (Thermo Scientific) using the designed primers and the pcDNA3.1-Pax9 cDNA as a template. The PCR product was resolved in a 1% gel to verify fragment size (Pax9 cDNA minus the VP motif). Resolved DNA was purified using a gel extraction purification kit (Qiagen) and ligated using T4 DNA ligase (Promega), followed by transformation into NEB 5α ultracompetent cells (NEB) according to manufacturer's protocol.

Transformed colonies were initially screened by colony PCR using the primers designed for the deletion (Table 2.5). Plasmid DNA from colonies showing the desired size was extracted by mini-prep and further confirmed by sequencing.

Table 2.5. Primers used for mutagenesis

Target	Oligo	Sequence
TBE-8Δ9+10	F	GAAGCCCCTGTTCATGGGAAA**aaa**TGATATCAGCAGAAATGGGGGCTC
	R	CTTCGGGGACAAGTACCCTTT**ttt**ACTATAGTCGTCTTTACCCCCGAG
VP deletion	F	CGCGCTGCCCTACAACCACA
	R	CGGTGATGGAGCGGATGCCC

2.9. Luciferase Assays

Luciferase assays were performed using the Dual-Luciferase Reporter Assay System (Promega) according to the manufacturer's protocol. Optimal seeding density and concentrations of plasmids for luciferase experiments were optimised and shown in appendix A.

JEG3 cells were plated at a density of 100,000 cells/well in 12-well plates in complete medium one day prior to transfections. The following day, cells were transfected with the DNA mixture containing the specific concentration of each plasmid as specified for each experiment, 20ng/well of a Renilla luciferase expression plasmid (pGL4.70; Promega) as a control reporter for normalisation of transfection efficiency, and XtremeGene9 transfection reagent (Roche) in a 3:1 ratio (µl transfection reagent: µg DNA) in 1x PBS (Life Technologies). 50µl of the transfection mixture was added drop-wise to each well and incubated for 48 hours. Each group was done in triplicate (i.e. 3 wells per group).

After 48 hours, culture medium was removed and cells were washed twice with cold 1x PBS; cells were lysed with 250µl of 1x passive lysis buffer (dual-luciferase reporter assay kit, Promega) and incubated at room temperature for 15 minutes with gentle rocking. Samples were then transferred to individual 1.5mL centrifuge tubes and centrifuged for 3 minutes at 3000g to pellet cell debris.

Firefly and Renilla luciferase were measured using a luminometer (Fluroskan, ThermoFisher); 25µl of each sample were dispensed into an opaque 96 well plate, followed by addition of 100µl of luciferase assay substrate (Promega) and Firefly luciferase was measured immediately. 100µl of Stop and Glo reagent (Promega) were then added to each well and Renilla luciferase was measured. A well containing just passive lysis buffer was measured every time as a blank and the value subtracted from the Firefly and Renilla measurements. Firefly luciferase measurements were then normalised against Renilla measurements for analysis.

A synthetic T-site reporter construct (2xTtkGL2, Zweier et al, 2007) was used in all experiments as a positive control for Tbx1 activity, whereas the same vector without the synthetic T-site (tkGL2) was used as a negative control. Likewise, two groups containing just the empty vectors (pGL3 or pcDNA3.1) were included in all experiments as negative controls.

The concentration of each plasmid was specific for each experiment, but the total DNA concentration (2µg) was matched in all groups with the empty pcDNA3.1 vector.

From the optimisation experiments, the optimal concentrations of reporter and plasmids were: 20ng of Renilla plasmid (pGL4.7), 1µg of 2xTtkGL2 reporter and 25ng (0.25µg) of Tbx1 to give the optimal activation of the 2xTtkGL2 reporter (appendix A).

2.10. Immunocytochemistry

To verify expression of the Tbx1 and Pax9 expression plasmids, immunofluorescence on JEG3 cells was performed as described below.

JEG3 cells were cultured on 300mm dishes and transfected with 5µg of Tbx1, Pax9 or both (total of 10µg) using XtremeGene9 transfection reagent (Roche) in a 3:1 ratio (µl transfection reagent: µg DNA). 48 hours later, culture media was removed and cells were washed once in PBS, and then fixed for 30 minutes at room temperature with ice-cold 4% PFA (in PBS).

Cells were then washed three times for 20 minutes with PBS at room temperature, and then blocked with 2% fetal bovine serum (v/v in PBS) for 30 minutes at room temperature.

Table 2.6. List of primary and secondary antibodies

Primary antibodies		
Antibody	Information	Dilution
Rat anti-Pax9	Abcam, ab28538	IP: 5µg/mL WB: 1µg/mL ICC: 10µg/mL
Rabbit anti-Tbx1	Abcam, ab18530	IP: 5µg/mL WB: 1µg/mL ICC: 1:100
Rabbit anti-Histone H3	Abcam, ab1791	IP: 5µg/mL
Rabbit IgG	Abcam, ab46540	IP: 5µg/mL
Secondary antibodies		
Anti-rat IgG-HRP	Jackson,1 12-036-003	WB: 1:20000
Anti-rabbit IgG-HRP	DAKO, P0448	WB: 1:2000
Anti-rat IgG Alexa Fluor 488	Life Technologies, A21208	ICC: 1:200
Anti-rabbit IgG Alexa Fluor 594	Life Technologies, A21207	ICC: 1:200

Blocking solution was removed and cells were incubated with primary antibody at the appropriate dilution (Table 2.6) in 0.1% Triton X-100 in PBS overnight at 4^{o}C.

Cells were then washed four times for 20 minutes in PBS at room temperature, and then incubated with the respective secondary antibody (Table 2.6) diluted 1:200 in PBS for 2 hours in the dark at room temperature.

Cells were then washed four times for 20 minutes with PBS at room temperature in the dark, and finally mounted with 5 drops of Vectashield plus DAPI and a round coverslip.

Dishes were let dry overnight and the edges were sealed with nail polish and the rims removed. Images were taken using a Fluorescence microscope (Zeiss Axioimager).

2.11. Chromatin Immunoprecipitation (ChIP)

2.11.1 ChIP From Embryos

For chromatin immunoprecipitation of the potential TBEs within the *Pax9* locus (section 5.2), nine E9.5 wild-type embryos were collected and pooled for each IP; while nine (E8.5), eight (E9.5) and twelve (E10.5) embryos were pooled for each IP of the *Gbx2* locus (section 5.4).

Wild-type embryos were collected and homogenised in ice-cold PBS containing protease inhibitors (Sigma); homogenised tissue samples were fixed in 1% formaldehyde and then neutralized in 125mM glycine. Tissue samples were then centrifuged for 1 minute at 3000g and washed twice in PBS; samples were then lysed in RIPA buffer (radioimmunoprecipitation assay buffer; 50mM Tris, 150mM NaCl, 0.1% SDS, 0.5% sodium deoxycholate, 1% Triton X) containing protease inhibitors, and chromatin was sonicated into 200–600bp long fragments. Sonication into the right size was assessed by electrophoresis in a 1% agarose gel.

The sonicated chromatin was divided equally into the number of samples required for each immunoprecipitation and controls (i.e Input, p-HH3, Tbx1, IgG, no antibody); the Input aliquot was stored at -20^{o}C until used, while the remaining samples were diluted 1:10 in RIPA buffer.
Diluted samples were pre-cleared with 20µl of pre-absorbed protein A/G sepharose beads (Sigma) for 1 hour rotating at room temperature.

Pre-cleared samples were then incubated with the respective primary antibody (Table 2.6), except for the 'no antibody/beads-only' sample; 20µl of pre-absorbed protein A/G sepharose beads was added to all samples and these were incubated overnight with rotation at 4^{o}C.

Samples were extensively washed as follows: samples were centrifuged for 1 minute at 3000g, the supernatant removed and samples were resuspended in wash buffer (20mM Tris-HCl pH 8.0, 150mM NaCl, 2mM EDTA, 1% Triton-X100, 0.1% SDS); the procedure was repeated six times, leaving samples in the final wash overnight at 4^{o}C with rotation.

Samples were washed one last time with LiCl buffer (0.25M LiCl, 10mM Tris-HCl pH 8.0, 1mM EDTA, 1% NP-40, 1% sodium deoxycholate). The immunocomplexes were then eluted in 120µl of elution buffer (100mM $NaHCO_3$, 1% SDS) and incubated for 15 minutes at 30^{o}C with rotation.

Cross-linking of the Input and immunoprecipitated DNA samples was reversed at 65°C for 4 hours with shaking, followed by treatment with 20mg/mL of proteinase K and 10mg/mL of RNAse A at 45°C for 1 hour.

The DNA was subsequently purified using the QIAquick PCR purification kit (Qiagen), and equal volumes of all samples were analysed by qPCR using SYBR Green JumpStart Taq ReadyMix (Sigma) and specific primers targeting the regions of interest (Table 2.7).

A sample incubated with an anti-IgG antibody was used as an isotype negative control for the immunoprecipitation, and a sample incubated only with the protein A/G beads and no primary antibody was also used as a negative control.

For qPCR, each sample was run in triplicate, and a Ct average value was obtained from the replicates; samples were then normalised with the Input sample and represented as a percentage of input (which was set as a 100% of total chromatin).

A sample containing genomic DNA (gDNA) was used as a positive control for the qPCR, whereas a sample with no DNA and only water was used as a negative control.

Table 2.7. List of primers used for ChIP

Target Gene	Primer Name	Sequence
Pax9	TBE-1-F	TGTCAGCTCGCCAGAACATCAGA
	TBE-1-R	GCAGGGTTGAGACAACAGCCCC
	TBE-2-F	ACGCAATCATACCATAGGAGGCTCA
	TBE-2-R	CCCGGGAAATTGCCGTGACC
	TBE-3-F	CGCCTTCAAAGCGGGAGGGG
	TBE-3-R	CCGATCAGCCGGGGTTGGTT
	TBE-4-F	CTGCCCGGTGCCAAGTGTGT
	TBE-4-R	TGGGGCGACCCCTTCTCTGG
	TBE-5-F	AAGAGGGCCGTGGCATTGGC
	TBE-5-R	CCCCTCCCTTCTGCGGGGTT
	TBE-6-F	CGGAGTGGGTTCCTGCACGC
	TBE-6-R	AGGCTGGAGACTGTGTGTGGCA
	TBE-7-F	GCAGCTACGAGTCCCCGCAC
	TBE-7-R	AGACCGAGACCTCCGTTTCCGA
	TBE-8+9+10-F	ACCTTAGTTGGAGACGTTGCCCT
	TBE-8+9+10-R	ACAAAAGGCAGTCGGTGGGC
	MusChr12C1-F	TGGGAAAGACAAGAGGATGC
	MusChr12C1-F	CTTGGAAAACTCCACCCTCA
Gbx2	Gbx2_T5b-F	GAGCTAGCCTCGGGCACTAT
	Gbx2_T5b-R	GTCTCCAAGGCCAAGAACTG
	Gbx2_T5c-F	TGGTGTGTCTGATGGGGAAT
	Gbx2_T5c-R	TCTTGCTCCTGGCCATAGTT
	Gbx2_T5d-F	TGGGTATCCCACAGACACCT
	Gbx2_T5d-R	TGTTGCATCCCTTCACTTCA
	Gbx2_T5e-F	GATGGAGCAGATAAAAGACTCG
	Gbx2_T5e-R	GACATTCTTAATCATCGCACCT
	Gbx2_P9-F	CCAAGGCCCTGGAGACAG
	Gbx2_P9-R	TTCTCTCTGCCTGTGATGTGA
	Gbx2_T5f-F	GCTGATTAATGAGACCCACGA
	Gbx2_T5f-R	TTTGAAGCTCAGACAAGTTGC
	Gbx2_P5-F	CTCTGGCCTGAGATGCTGTT
	Gbx2_P5-R	CCGGTCTGTGCACTTCTGAT
Synthetic T-site	2xTt-F1	TGTAACTGAGCTAACATAACCCGGGAA
	2xTt-R2	TGACGCGTGTGGCCTCGAAC

For ChIP-western blot (section 5.4), a 20µl aliquot was taken from the samples incubated with Tbx1 and Pax9 antibodies after immunoprecipitation and prior reversing the cross-linking. Samples were then incubated with 20µl of 2x SDS-PAGE buffer (2% SDS, 5% β-mercaptoethanol, 10% glycerol, 0.05% bromophenol blue, 62.5mM Tris pH 6.8) at 95^{o}C for 30 minutes, followed by centrifugation at 14,000g for 5 minutes. Supernatants were then used for western blot as described below (section 2.13).

2.11.2 ChIP From MEFs

For chromatin immunoprecipitation from MEFs, two confluent T75 flasks were used; formaldehyde was added drop-wise to each flask to a final concentration of 1%, and incubated at room temperature for 10 minutes. Glycine was then added to a final concentration of 125mM and incubated for further 5 minutes at room temperature; cells were then rinsed twice with cold PBS, scraped thoroughly with a cell scraper and transferred into a 50mL centrifuge tube. Cells were centrifuged at 1000g for 5 minutes; supernatant was discarded and cells were resuspended in 750µl of RIPA buffer and incubated for 10 minutes on ice. Chromatin was then sonicated and samples treated as previously described for IP.

2.11.3 2xTtkGL2 ChIP From JEG3 Cells

To determine binding of Tbx1 to the 2xTtkGL2 reporter (section 5.3), JEG3 cells were cultured on 6-well plates; when 80% confluency was reached, cells were transfected with 1µg of 2xTtkGL2 construct, 0.25µg of Tbx1-expressing vector and increasing concentrations (0, 0.01, 0.05, 0.1, 0.25 and 0.5µg) of Pax9-expressing plasmid using XtremeGene9 transfection reagent (Roche) in a 3:1 ratio (µl transfection reagent: µg DNA). Each group was done in triplicate (i.e. 3 wells per group); after 24 hours post transfection, formaldehyde was added drop-wise to each flask to a final concentration of 1%, and incubated at room temperature for 10 minutes. Glycine was then added to a final concentration of 125mM and incubated for a further 5 minutes at room temperature; cells were then rinsed twice with cold PBS.

Cells were scraped thoroughly from the wells with a cell scraper and triplicates were pooled into 50mL centrifuge tubes. Cells were centrifuged at 1000g for 5 minutes; supernatant was discarded and cells were resuspended in 500µl of RIPA buffer and incubated for 10 minutes on ice. DNA was then briefly sonicated and samples treated as previously described for IP using an anti-Tbx1 antibody, an IgG and a 'no antibody' sample. No anti-Histone H3 antibody was used as the target DNA was from a plasmid and not from the chromatin. A PCR from the pure plasmid was used as a positive control for PCR, while a PCR from genomic DNA was used as a negative control.

ChIP for the 2xTtkGL2 reporter was assessed by end-point PCR, using specific primers (Table 2.7) targeting the 2xT site.

2.12. Co-Immunoprecipitation

Co-immunoprecipitation was used to detect a physical interaction between Pax9 and Tbx1 *in vivo*; for this purpose, E9.5 wild-type embryos were collected and pooled in ice-cold PBS with protease inhibitors.
Pooled embryos were homogenised in 250µl of cold RIPA buffer with protease inhibitors and incubated with constant agitation for 2 hours at 4^{o}C.

The lysed sample was then centrifuged for 20 minutes at 14,000g at 4^{o}C to remove cell debris; supernatant was transferred into a fresh tube and kept on ice, the pellet was discarded.

The lysate was pre-cleared with 5% normal serum for 1 hour on ice, followed by addition of 100µl of protein A/G beads and incubation for 30 minutes at 4^{o}C with gentle agitation.

Lysate was then centrifuged at 14,000g for 10 minutes at 4^{o}C; the pellet was discarded and supernatant used for immunoprecipitation. The lysate was divided equally in two aliquots for IP with anti-Tbx1 and anti-Pax9 antibodies.

Each sample was then incubated with 50µl of protein A/G and 5µg of the respective antibody (Table 2.6) overnight at 4^{o}C on a rotating wheel.

Samples were then centrifuged at 10,000g for 5 minutes at 4^{o}C; supernatants were discarded and samples were washed five times with cold RIPA buffer. After the final wash, supernatant was discarded and 50µl of 2x SDS-PAGE buffer was added to each sample.

Diluted samples were denatured at 95^{o}C for 5 minutes, followed by centrifugation at 14,000g for 5 minutes; supernatants were used for Western blotting as described below.

For co-immunoprecipitation from JEG3 cells, cells were cultured in a 6-well plate; when 80% confluency was reached, cells were transfected with 5µg of Tbx1-expressing vector and 5µg of Pax9-expressing plasmid using XtremeGene9 transfection reagent (Roche) in a 3:1 ratio (µl transfection reagent: µg DNA) and incubated for 24 hours.

Cells were then washed twice with cold PBS, and 100µl of RIPA buffer with protease inhibitors was added to each well; all wells were pooled and RIPA buffer was added to a total of 1mL. Lysed cells were incubated for 30 minutes at 4^{o}C in a rotating wheel.

The sample was then centrifuged at 10,000g for 5 minutes at 4^{o}C; supernatant was transferred into a fresh tube and kept on ice.

Lysate was then pre-cleared and immunoprecipitated as described above using antibodies for Tbx1 and Pax9 (Table 2.6). Immunoprecipitated samples were then used for Western blot as next described.

2.13. Western Blot

Samples from IP or ChIP were diluted in 2x SDS-PAGE buffer and denatured at 95^{o}C for 5 minutes as previously mentioned prior to polyacrylamide electrophoresis. 10 µl of each sample were loaded into 10% Tris/glycine pre-cast gels (Bio-rad) along with a pre-stained protein ladder (Thermo Scientific).

Gels were run in 1x running buffer (25mM Tris pH8.0, 190mM glycine, 0.1% SDS) for 45 minutes at 180V. Resolved samples were then transferred into polyvinyl difluoride (PVDF) membranes for immunoblotting.

PVDF membranes were activated prior to transfer; to activate them, membranes were immersed in 100% methanol for 30 seconds, rinsed in dH_2O for 5 minutes and equilibrated in ice-cold transfer buffer (48mM Tris, 39mM glycine, 0.04% SDS, 20% methanol) for 20 minutes.

The resolved gels and activated membranes were stacked together in-between two sheets of blotting paper and sponge on either side. The samples were wet-transferred for 1 hour at 100V in cold transfer buffer; transfer was performed in a cold room, maintaining gentle agitation of the transfer buffer inside the tank using a magnetic stirrer.

After transfer, membranes were blocked in 5% (w/v) skimmed-milk in TBST (50mM Tris pH7.0, 150mM NaCl, 0.05% Tween-20) for 1 hour with gentle agitation. Blocking solution was then replaced with the corresponding primary antibody at the appropriate dilution (Table 2.6); primary antibody was diluted in 5% milk/TBST and incubated overnight at 4^oC with constant agitation.

The primary antibody was then removed and membranes were washed four times in 5% milk/TBST for 10 minutes. Membranes where then incubated with the corresponding horseradish peroxidase (HRP) linked-secondary antibody (Table 2.6) diluted (1:20,000) in 5% milk/TBST for 1 hour at room temperature with gentle agitation. Membranes were then washed four times in 5% milk/TBST for 10 minutes, followed by four washes in TBST for 10 minutes prior to development.

Immunocomplexes were detected by chemiluminescence using the Supersignal West Dura substrate (Thermo Scientific); solutions A and B were mixed (1:1), and added to the membrane and incubated for 5 minutes. Excess substrate was drained, and the membrane wrapped in a plastic sheet; membranes were exposed to an X-ray film sheet (Amersham Hyperfilm, GE Healthcare), and exposed film was developed in an automated Film developer (Konica Minolta).

2.14. Quantitative PCR

Expression of Pax9 and Tbx1 mRNA in double heterozygous was analysed by quantitative PCR. Complementary DNA (cDNA) samples from wild-type, *Pax9*$^{+/-}$, *Tbx1*$^{+/-}$ and double heterozygous embryos was previously generated in the lab from the dissected pharyngeal region of E9.5 embryos; six samples of each genotype were used for qPCR, and each sample was done in triplicate.

qPCR was performed using SYBR Green Taq ready mix (Sigma) in a mix containing 1x SYBR green mix, 1x internal reference dye (Rox), 1mM of each primer and 2µl of diluted cDNA (1:10). Samples were loaded into a 384-well plate sealed with optical adhesive film; the plate was run on a 7900HT Real-time PCR system (Applied Biosystems) under a standard thermo-cycling program: an initial denaturation step of 95^{o}C for 15 minutes, followed by 39 cycles of a denaturation step of 95^{o}C for 30 seconds, an annealing stage at 60^{o}C for 30 seconds, an elongation step of 72^{o}C for 30 seconds, and a data collection point of 79.5^{o}C for 10 seconds at the end of each cycle; followed by a final data collection ramp from 68^{o}C to 99^{o}C.

Specific primers targeting Pax9 and Tbx1 mRNA (Table 2.8) were used for qPCR, along with primers targeting GAPDH as a housekeeping gene for relative quantification analysis.

Relative gene expression was analysed by the comparative Ct method (ΔCt; Schmittgen and Livak, 2008). In qPCR, a product is detected by accumulation of a fluorescent signal; the Ct (cycle threshold) value is the number of cycles required for the fluorescent signal to pass the threshold of background signal, Ct values are therefore inversely proportional to the amount of target RNA.

For relative quantification, the average Ct value of triplicates is calculated for all samples; the average Ct of the target gene is then normalised to the housekeeping (GAPDH) average Ct value (Ct target gene – Ct GAPDH).

Based on the assumption of a 100% efficiency of the PCR reaction to produce 2 copies of each gene at each cycle, the ΔCt of each sample is calculated by 2 raised to the power of the negative normalised Ct value.

$$\Lambda Ct = 2^{-(Ct\ target\ gene - Ct\ housekeeping\ gene)}$$

The average ΔCt of the six samples of each genotype was calculated; the average ΔCt of *Tbx1*$^{+/-}$, *Pax9*$^{+/-}$ and double heterozygous samples was then normalised to the wild-type ΔCt of each gene (ΔCt mutant/ΔCt wild-type) and this change was plotted as the fold change over the wild-type relative expression.

Table 2.8. List of primers used in qPCR

Target Gene	Primer name	Sequence
GAPDH	Gapdh-f	TGTGCAGTGCCAGCCTCGTC
	Gapdh-r	TGACCAGGCGCCCAATACGG
Pax9	Pax9-F	GGGCCGGGTTGGTGTACTGC
	Pax9-R	GGTCGGATGCCCAGTTGGGC
Tbx1	Tbx1-F	AGGCGGAAGGAAGTGGTATT
	Tbx1-R	CTCGGTCGTCTACACTGCAA

2.15. Statistics

Statistical differences between the incidences of cardiovascular defects among different genotypes were calculated using the one tailed Fisher's exact test. Statistical significance in luciferase assays and qPCR was calculated using a two-paired T-test.

Statistical significance was considered when p-value<0.05.

Chapter 3. *Tbx1*- And *Pax9*-null Phenotypes

3.1. Introduction

Tbx1 mutant mice have been thoroughly studied and are considered a model of 22q11 deletion syndrome. *Tbx1* knockout mice have severe cardiovascular defects, mostly persistent truncus arteriosus, and pups die soon after birth due to cardiovascular and respiratory insufficiency (Lindsay et al, 2001; Jerome and Papaioannou, 2001). However, *Tbx1* heterozygous mice present with 4th PAA-derived defects although their incidence varies greatly as seen in different previously published studies, as summarized in Table 3.1.

Table 3.1. Summary of reported incidences of cardiovascular defects in *Tbx1* heterozygotes at late embryogenesis.

Age	n	Abnormal (%)	IAA-B	ARSA	C-AoA	Reference
E18.5	41	11 (26.8%)	3 (7.3%)	6 (14.6%)	2 (4.8%)	Vitelli et al, 2002
E17.5	5	0 (0%)	0 (0%)	0 (0%)	0 (0%)	Aggarwal et al, 2006
E16.5	18	6 (33.3%)	0 (0%)	4 (22.2%)	1 (5.5%)	Guris et al, 2006
E18.5	29	11 (37.9%)	1 (3.4%)	8 (27.5%)	NR	Zhang et al, 2008
E15.5	19	5 (26.3%)	2 (10.5%)	2 (10.5%)	NR	Calmont et al, 2009
E14.5	25	6 (24%)	1 (4%)	4 (16%)	1 (4%)	Randall et al, 2009
E14.5 - E18.5	36	9 (25%)	1 (2.7%)	4 (11.1%)	4 (11.1%)	Ryckebush et al, 2010
E15.5	17	5 (29%)	2 (11.7%)	3 (17.5%)	0 (0%)	Papangeli and Scambler, 2013

NR, Not reported

Tbx1 haploinsufficiency mainly affects the 4th PAAs either unilaterally or bilaterally. The proportion of affected *Tbx1*$^{+/-}$ embryos at mid embryogenesis (Table 3.2) is higher than the incidence of 4th PAA-derived defects seen at late embryogenesis (Table 3.1). The lower incidence seen at later stages is considered to be due to some form of recovery occurring during the remodeling process (between E11.5 and E13.5), where hypoplastic vessels may be able to recover and develop normally (Lindsay and Baldini, 2001; Calmont et al, 2009; Papangeli and Scambler, 2012).

Table 3.2. Summary of reported 4th PAAs abnormalities in *Tbx1* heterozygotes at mid embryogenesis

Age	n	Abnormal (%)	Unilateral defects	Bilateral defects	Reference
E10.5	48	48 (100%)	NR	NR	Lindsay and Baldini, 2001
E10.5	11	5 (46%)	3	2	Calmont et al, 2009
E10.5	14	9 (64%)	6	3	Randall et al, 2009
E10.5	17	14 (82%)	6	8	Ryckebush et al, 2010
E10.5	29	21 (71%)	15	6	Papangeli and Scambler, 2013
E11.5	23	22 (95%)	NR	NR	Caprio and Baldini, 2014

NR, not reported

In order to establish a baseline of the penetrance of *Tbx1* heterozygous defects for further analysis in the context of *Pax9* heterozygosity, as well as to compare the penetrance of our study with previous reports, *Tbx1* heterozygous embryos were analysed by MRI and hematoxylin and eosin (H&E) staining at E15.5, and by intracardiac ink injections at E10.5.

3.2. *Tbx1* Mouse Phenotype

3.2.1. Cardiovascular Phenotype Of Tbx1 Mutant Embryos

Tbx1 mice were bred by intercrossing *Tbx1*$^{+/-}$ mice; no *Tbx1*-null mice were found alive after weaning, concordant with perinatal lethality previously reported (Lindsay et al, 2001; Jerome and Papaioannou, 2001).

Tbx1 heterozygous embryos from double heterozygous (*Pax9*$^{+/-}$ with *Tbx1*$^{+/-}$) crosses were collected at E15.5 and analysed by MRI and histology to determine the penetrance of *Tbx1* haploinsufficiency defects to set the basis for future analysis of double heterozygotes. As seen in Table 3.3 and Figure 3.1, *Tbx1* heterozygosity leads to various cardiovascular defects including VSD, ARSA, IAA-B, coRSA, coAA (Figure 3.1b).

The penetrance of each of these defects is summarised in Table 3.3. Only 1 (5%) *Tbx1*$^{+/-}$ embryo had an interrupted aortic arch type B (IAA-B) and ventricular septal defect (VSD), 2 (10%) *Tbx1*$^{+/-}$ embryos had a cervical aortic arch (coAA), 5 (26%) *Tbx1*$^{+/-}$ embryos had a cervical right subclavian artery (coRSA), and 7 out of 19 (36%) presented with a retro-esophageal right subclavian artery (ARSA, Figure 3.1b).

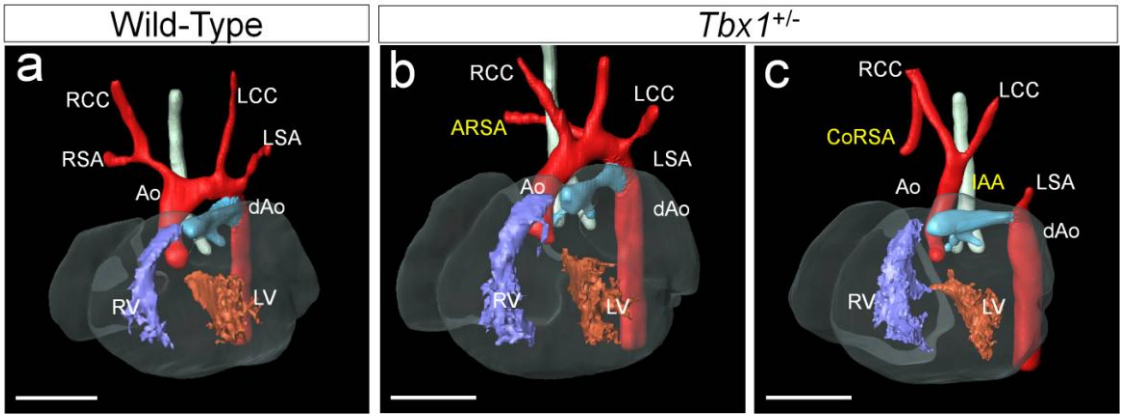

Figure 3.1. Cardiovascular phenotype of E15.5 *Tbx1* heterozygous embryos.
(a) Wild-Type embryos present with normal branching of the great arteries, whereas **(b, c)** *Tbx1* heterozygous embryos (*Tbx1*$^{+/-}$) present with some cardiovascular defects including anomalous retro-esophageal right subclavian artery (ARSA), cervical right subclavian artery (CoRSA). Ao, aorta; dAo, dorsal aorta; RV, right ventricle; LV, left ventricle; RSA, right subclavian artery; RCC, right common carotid artery; LSA, left subclavian artery; LCC, left common carotid artery; ARSA, anomalous retro-esophageal right subclavian artery. Scale 500µm.

Table 3.3. Incidence of cardiovascular defects in E15.5 *Tbx1* heterozygous embryos.

Genotype	n	VSD	Cervical Ao	IAA	Cervical RSA	ARSA
Wild-Type	16	0	0	0	0	0
***Tbx1*$^{+/-}$**	19	1 (5.3%)	2 (10.5%)	1 (5.3%)	5* (26.3%)	7* (36.8%)

Fisher's exact test, *p<0.05

It is well known that *Tbx1* haploinsufficiency mostly affects the development of the pharyngeal arch arteries causing the PAA-derived defects previously discussed.

Therefore, the development of the PAAs in *Tbx1*$^{+/-}$ embryos was analysed by intracardiac ink injection to visualise the patterning of the PAAs at E10.5.

3.2.2 Development Of The Pharyngeal Arch Arteries In Tbx1 Mutant Embryos

Tbx1$^{+/-}$ embryos present defects mostly derived from abnormal development of the PAAs as described before (Figure 3.1). To analyse the patterning of the PAAs in *Tbx1*$^{+/-}$ embryos India ink was injected directly into the beating left ventricle to be pumped into the PAAs to visualise their patency.

As seen in Figure 3.2, all *Tbx1*$^{+/-}$ embryos present abnormal patterning of the 4th PAAs, which can be a hypoplastic or a completely absent vessel either unilateral or bilaterally (Figure 3.2b, Table 3.4). Four out of eight (50%) *Tbx1*$^{+/-}$ embryos have bilaterally abnormal 4th PAAs (Table 3.4), mainly showing a hypoplastic artery (Figure 3.2b).

As can be seen in Table 3.4, the incidence of abnormal *Tbx1*$^{+/-}$ embryos (100%) is much higher compared to the incidence of defects seen at E15.5 (Table 3.3), which can be explained by the proposed recovery during the remodelling process (Calmont et al, 2009; Papangeli and Scambler, 2012).

Interestingly, we also found that 9 out of 19 (50%) of *Tbx1* heterozygous adult mice have an ARSA (Figure 3.3), which did not appear to affect their viability, and correlates with the incidence of non-patent 4th right PAA at mid embryogenesis (Table 3.4).

The incidence of 4th PAA-derived defects in *Tbx1* heterozygous mice varies among different studies as discussed before; similarly, the incidence and severity of cardiovascular defects in human patients with 22q11DS varies among individuals, suggesting such cardiovascular defects are not monogenic due to only *Tbx1* loss but a result in the disruption of other genes or pathways that modify the phenotype.

In this context, several reports have studied potential genetic interactions between *Tbx1* and other genes involved in cardiovascular development as discussed in section 1.5 (reviewed in Scambler, 2010).

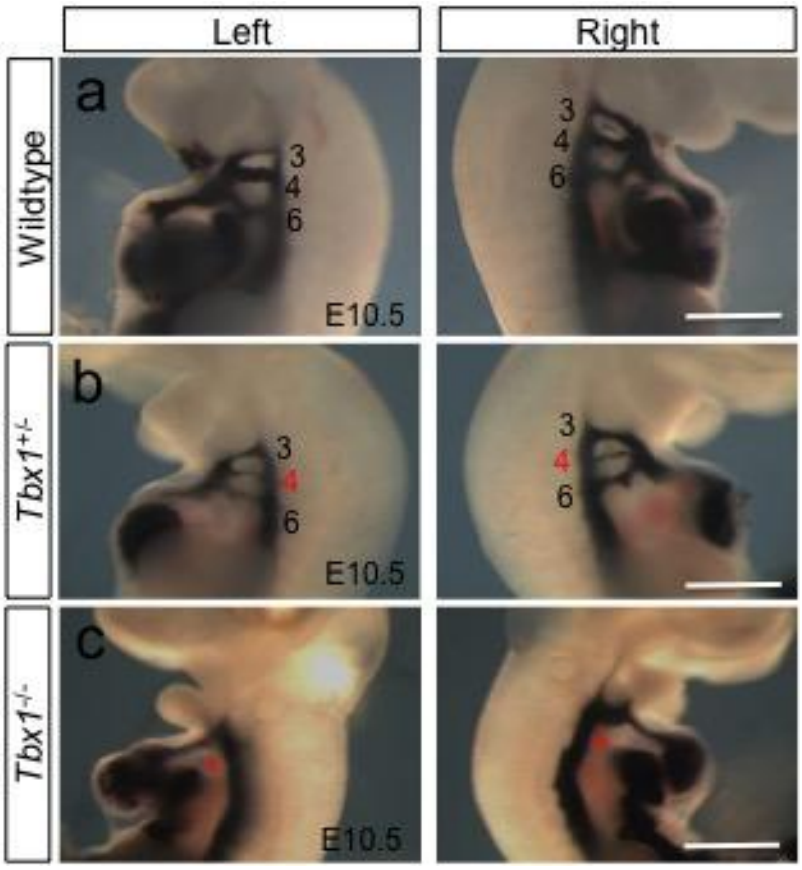

Figure 3.2. Pharyngeal arch artery defects in *Tbx1* mutant embryos.
Patterning of the pharyngeal arch arteries at E10.5 was visualised by intracardiac injection of India ink. **(a)** Wild-type embryos present normal patterning of the 3rd, 4th and 6th PAAs on both sides, whereas *Tbx1*$^{+/-}$ embryos **(b)** present abnormal 4th PAAs on both sides, mainly displaying hypoplastic vessels. *Tbx1*$^{-/-}$ embryos **(c)** present a more severe phenotype with no caudal pharyngeal arches being formed (red asterisk), showing only formation of the 1st and 2nd PA; consequently, the PAAs are not formed and a single vessel connects the aortic sac with the paired dorsal aortas on both sides. Scale 500μm.

Table 3.4. Incidence of 4th PAA abnormalities in E10.5 *Tbx1* heterozygous embryos.

Genotype	n	Abnormal (%)	Bilateral defects	Bilateral defects		
				Hypo/Hypo	Hypo/NP	NP/NP
Wild-type	6	0	0	-	-	-
Tbx1$^{+/-}$	8	8* (100%)	4* (50%)	3	1	-

Fisher's exact test, *p<0.001

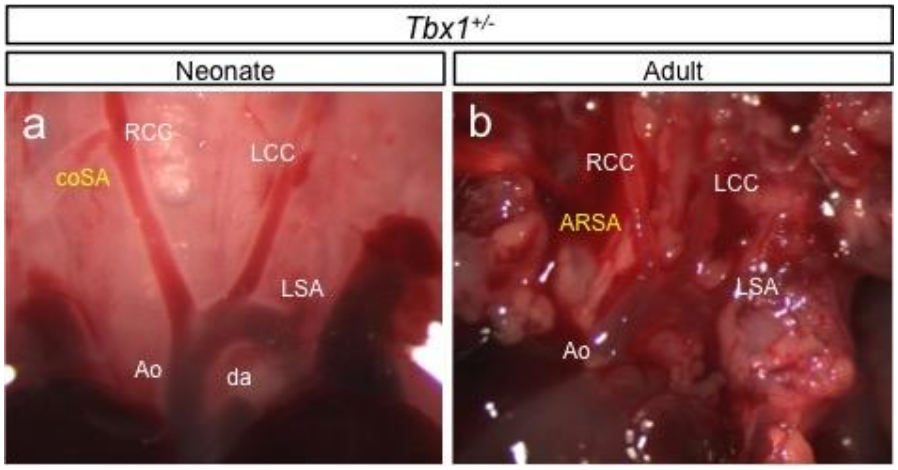

Figure 3.3. Great artery defects in neonate and adult *Tbx1* heterozygous mice.
Neonate **(a)** and adult **(b)** *Tbx1* heterozygous mice were dissected to visualise the heart and great arteries, revealing 4th PAA-derived defects, with some mice presenting a right subclavian with cervical origin (coRSA), and many presenting a retro-esophageal right subclavian artery (ARSA). Ao, aorta; RCC, right common carotid; LCC, left common carotid; LSA, left subclavian artery; da, ductus arteriosus; coRSA, cervical origin of the right subclavian; ARSA, anomalous retro-esophageal right subclavian artery.

Epistasis between *Tbx1* and other genes such as *Vegf* (Stalmans et al, 2003), *Crkl* (Guris et al, 2006), *Cdh7* (Randall et al, 2009), *Aldh1a2* (Ryckebusch et al, 2010), or direct downregulation of *Tbx1* target genes including *Fgf8* (Vitelli et al, 2002), *Gbx2* (Calmont et al, 2009; Caprio and Baldini, 2014) and *Wnt5a* (Chen et al, 2012) have been shown to modify the *Tbx1*$^{+/-}$ phenotype (reviewed in Aggarwal and Morrow, 2008).

However, more than 200 genes have been found affected by homozygous deletion of *Tbx1* (Ivins et al, 2005; Liao et al, 2008), that could potentially be involved in cardiovascular development and modify the *Tbx1* phenotype. Among those affected genes, *Pax9* is found significantly downregulated in *Tbx1*-null embryos at E8.5, E8.75 and E9.5 (Ivins et al, 2005; Liao et al, 2008).

3.2.3 Pax9 Is Downregulated In Tbx1 Knockout Embryos

Microarray analysis of *Tbx1*-null embryos revealed *Pax9* to be significantly down-regulated, and it was further confirmed by *in situ* hybridisation and qPCR, showing about a 50% reduction of *Pax9* expression in *Tbx1*-null embryos (Ivins et al, 2005; Liao et al, 2008). To confirm this *Pax9* reduction in our model, *Tbx1*-null, heterozygous and wild-type embryos were collected at E9.5 and *in situ* hybridisation was performed using a probe against *Pax9* mRNA.

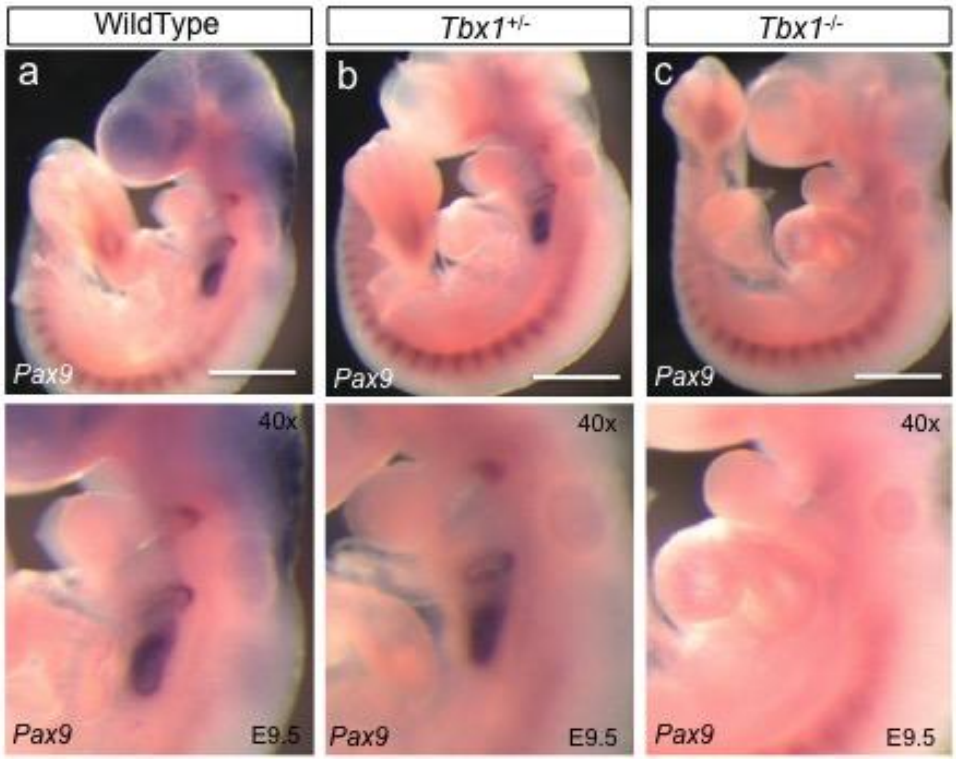

Figure 3.4. *Pax9* mRNA expression is reduced in *Tbx1*-null embryos
Whole-mount in situ hybridisation using a *Pax9* riboprobe shows an obvious decrease of *Pax9* expression within the pharyngeal region of *Tbx1*-null embryos **(c)** compared to wild-type **(a)** and *Tbx1*$^{+/-}$ embryos **(b)** at E9.5. Scale bar 500µm.

As seen in Figure 3.4, *Pax9* expression does not seem to be qualitatively affected by *Tbx1* haploinsufficiency (Figure 3.4b) as compared to wild-type embryos (Figure 3.4a), whereas *Tbx1*-null embryos show a significant reduction in *Pax9* expression (Figure 3.4c), concordant with what has been previously reported by Ivins et al (2005).

3.3 *Pax9* mouse

Expression of *Pax9* is significantly down-regulated in *Tbx1*-null embryos as previously mentioned, suggesting *Pax9* could be a down-stream target of Tbx1. Additionally, both Pax9 and Tbx1 are co-expressed at E9.5 and E10.5 within the pharyngeal endoderm (Figure 3.5).

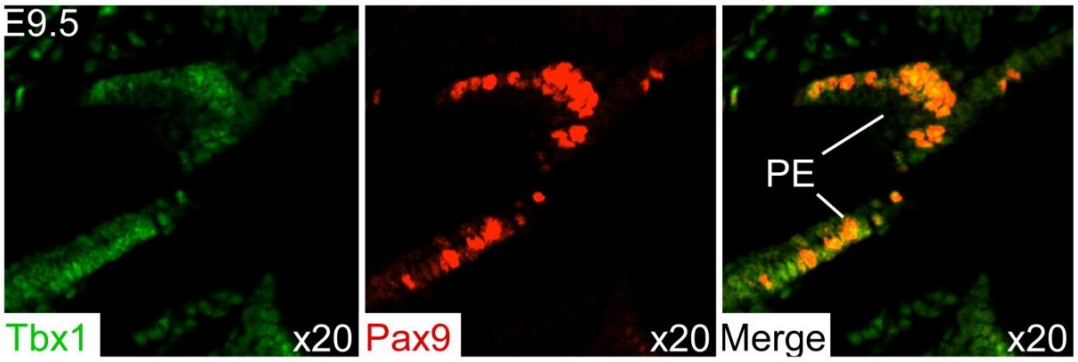

Figure 3.5. *Pax9* and *Tbx1* are co-localised within the pharyngeal endoderm.
Fluorescence double immunohistochemistry staining for *Tbx1* (green) and *Pax9* (red) on coronal sections from wild-type E9.5 embryos shows both proteins co-localise within cells in the pharyngeal endoderm (pe). Representative picture showing co-localization within the pharyngeal endoderm in the 3rd pouch. Image provided by Kathleen Allison.

Both *Pax9* and *Tbx1* knockout embryos present with abnormal development of the thymus, parathyroids and with craniofacial defects (Peters et al, 1998; Lindsay et al, 2001; Jerome and Papaioannou, 2001), showing some overlap between both knockout phenotypes. This overlapping of phenotypes, as a phenocopy, is suggestive of a genetic interaction or a common genetic pathway (Aggarwal and Morrow, 2008) between *Tbx1* and *Pax9*.

Although the craniofacial and skeletal defects, along with abnormal development of pharyngeal arch-derived glands in *Pax9* knockout embryos has been reported (Peters et al 1998; Kist et al, 2005), cardiovascular development has not been investigated in *Pax9*-null embryos.

Preliminary results from our group indicate that *Pax9* knockout embryos have some cardiovascular defects (Figure 3.6, Simon Bamforth unpublished data). In this context, E14.5 *Pax9*-null embryos were analysed by hematoxylin and eosin (H&E) staining. As seen in Figure 3.6, *Pax9*$^{-/-}$ embryos present DORV, IAA-B and ARSA (Figure 3.5e-h).

Therefore, the second aim of this chapter was to analyse the development of the heart and great arteries in *Pax9*-null embryos in detail, by MRI and H&E staining at E15.5.

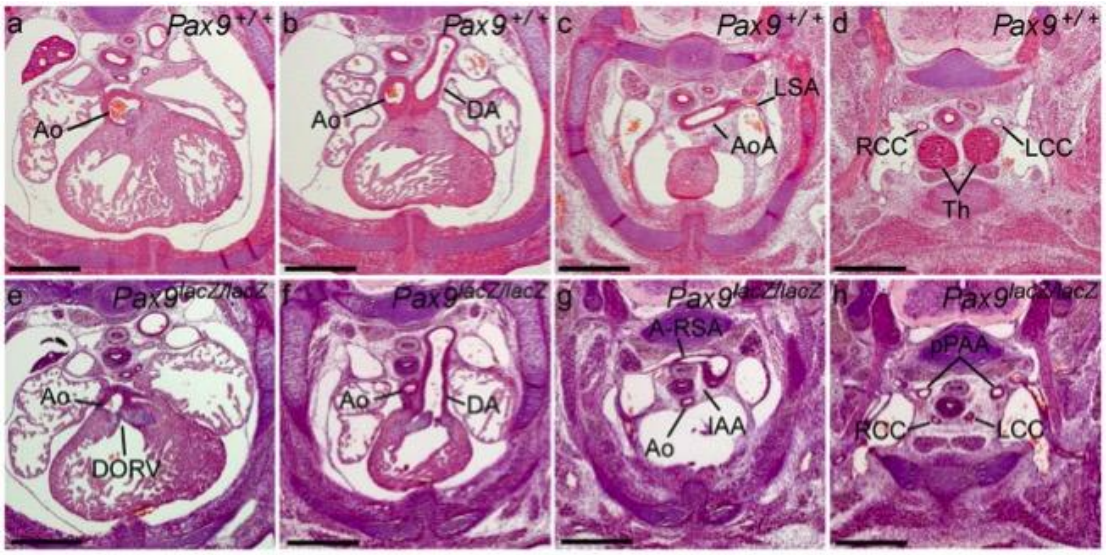

Figure 3.6. *Pax9*-null embryos present many cardiovascular defects at E14.5.
Histological analysis of E14.5 embryos revealed defects within the heart of *Pax9*-null embryos (**e-h**), including double outlet right ventricle (DORV) with the aorta ascending from the right ventricle **(e)**; *Pax9*-null embryos also present with interruption of the aortic arch (IAA) (**g**), retro-esophageal right subclavian artery (ARSA) (g), and abnormal origin of the carotid arteries (h). Additionally, the thymus is not apparent in *Pax9*-null embryos compared to wild-type embryos where the thymus (Th) is clearly visible **(d)**. Ao, aorta; DA, ductus arteriosus; AoA, aortic arch; LSA, left subclavian artery; RCC, right common carotid; LCC, left common carotid; Th, thymus; DORV, double outlet right ventricle; IAA, interruption of the aortic arch; A-RSA, anomalous retro-esophageal right subclavian artery. Scale bar, 100μm. (Simon Bamforth, unpublished data).

3.3.1. Cardiovascular phenotype of E15.5 Pax9-mutant *embryos*

Pax9-null embryos were generated by intercrossing $Pax9^{+/-}$ mice; embryos were collected at E15.5 and imaged by MRI (Section 2.3) and 3D models of the heart and great arteries were reconstructed from the data sets using Amira software (Visage Imaging). Wild-type (n=2), $Pax9^{+/-}$ (n=2) and $Pax9^{-/-}$ (n=4) embryos were analysed by MRI and subsequently embedded in wax, sectioned and stained with haematoxylin and eosin for detailed histological analysis.

Externally *Pax9*-null embryos are indistinguishable from Wild-type and heterozygous embryos (Figure 3.7), except for an extra limb digit seen in *Pax9* knockout embryos (not shown), as previously described (Peters et al, 1998). Additionally, all *Pax9* knockout embryos have cleft palate and ectopically placed hypoplastic thymus (Peters et al, 1998).

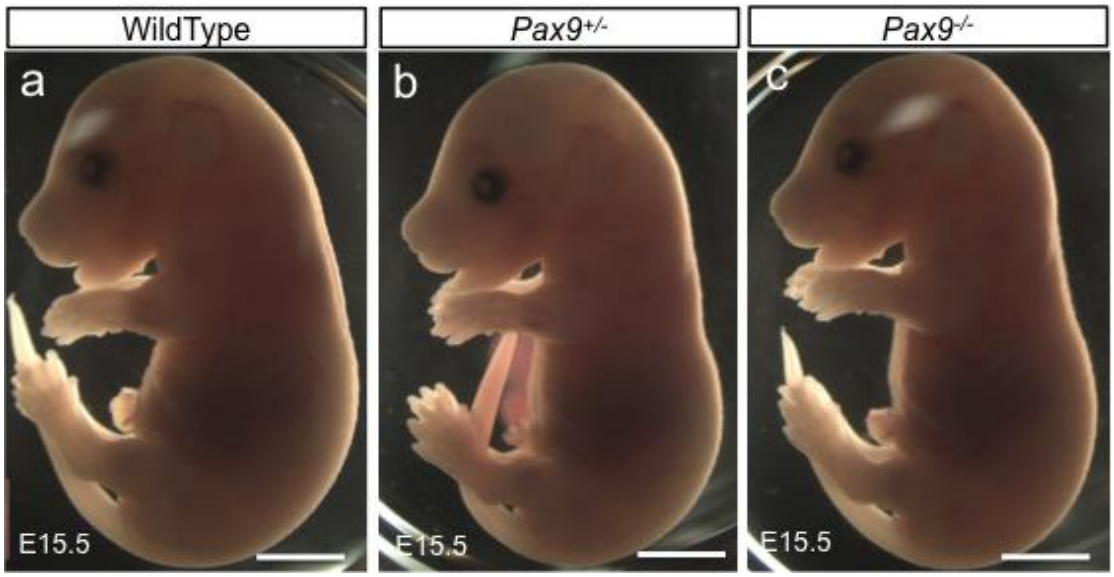

Figure 3.7. External phenotype of *Pax9* mutant embryos.
Pax9-null embryos **(c)** are indistinguishable from wild-type **(a)** and *Pax9*$^{+/-}$ **(b)** embryos externally. Scale bar, 1mm.

MRI (Figure 3.8) and histological analysis (Figure 3.9) shows Wild-type and *Pax9* heterozygous (*Pax9*$^{+/-}$) embryos display normal morphology of the heart and great arteries (Figure 3.8a, b), where the ascending aorta (Ao) arises from the left ventricle (LV) forming the aortic arch to join the descending aorta (dAo). Normal branching of the great arteries can be seen with the brachiocephalic artery arising as the first branch of the aortic arch and the left common carotid (LCC) and left subclavian (LSC) arising from the aortic arch as the second and third branch, respectively. Branching of the brachiocephalic artery into the right subclavian artery (RSA) and right common carotid (RCC) is normal in both wild-type and *Pax9*$^{+/-}$ embryos. Further normal branching of the common carotids into the internal and external carotids is observed in both wild-type (Figure 3.8a) and *Pax9*$^{+/-}$ (Figure 3.8b) embryos. Moreover, Wild-type and *Pax9*$^{+/-}$ hearts don't present any abnormalities within the ventricles or atrial chambers, showing normal size of the chambers and proper septation (Figure 3.9a).

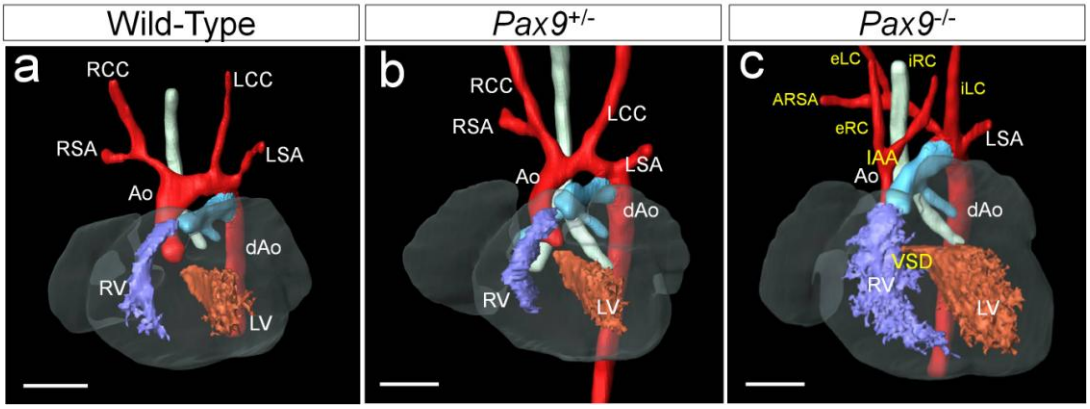

Figure 3.8. Cardiovascular phenotype of E15.5 *Pax9*-null embryos.
(a) Wild-Type and *Pax9*$^{+/-}$ **(b)** embryos present with normal branching of the great arteries; **(c)** All Pax9-null (*Pax9*$^{-/-}$) embryos present with some form of cardiovascular defect affecting the branching of the great arteries displaying interruption of the aortic arch type B (IAA), anomalous retro-esophageal right subclavian artery (ARSA), and unilateral or bilateral absence of the common carotids, consequently causing the internal and external carotids to arise directly from the aortas; additionally all *Pax9*-null embryos present VSD and DORV. LV, left ventricle; RSA, right subclavian artery; RCC, right common carotid artery; LSA, left subclavian artery; LCC, left common carotid artery; iRC, internal right carotid artery; eRC, external right carotid artery; iLC, internal left carotid artery; eLC, external left carotid artery; ARSA, anomalous retro-esophageal right subclavian artery; IAA, interruption of the aortic arch; VSD, ventricular septal defects. Scale 500µm.

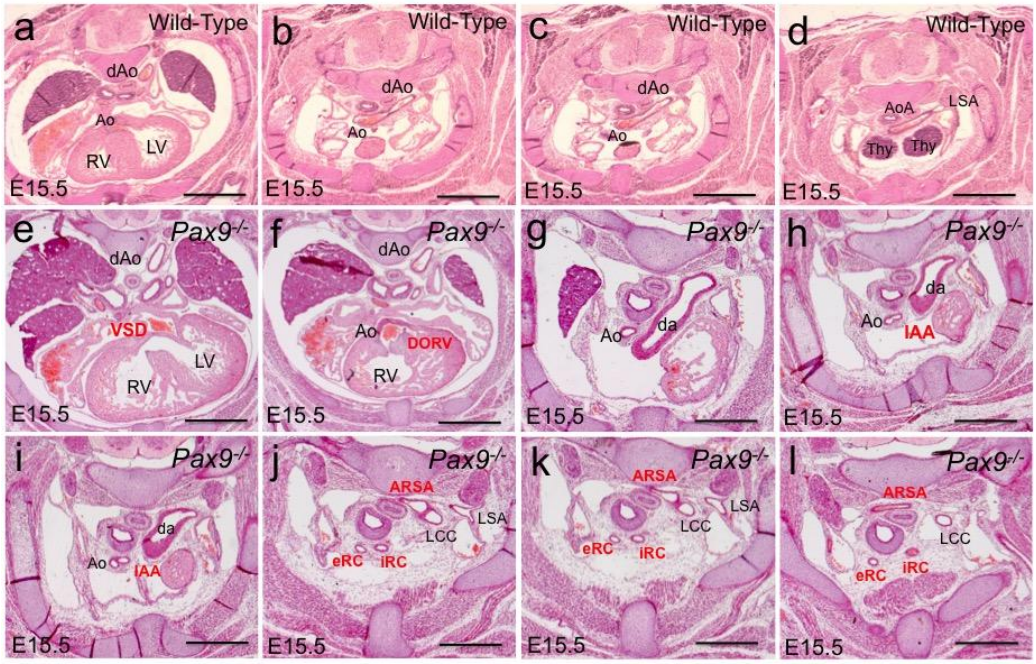

Figure 3.9. Histological analysis of E15.5 *Pax9*-null embryos.
Histological analysis shows in more detail the cardiovascular defects in *Pax9*-null embryos (*Pax9*$^{-/-}$) including VSD **(e)**, DORV **(f)**, IAA **(h, i)**, and ARSA **(j-l)**. The internal (iRC) and external right carotid (eRC) arteries can be seen arising directly from the aorta (Ao) as a consenquence of absent right common carotid **(j-l)**. LV, left ventricle; RSA, right subclavian artery; RCC, right common carotid artery; LSA, left subclavian artery; LCC, left common carotid artery; iRC, internal right carotid artery; eRC, external right carotid artery; iLC, internal left carotid artery; eLC, external left carotid artery; ARSA, anomalous retro-esophageal right subclavian artery; IAA, interruption of the aortic arch; VSD, ventricular septal defects; DORV, double outlet right ventricle; Thy, thymus. Scale bar, 100µm.

Pax9-null (*Pax9*$^{-/-}$) embryos however, display several abnormalities within the heart and great arteries. All *Pax9*$^{-/-}$ embryos show an absence of the common carotid arteries, either unilaterally or bilaterally (Figure 3.8c). Three out of four *Pax9*-null embryos analysed lack both (right and left) common carotids (Figure 3.8c), and one *Pax9*-null embryo had the left common carotid (LCC) but lacked the right common carotid. Such absence of the common carotids consequently causes the internal (iRCA, iLCA) and external (eRCA, eLCA) carotids to arise directly from the ascending and descending aorta (Figure 3.8c, Figure 3.9j-l).

Furthermore, the four *Pax9*-null embryos presented interruption of the aortic arch type B (IAA-B, Figure 3.8c, Figure 3.9h), ARSA (Figure 3.8c, Figure 3.9j-i), VSD (Figure 3.8c, Figure h, i), DORV (Figure 3.9f), bicuspid aortic valves (BAV) and a hypoplastic aorta.

The penetrance of these cardiovascular defects at E15.5 was further confirmed with data already available in the lab from the analysis of 15 more embryos, for a total of 19 *Pax9*$^{-/-}$ embryos (Table 3.5).

Table 3.5. Incidence of cardiovascular defects in E15.5 *Pax9*-null embryos.

n	**VSD**	**IAA**	**ARSA**	**CoRSA**	**Absent CC**	**Abnormal thymus**	**Cleft palate**
19	19 (100%)	17 (15.8%)	14 (73.7%)	2 (10.5%)	15 (79%)	19 (100%)	19 (100%)

Since all *Pax9*$^{-/-}$ embryos display abnormal patterning of the great arteries, the development of the pharyngeal arch arteries was analysed at E10.5 by India ink injection.

3.3.2. Pharyngeal Arch Artery Phenotype Of E10.5 Pax9-null Embryos

To analyze the development of the pharyngeal arch arteries (PAAs), *Pax9*-null embryos were collected at E10.5 and India ink was injected into the left ventricle, and allowed to be circulated to visualize the patterning of the pharyngeal arch arteries.

As observed in Figure 3.10, wildtype (a) and *Pax9*$^{+/-}$ (b) embryos display normal patterning of the 3rd, 4th and 6th pharyngeal arch arteries on both sides, connecting the aortic sac (as) with the paired dorsal aortas (dAo) at E10.5. By this stage the 1st and 2nd PAAs have already remodeled and are no longer visible. In contrast, all *Pax9*-null embryos present with abnormal patterning of the pharyngeal arch arteries at E10.5 (Table 3.6), showing delayed remodeling of the 1st and 2nd pharyngeal arch arteries bilaterally (Figure 3.10c), with 50% of *Pax9*$^{-/-}$ embryos exhibiting patent 1st PAAs and 20% embryos showing patent 2nd PAAs. Moreover, 50% of *Pax9*$^{-/-}$ embryos show hypoplastic 3rd arteries, and 100% of Pax9$^{-/-}$ embryos show non-patent 4th PAAs on both sides (Figure 3.10c; Table 3.6).

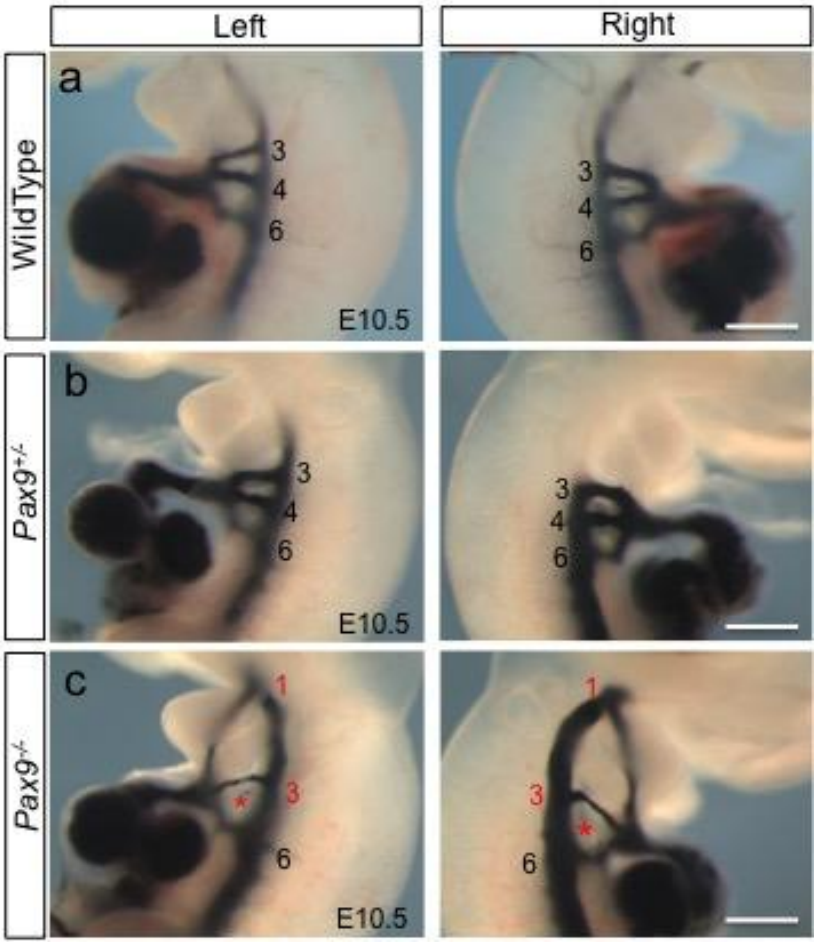

Figure 3.10. Pharyngeal arch artery defects in *Pax9* mutant embryos.
Patterning of the pharyngeal arch arteries at E10.5 was visualised by intracardiac injection of India ink. **(a)** Wild-type and *Pax9*$^{+/-}$ **(b)** embryos present normal patterning of the 3rd, 4th and 6th PAAs on both sides, whereas *Pax9*$^{-/-}$ embryos **(c)** show abnormal patency of the 1st PAAs on both sides at E10.5, suggesting a delay in their remodelling; *Pax9*-null embryos also display abnormal hypoplastic 3rd PAAs and the 4th PAAs (red asterisk) are non-patent to ink on both sides **(c)**. Scale 500µm.

Table 3.6. Pharyngeal arch artery defects in E10.5 *Pax9*-null embryos.

n	PAA	Abnormal (%)	Defects		
			Patent	Hypoplastic	Non-patent
10	1st	5 (50%)	5	-	-
	2nd	2 (20%	2	-	-
	3rd	6 (60%)	-	3	1
	4th	10 (100%)	-	2	8

Delayed regression of the 1st and 2nd PAA together with the hypoplastic 3rd PAA could explain the abnormal patterning of the carotids seen at E15.5, where the common carotids are absent as these are formed from the 3rd PAAs. Therefore, abnormal regression of the 3rd PAAs causes the internal and external carotids to arise directly from the ascending and dorsal aorta. Furthermore, the absence of the 4th pharyngeal arch arteries in *Pax9*$^{-/-}$ embryos explains the IAA-B and ARSA seen at E15.5 (Figure 3.8), as the aortic arch is formed by the left 4thPAA, while the right 4th PAA forms the distal portion of the right subclavian artery (RSA).

3.4. Discussion

The results shown in the first section of this chapter further confirm the crucial role of *Tbx1* for pharyngeal arch artery development and their derived structures (i.e. the great arteries). Although the incidence of *Tbx1* heterozygous defects varies among different studies at late embryogenesis, our results along with previous studies show the 4th PAAs as the main affected vessels at mid embryogenesis (Figure 3.3).

The recovery that takes place during the remodelling of the PAAs highly increases this variability, however, given the high phenotypic variability seen in 22q11DS patients, it is likely that genetic modifiers in epistasis with TBX1 modify the presentation of the phenotype. In this context, various genes have been shown to be in direct epistasis with *Tbx1* modifying the penetrance of *Tbx1*-heterozigosity defects (reviewed in Aggarwal and Morrow, 2008), including *Vegf* (Stalmans et al, 2003), *Crkl* (Guris et al, 2006), *Pitx2* (Nowotschin et al, 2006), *Gbx2* (Calmont et al, 2009), and *Aldh1a2* (Ryckebusch et al, 2010).

Moreover, expression of many other genes is affected by loss of *Tbx1* (Ivins et al, 2005; Liao et al, 2008), however their role in cardiovascular development or as potential modifiers of the *Tbx1* phenotype has not been studied for many of those genes. Among them, the transcription factor *Pax9* is found significantly downregulated in *Tbx1*-null embryos (Ivins et al, 2005; Figure 3.4).

Pax9 transcription factor is required for development of some pharyngeal arch-derived tissues including the thymus, parathyroids and ultimobranchial bodies (Peters et al, 1998), which are also affected in 22q11DS patients.

The results in this chapter show the a novel role for *Pax9* during cardiovascular development; particularly, *Pax9* is required for correct development of the pharyngeal arch arteries at mid embryogenesis, since homozygous deletion of *Pax9* causes a delay in the remodelling of the cranial 1st and 2nd PAAs, abnormal regression of the 3rd PAAs and completely disrupts the formation of the 4th PAAs (Figure 3.10).

The lack of formation of the 4th PAA on the left side prevents the formation of the aortic arch, whereas the absent right 4th PAA results in the right subclavian artery to abnormally originate on the left side and migrate behind the esophagous towards the right side forming a retro-esophageal right subclavian artery (ARSA).

Although the presence of ARSA can be asymptomatic and patients may not present with further complications, IAA is perinatally lethal, and patients need pharmacological and surgical attention immediately as previously mentioned.

Additionally, *Pax9*-null embryos display the internal and external carotids arising directly from the aortic arch due to absence of the common carotids as a consequence of the abnormal regression of the 3rd PAAs at E10.5. Such absence of the common carotids as a consequence of abnormal regression of the 3rd PAAs and persistence of the carotid duct has been previously reported in a female patient, who presented bilateral absence of the common carotids with the internal and external carotids arising directly from the aortic arch (Roberts and Gerald, 1978).

Although there is no direct evidence to date associating *PAX9* with cardiovascular development in humans, a few published papers have found patients with *PAX9* deletions presenting cardiovascular anomalies.

In 1999, Schuffenhauer et al reported a male patient with 14q chromosomal deletion that included *PAX9* presenting persistent ductus arteriosus and pulmonary stenosis. In 2001, Kamnasaran and colleagues reported another patient with persistent ductus arteriosus also with 14q deletion that included *PAX9*. Furthermore, Santen et al (2012) recently reported a case of a patient carrying a 14q13 deletion that included *PAX9,* presenting severe cardiovascular malformations including interrupted aortic arch type B, bicuspid aortic valve, ventricular septal defect and hypoplastic aorta; interestingly, these cardiovascular anomalies greatly overlap with the phenotype seen in *Pax9*-null embryos presented in this chapter.

Although *TBX1* deletion was excluded in the last report of a patient with *PAX9* deletion (Santen et al, 2012), the possibility of mutations or deletions of *PAX9* in patients with 22q11DS has not been analysed to date, leaving open the possibility of *PAX9* being a modifier gene of the 22q11DS phenotype. Therefore, a potential genetic interaction between *Tbx1* and *Pax9* during cardiovascular development was studied in the next chapter.

Chapter 4. *Pax9* And *Tbx1* Genetically Interact During Cardiovascular Development

4.1 Introduction

As described in section 3.3, *Pax9* is required for normal cardiovascular development as homozygous deletion of *Pax9* leads to severe cardiovascular anomalies including IAA-B, ARSA, VSD, DORV and absence of the common carotids (Figure 3.8). Furthermore, *Pax9* homozygous deletion affects the development of the pharyngeal arch arteries, as *Pax9*-null embryos show abnormal remodelling of the 1st, 2nd and 3rd PAAs, and complete lack of formation of the 4th PAAs (Figure 3.10).

The similarity between both *Pax9* knockout and *Tbx1* heterozygous phenotypes showing ARSA and IAA, which are caused by abnormal development of the 4th PAAs suggests both *Pax9* and *Tbx1* are required for normal 4th PAAs development. Moreover, Tbx1 and Pax9 are co-expressed within the pharyngeal endoderm at E9.5 and E10.5 (Figure 3.5), and *Pax9* expression is significantly downregulated in *Tbx1*-null embryos (Ivins et al, 2005; Figure 3.4), suggesting *Pax9* as a potential down-stream target of Tbx1.

Therefore, to investigate whether *Pax9* and *Tbx1* interact during cardiovascular development either as part of the same pathway or working in parallel pathways, *Pax9*$^{+/-}$ mice were crossed with *Tbx1*$^{+/-}$ mice and their progeny were analyzed for cardiovascular defects at different embryonic and postnatal stages.

4.2 Perinatal survival of double heterozygous mice

Pax9$^{+/-}$ mice were crossed with *Tbx1*$^{+/-}$ mice to generate compound heterozygotes for analysis. From this cross it is expected that 25% will be wild-type (i.e. *Pax9*$^{+/+}$;*Tbx1*$^{+/+}$), 25% will be *Pax9*$^{+/-}$, 25% *Tbx1*$^{+/-}$, and the final 25% being doubly heterozygous (i.e. *Pax9*$^{+/-}$;*Tbx1*$^{+/-}$). Interestingly, only 2 double heterozygous mice (out of 168 pups weaned) were found alive after weaning at 3 weeks old.

Table 4.1. Survival of double heterozygous mice after weaning

Genotype	Wildtype	*Pax9*$^{+/-}$	*Tbx1*$^{+/-}$	*Pax9*$^{+/-}$;*Tbx1*$^{+/-}$	Total
Observed (3 weeks old)	55	68	43	2*	168
Expected	42	42	42	42	168

*Fisher's exact test, p<0.0001

This is a significant deviation from the expected Mendelian ratio, where 42 pups of each genotype were expected (p<0.0001). Whereas all other genotypes were found within Mendelian ratios (Table 4.1).

Although all *Pax9*$^{+/-}$ and the majority (95%) of *Tbx1*$^{+/-}$ mice are viable, all homozygous null mice die soon after birth as previously mentioned. To determine whether double heterozygotes were dying during the foetal period or after birth, neonates were collected within 48 hours of birth.

All pups from *Pax9*$^{+/-}$ and *Tbx1*$^{+/-}$ mice crosses were born alive, however all double heterozygous pups (n=7, Table 4.2) died within 48 hours, with the rest of the pups surviving. When dissected, 5 out of 7 double heterozygotes had an interrupted aortic arch (Figure 4.1c, Table 4.2) and no visible brachiocephalic or right subclavian artery, suggesting they had a retro-esophageal right subclavian artery (ARSA, arrow in Figure 4.1c). No wild-type or *Pax9*$^{+/-}$ mice had cardiovascular defects, whereas 3 out of 5 *Tbx1*$^{+/-}$ pups had ARSA and one presented with IAA-B (Table 4.2).

The analysis of neonatal survival indicates that double heterozygous mice die after birth, the majority likely dying from the consequence of having an interrupted aortic arch, with the time of death being variable depending on the time of closure of the ductus arteriosus (Figure 4.1).

To analyse in more detail the cardiovascular defects in double heterozygotes, E15.5 embryos were collected and analysed by MRI and histology.

Table 4.2 Perinatal lethality of double heterozygous mice.

Genotype	Wild type	*Pax9*$^{+/-}$	*Tbx1*$^{+/-}$	*Pax9*$^{+/-}$;*Tbx1*$^{+/-}$	Total
Observed	5	10	5	7	27
Expected	6.75	6.75	6.75	6.75	27
Abnormal	0	0	1[a]	6*[b]	

*Fisher's exact test, p<0.005 (compared to abnormal Tbx1+/- mice)
a, one embryo presented IAA
b, six embryos presented IAA

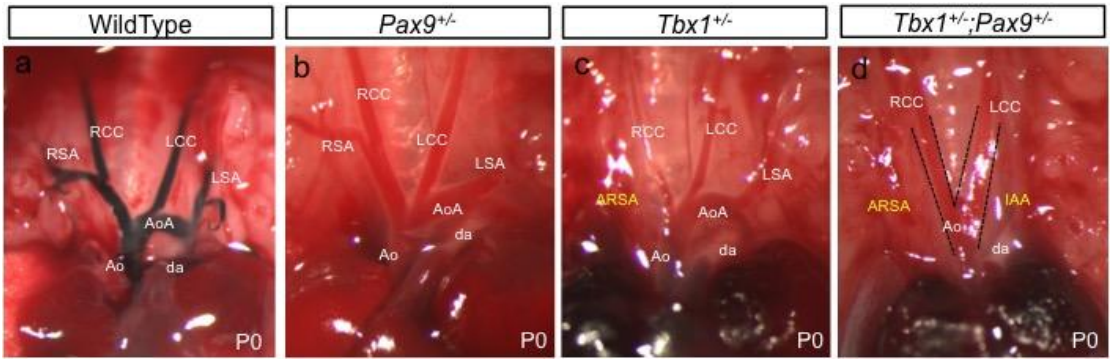

Figure 4.1. Cardiovascular defects in neonate double heterozygous mice.
Dissection of neonate mice (P0) revealed double heterozygotes (*Tbx1*$^{+/-}$;*Pax9*$^{+/-}$) present with interruption of the aortic arch (IAA) and retro-esophageal right subclavian artery (ARSA) **(d)**; some *Tbx1*$^{+/-}$ pups **(c)** displayed ARSA, whereas *Pax9*$^{+/-}$ **(b)** do not have any cardiovascular defects. Ao, aorta; da, ductus arteriosus; AoA, aortic arch; RSA, right subclavian artery; LSA, left subclavian artery; RCC, right common carotid; LCC, left common carotid; IAA, interruption of the aortic arch; ARSA, anomalous retro-esophageal right subclavian artery.

4.3 Cardiovascular phenotype of double heterozygotes

Embryos from *Pax9*$^{+/-}$ and *Tbx1*$^{+/-}$ mice crosses were collected at E15.5, imaged by MRI and analysed by histology afterwards. Wild-type (n=16), *Pax9*$^{+/-}$ (n=15), *Tbx1*$^{+/-}$ (n=19) and *Pax9*$^{+/-}$;*Tbx1*$^{+/-}$ (n=20) embryos were imaged and 3D models of the heart and great arteries were built from the MRI data sets (Figure 4.2).

As can be seen in Table 4.3, Wild-type and *Pax9* heterozygous embryos do not present any cardiovascular defects (Table 4.3, Figure 4.2a, b), whereas a proportion of *Tbx1* heterozygotes (Table 4.3) have some form of cardiovascular defect mainly affecting the great arteries (Figure 4.2c).

As described before in section 3.1, ARSA is most commonly found in *Tbx1* heterozygous embryos with 7 out of 19 (36%) presenting ARSA (Figure 4.2c). Five (26%) *Tbx1*$^{+/-}$ embryos also presented with cervical right subclavian artery (coRSA), and 2 (10%) *Tbx1*$^{+/-}$ embryos had a cervical aortic arch (coAoA). Only 1 (5%) *Tbx1*$^{+/-}$ embryo had IAA-B with VSD (Table 4.3).

However, all double heterozygous (*Pax9*$^{+/-}$;*Tbx1*$^{+/-}$) embryos had some form of cardiovascular defect affecting the great arteries (Table 4.3). Of particular interest is that double heterozygous embryos showed a statistically significant increase ($p<0.001$) in the incidence of IAA-B (Table 4.3, Figure 4.2 d-f, Figure 4.3f,g), with 14 out of 20 (70%) *Pax9*$^{+/-}$;*Tbx1*$^{+/-}$ embryos being affected, compared to only one (5%) *Tbx1* heterozygote with an IAA-B. Three (15%) double heterozygotes had a cervical aortic arch, 11 (55%) double heterozygotes had a coRSA (Figure 4.2d, f), and 9/20 (45%) had ARSA (Figure 4.2e, Figure 4.3f-h).

Moreover, double heterozygotes had a statistically significant increase (p-value <0.005) in the incidence of VSD, with 6 (30%) double heterozygous embryos affected (Table 4.3, Figure 4.2d, Figure 4.3e) compared to only one *Tbx1* heterozygous embryo (Table 4.3).

All *Tbx1*$^{+/-}$ and double heterozygous embryos were externally indistinguishable from wild-type and *Pax9* heterozygotes (Figure 4.4). However, 4 (21%) *Tbx1* heterozygous embryos had an abnormal thymus, whereas 17 (85%) double heterozygotes displayed an abnormally developed thymus, where the thymus appears hypoplastic and asymmetric with unfused lobes.

The great arteries appear to be mainly affected by *Pax9* and *Tbx1* double haploinsufficiency, and it is well known *Tbx1* heterozygosity affects the development of the pharyngeal arch arteries as discussed in sections 1.4 and 3.1. Therefore, the development of the PAAs in double heterozygous embryos was analysed by intracardiac ink injection at E10.5.

Table 4.3. Incidence of cardiovascular defects in E15.5 double heterozygous embryos.

Genotype	n	VSD	Cervical Ao	IAA	Cervical RSA	ARSA
WildType	16	0	0	0	0	0
***Pax9*$^{+/-}$**	15	0	0	0	0	0
***Tbx1*$^{+/-}$**	19	1 (5.3%)	2 (10.5%)	1 (5.3%)	5 (26.3%)	7 (36.8%)
***Pax9*$^{+/-}$*;Tbx1*$^{+/-}$**	20	6* (30.0%)	3 (15.0%)	13** (65.0%)	11 (55.0%)	9 (45.0%)

Fisher's exact test, *p<0.05 ** p<0.001

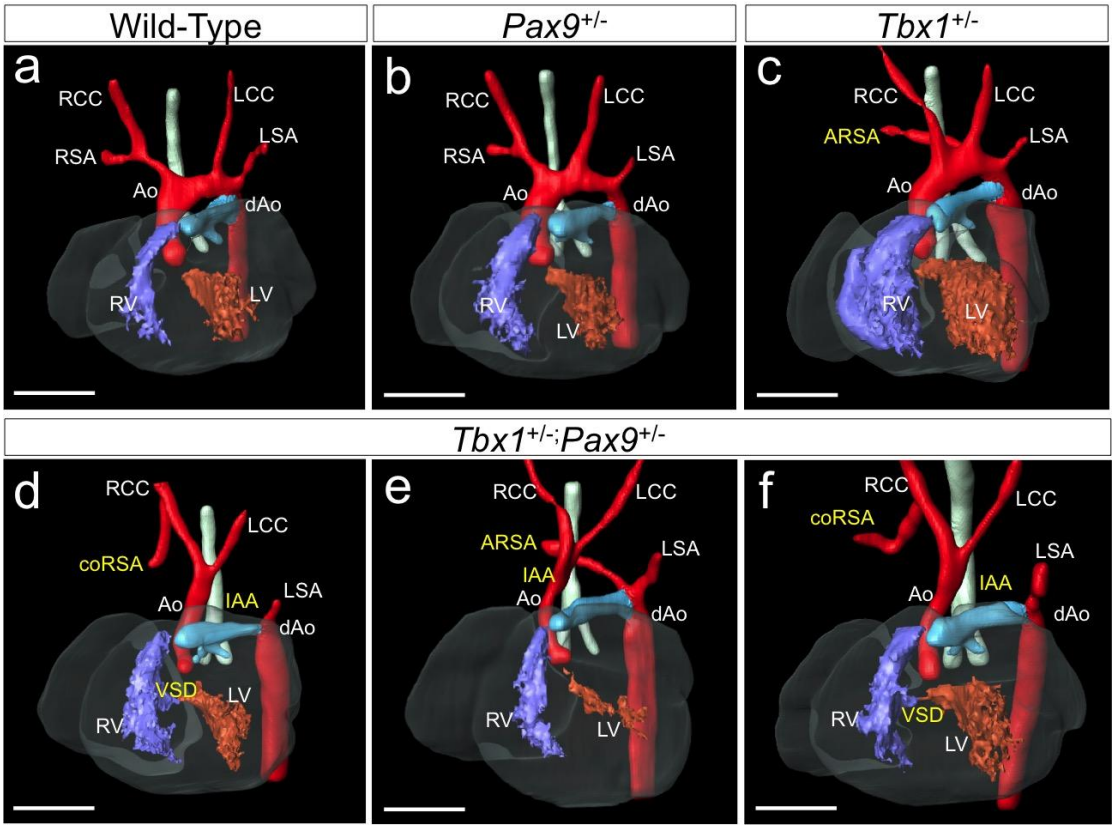

Figure 4.2. Cardiovascular phenotype of E15.5 double heterozygous embryos.
(a) Wild-Type and *Pax9*$^{+/-}$ **(b)** embryos present with normal branching of the great arteries where the aorta (Ao) arises from the left ventricle (LV) forming the aortic arch to connect with the descending aorta (dAo), the brachiocephalic artery arising from the right side of aortic arch and branching into the righ subclavian artery (RSA) and the right common carotid artery (RCC), while the left common carotid (LCC) and the left subclavian artery (LSA) arise from the left side of the aortic arch; **(c)** *Tbx1*$^{+/-}$ embryos present with some cardiovascular defects, including anomalous retro-esphageal right subclavian artery (ARSA), whereas **(d-f)** double heterozygous embryos (*Tbx1*$^{+/-}$;*Pax9*$^{+/-}$) present with a higher incidence of cardiovascular defects, including ventricular septal defects (VSD), cervical origin of the right subclavian artery (coRSA, **d, f**), anomalous right subclavian artery **(e)**, and interruption of the aortic arch type B (IAA, **d, e**). LV, left ventricle; RSA, right subclavian artery; RCC, right common carotid artery; LSA, left subclavian artery; LCC, left common carotid artery; ARSA, anomalous retro-esophageal right subclavian artery; coRSA, cervical origin of the right subclavian artery; IAA, interruption of the aortic arch; VSD, ventricular septal defects. Scale 500µm.

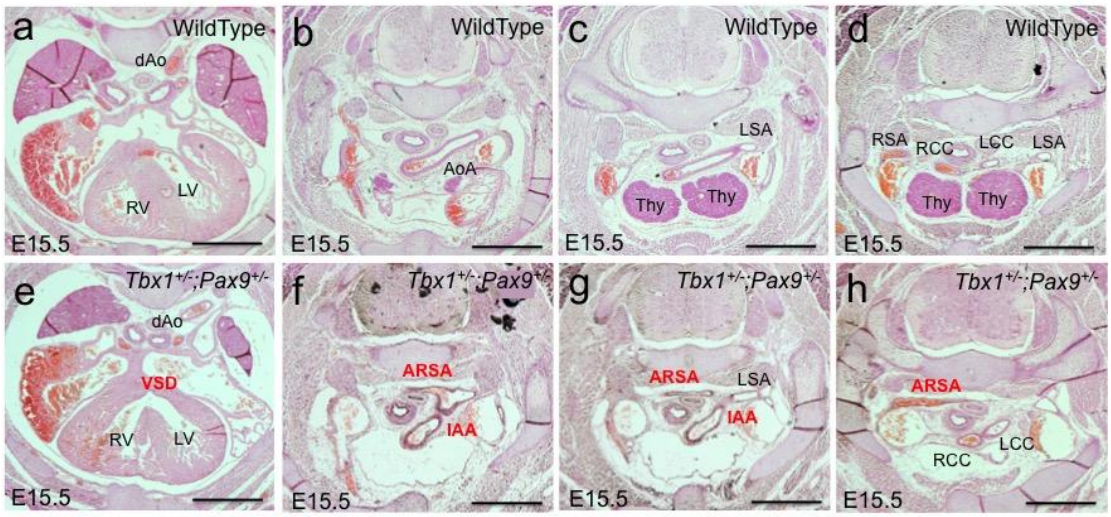

Figure 4.3. Histological analysis of E15.5 double heterozygous embryos.
Histological analysis shows in more detail the cardiovascular defects in double heterozygous embryos (*Tbx1*$^{+/-}$;*Pax9*$^{+/-}$) including VSD **(e),** IAA **(f,g)** and ARSA **(f-h)**. Additionally, the thymus is not apparent in double heterozygous embryos compared to wild-type embryos where the thymus is clearly visible **(c,d)**. Ao, aorta; AoA, aortic arch; dAo, descending aorta; LV, left ventricle; RSA, right subclavian artery; RCC, right common carotid artery; LSA, left subclavian artery; LCC, left common carotid artery; ARSA, anomalous retro-esophageal right subclavian artery; IAA, interruption of the aortic arch; VSD, ventricular septal defect; Thy, thymus. Scale bar, 100μm.

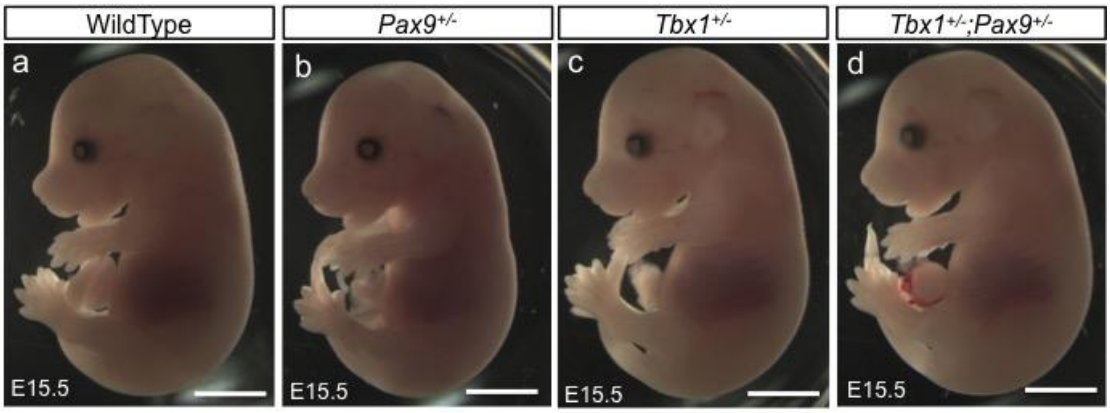

Figure 4.4. Double heterozygous embryos do not present external abnormalities.
Tbx1$^{+/-}$;*Pax9*$^{+/-}$ embryos **(d)** are indistinguishable externally from wild-type **(a)**, *Pax9*$^{+/-}$ **(b)** and *Tbx1*$^{+/-}$ **(c)** embryos and do not present any external abnormalities. Scale bar, 1mm.

4.4 Pharyngeal Arch Artery Remodelling In Double Heterozygotes

To analyse the development of the pharyngeal arch arteries, E10.5 embryos were collected and India ink was injected directly into the left ventricle to be pumped by the heart through the pharyngeal arch arteries.

Wild-type and *Pax9*$^{+/-}$ embryos (Figure 4.5a, b) present normal patency of the 3rd, 4th and 6th pharyngeal arch arteries on both sides, as expected at this stage, whereas all *Tbx1*$^{+/-}$ embryos (Figure 4.5c) present abnormal 4th PAAs, with 50% of them showing bilateral defects (Table 4.4). *Tbx1*$^{+/-}$ embryos mainly display hypoplastic 4th PAAs as seen in Figure 4.5c and Table 4.4. Interestingly, the incidence of bilaterally absent 4th PAAs was significantly increased ($p<0.005$) in double heterozygous embryos, with 7 out of 9 embryos showing absent 4th PAAs on both sides (Table 4.4, Figure 4.5d).

Table 4.4. Incidence of 4th PAA abnormalities in E10.5 double heterozygous embryos.

Genotype	n	Abnormal (%)	Bilateral defects	Bilateral defects		
				Hypo/Hypo	Hypo/NP	NP/NP
Wild-type	6	0	0	-	-	-
***Pax9*$^{+/-}$**	4	0	0	-	-	-
***Tbx1*$^{+/-}$**	8	8 (100%)	4 (50%)	3	1	-
***Pax9*$^{+/-}$*;Tbx1*$^{+/-}$**	9	9 (100%)	8* (88%)	-	1	7**

Fisher's exact test, *$p<0.05$, compared to *Tbx1*$^{+/-}$ bilateral defects; **$p<0.001$ compared to NP/NP bilateral defects in *Tbx1*$^{+/-}$

The penetrance of 4th PAA defects seen at E10.5 by ink injection in double heterozygous embryos (Table 4.4) corresponds to the penetrance of 4th PAA-derived defects seen at E15.5 by MRI and histology (Table 4.3). Particularly, the incidence of non-patent left 4th PAA (77%, Table 4.4) corresponds to about 70% of IAA seen in double heterozygotes at E15.5 (Table 4.3). Although nearly all double heterozygotes died after birth as previously discussed, two male double heterozygous mice survived until adulthood. We crossed these double heterozygous mice with *Pax9*$^{+/-}$ females to generate embryos that would include the *Pax9*$^{-/-}$;*Tbx1*$^{+/-}$ genotype, and analysed their PAA phenotype by ink injections at E10.5.

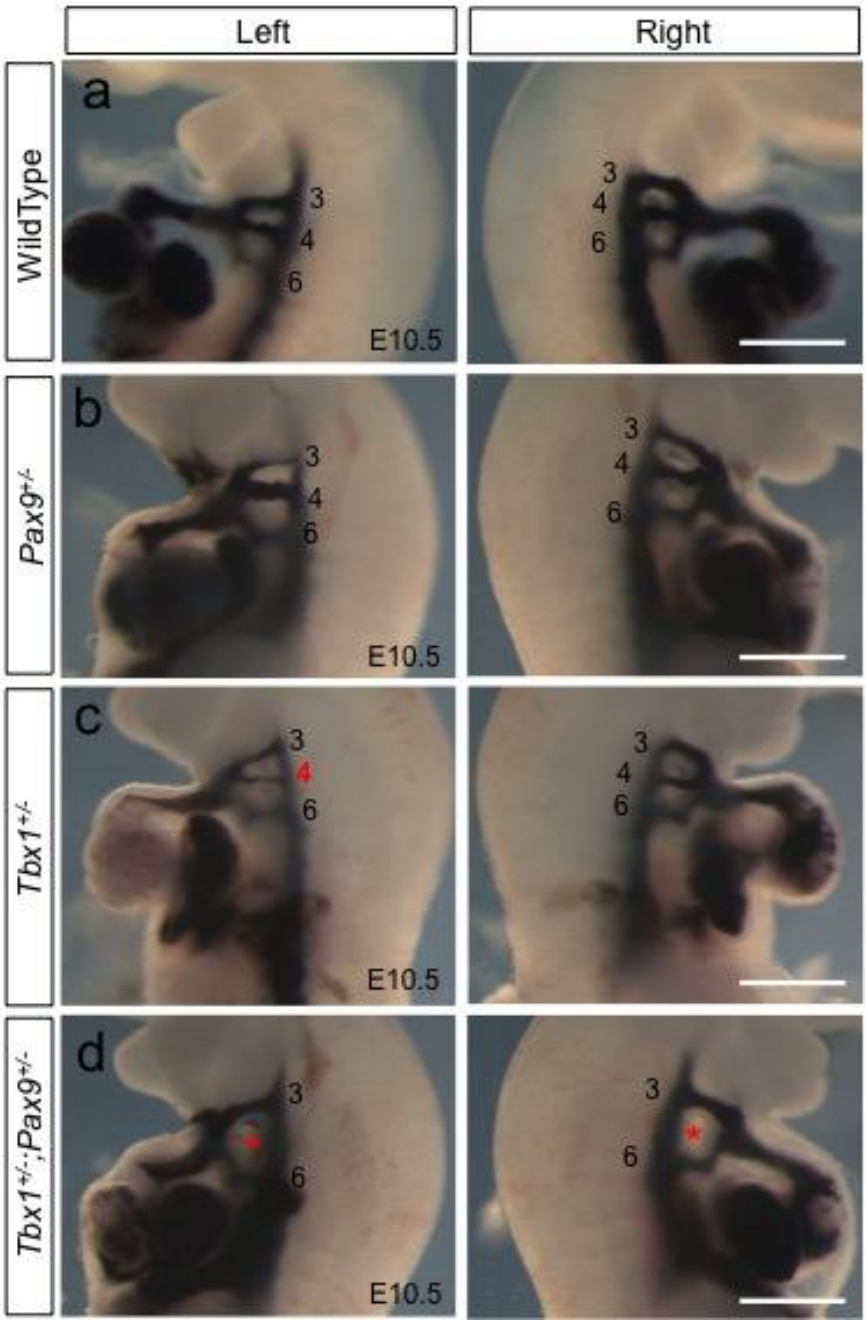

Figure 4.5. Pharyngeal arch artery defects in double heterozygous embryos.
Patterning of the pharyngeal arch arteries at E10.5 was visualised by intracardiac injection of India ink. **(a)** Wild-type and *Pax9*$^{+/-}$ **(b)** embryos present normal patterning of the 3rd, 4th and 6th PAAs on both sides, whereas *Tbx1*$^{+/-}$ embryos **(c)** display abnormal hypoplastic 4th PAAs unilateral or bilaterally. *Tbx1*$^{+/-}$;*Pax9*$^{+/-}$ **(d)** present abnormal 4th PAAs which are non-patent to ink on both sides **(d)**. Scale 500µm.

As seen in Figure 4.6, all double heterozygous embryos present abnormal 4th PAAs that are non-patent to ink as described before (Figure 4.6a), whereas *Pax9*$^{-/-}$;*Tbx1*$^{+/-}$ embryos display the *Pax9*-null phenotype (Figure 4.6b), with delayed regression of the 1st and 2nd PAAs, and completely absent 4th PAAs on both sides (Figure 4.6b). *Pax9*$^{+/-}$;*Tbx1*$^{-/-}$ embryos were not generated (by crossing the double heterozygous males with *Tbx1*$^{+/-}$ females) since *Tbx1* homozygous deletion disrupts the formation of the caudal pharyngeal arches and consequently the PAAs below the 2nd PAA are not formed. As this is already a severe phenotype with most of the PAA not formed, it was therefore decided not to try and look at the effect of *Pax9* heterozygosity in combination with complete *Tbx1* loss on the development of the PAAs.

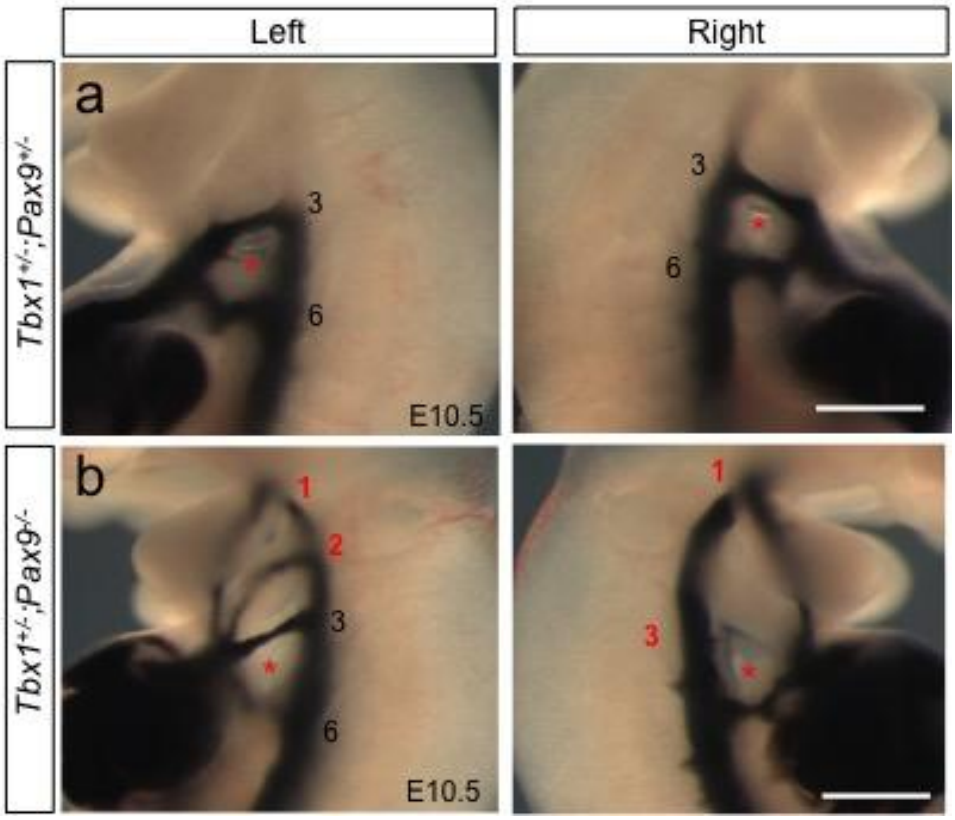

Figure 4.6. Pharyngeal arch artery defects in *Tbx1*$^{+/-}$;*Pax9*$^{-/-}$ embryos.
Patterning of the pharyngeal arch arteries at E10.5 was visualised by intracardiac injection of India ink. *Tbx1*$^{+/-}$;*Pax9*$^{+/-}$ embryos **(a)** present with abnormal 4th PAAs which are non-patent to ink on both sides as previously described; however, *Tbx1*$^{+/-}$;*Pax9*$^{-/-}$ embryos **(b)** display the *Pax9*-null phenotype with patent 1st and 2nd PAAs at E10.5, abnormal 3rd PAAs unilateral or bilaterally, and bilateral non-patent 4th PAAs (red asterisk). Scale 500µm.

4.5 *Pax9* Down-regulation In Double Heterozygous Embryos

The results from the analysis of double heterozygous embryos at E15.5 clearly shows a significant increase in the penetrance of IAA (70%) compared to *Tbx1*$^{+/-}$ embryos (5%), as well as a significant increase in the incidence of absent 4th PAAs and bilateral defects at E10.5. Given that the incidence of IAA in *Tbx1*$^{+/-}$ embryos is very low (5%) and *Pax9*$^{+/-}$ embryos do not have any defects, such significant increase suggests some form of synergy between *Pax9* and *Tbx1* heterozygosity.

Moreover, *Pax9* expression is significantly downregulated in *Tbx1*-null embryos by quantitative real-time PCR (qPCR) by approximately 50% compared to wild-type embryos (Ivins et al, 2005). This downregulation of *Pax9* mRNA in *Tbx1*-null embryos is also confirmed in this thesis by whole-mount *in situ* hybridisation (section 3.2.3, Figure 3.4).

To determine whether *Pax9* and *Tbx1* mRNA levels are affected by double haploinsufficiency, total RNA was extracted from the pharyngeal region of E9.5 double heterozygous embryos (six embryos of each genotype), cDNA was synthesized and mRNA levels were analysed by qPCR.

As seen in Figure 4.7a, *Tbx1* mRNA expression (white bars) is reduced to 58% in *Tbx1*$^{+/-}$ embryos compared to wild-type embryos and it is not affected by *Pax9* haploinsufficiency nor double heterozygosity. *Pax9* mRNA (black bars) expression is reduced to 52% in *Pax9*$^{+/-}$ embryos compared to wild-type embryos and it is not significantly affected by *Tbx1* heterozygosity. However, double heterozygous embryos show a statistically significant ($p<0.005$) further 21% reduction compared to *Pax9*$^{+/-}$ embryos. This further downregulation in double heterozygous embryos compared to *Pax9*$^{+/-}$ embryos suggests that some form of synergy between *Pax9* and *Tbx1* may exist. To further confirm this down-regulation, *in situ* hybridisation using a probe against *Pax9* mRNA was performed in double heterozygotes (three embryos per genotype). As seen in Figure 4.7b, double heterozygous embryos (*Pax9*$^{+/-}$;*Tbx1*$^{+/-}$) display an obvious reduction in *Pax9* expression compared to *Pax9*$^{+/-}$ embryos (Figure 4.7b).

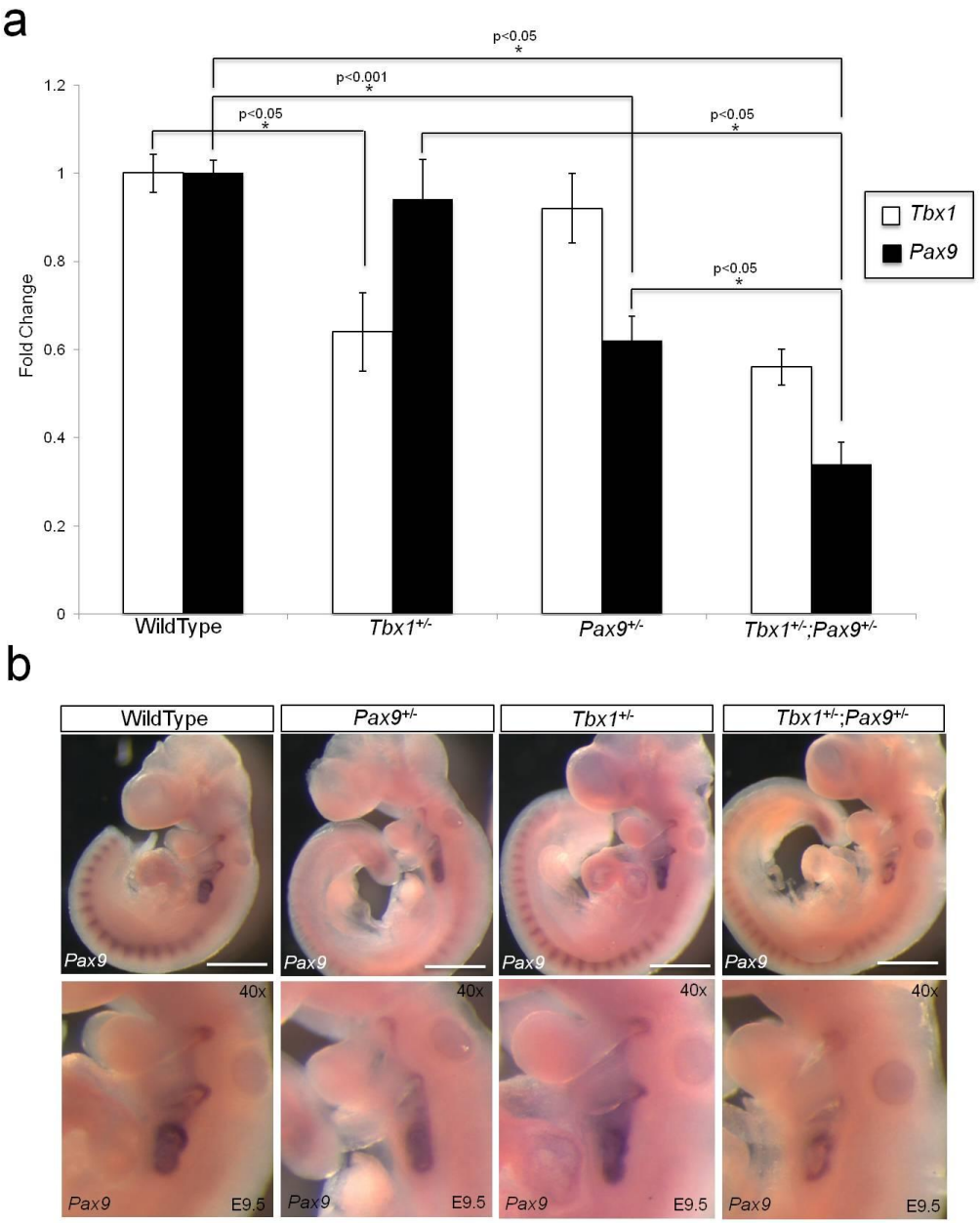

Figure 4.7. *Pax9* mRNA levels are further reduced in double heterozygous embryos.
(a) *Pax9* and *Tbx1* mRNA levels were analysed by qPCR from the dissected pharyngeal region of E9.5 embryos (six embryos per genotype). Relative expression was normalised against wild-type embryos and plotted as the fold change over the wild-type samples. *Tbx1* levels (white bars) are significantly reduced to 58% in *Tbx1*$^{+/-}$ embryos ($p<0.05$) compared to wild-type levels, and are not affected in *Pax9*$^{+/-}$ embryos nor double heterozygous embryos. *Pax9* levels (black bars) are not significantly affected in *Tbx1*$^{+/-}$ embryos, but significantly reduced to 52% in *Pax9*$^{+/-}$ samples ($p<0.001$) compared to wild-type samples. Interestingly, *Pax9* levels are significantly reduced to 31% in double heterozygous embryos ($p<0.05$) compared to wild-type and *Pax9*$^{+/-}$ embryos, representing a significant further 21% reduction ($p<0.05$) compared to *Pax9*$^{+/-}$ embryos. Error bars represent standard error of the mean (SEM) from triplicates of each sample. Statistical significance was calculated using a two-paired T-test.
(b) Whole-mount in situ hybridisation using a *Pax9* riboprobe was performed to further confirm *Pax9* down-regulation in double heterozygous embryos. *Pax9* levels appear visibly reduced in double heterozygous embryos (*Tbx1*$^{+/-}$;*Pax9*$^{+/-}$) compared to wild-type, *Pax9*$^{+/-}$ and *Tbx1*$^{+/-}$ embryos (n=3 per genotype); the pharyngeal region is enlarged in the bottom panels for better appreciation. Scale bar, 500µm.

4.6 Discussion

The results presented in this chapter show a strong genetic interaction between *Tbx1* and *Pax9* for the formation of the 4th PAAs, with double heterozygous embryos showing a significant increase in the frequency of bilateral 4th PAA defects at mid embryogenesis and a significant increase in the incidence of IAA-B at later fetal stages.

This interaction is very strong with a 100% penetrance in double heterozygous embryos, and also very specific only affecting the formation of the 4th PAAs and their derived structures, the aortic arch and right subclavian artery.

The specificity of *Tbx1* and *Pax9* double haploinsufficiency affecting only the 4th PAA implies that 4th PAA precursors are molecularly distinct from the other PAAs as they respond differently to changes in *Pax9* and *Tbx1* mRNA levels.

Although other genes have been shown to interact with *Tbx1*, particularly in the development of the 4th PAAs, such interactions are not typically as strong as that observed here in *Pax9* and *Tbx1* double heterozygotes. For instance, only 10% of *Tbx1* and *Smad7* double heterozygous present with IAA (Randall et al, 2009), while only 9% of *Moz* and *Tbx1* double heterozygous embryos have IAA (Voss et al, 2012), compared to 65% of *Tbx1*$^{+/-}$;*Pax9*$^{+/-}$ embryos that present IAA-B.

In other cases where a higher penetrance of IAA is seen, the interaction requires homozygous deletions to observe an increased incidence, such as complete deletion of *Bmp4* expression in *Tbx1* expressing cells with a 40% penetrance of IAA (Nie et al, 2011).

The model presented here suggests some form of synergy between *Pax9* and *Tbx1* exists, since 65% of double heterozygous embryos display IAA-B, but *Pax9*$^{+/-}$ embryos do not present cardiovascular defects and only 5% of *Tbx1*$^{+/-}$ embryos have IAA-B, ruling out the possibility of an additive effect.

Although interruption of the aortic arch is a rare congenital cardiovascular defect, it is commonly associated with 22q11DS, with 50% of patients with IAA presenting 22q11 deletion.

Moreover, IAA is one of the most severe CCVM, requiring immediate attention on the newborn to keep the ductus arteriosus open to preserve the flow of blood, followed by open heart surgery to graft a connection between the ascending and thoracic aortas; if untreated, IAA can lead to mortality within 4 days.

The analysis of perinatal survival shows double heterozygous mice die after birth, likely as a consequence of having an interrupted aortic arch; however, the time of death was variable (between 24 and 48 hours) depending on the time of closure of the ductus arteriosus.

Given that in double heterozygous embryos only the 4th PAAs are affected and not the 1st, 2nd and 3rd PAAs as occurs in *Pax9*-null embryos, *Pax9* heterozygosity seems to exacerbate the *Tbx1*$^{+/-}$ phenotype, suggesting *PAX9* could be a modifier of the 22q11DS phenotype, increasing the prevalence of 4th PAA defects and consequently increasing the incidence of IAA.

In this context, mutations leading to *PAX9* heterozygosity in patients with 22q11 deletion would imply a more severe presentation of the 22q11 syndrome including IAA-B.

Additionally, the possibility of *PAX9* mutations in humans leading to cardiovascular defects including IAA may be supported by the report of a patient with *PAX9* deletion presenting IAA-B, BAV, DORV and hypoplastic aorta (Santen et al, 2012), which resembles the phenotype seen in the *Pax9*-null mouse model presented in chapter 3.

Chapter 5. *Tbx1-Pax9* Mechanism of Interaction

5.1 Introduction

The phenotype seen in double heterozygous embryos (*Tbx1*$^{+/-}$;*Pax9*$^{+/-}$) clearly show a genetic interaction between *Pax9* and *Tbx1* as the incidence of bilaterally abnormal 4th PAAs at mid embryogenesis and the incidence of IAA at later stages are significantly increased compared to the *Tbx1* heterozygous embryos. This genetic interaction results in a 100% penetrance specifically in 4th PAA defects in the double heterozygotes.

Therefore, the aim of this chapter was to identify the mechanism by which *Pax9* and *Tbx1* interact at a molecular level.

Microarray analysis of *Tbx1*-null embryos previously revealed *Pax9* expression to be significantly downregulated (Ivins et al, 2005; Liao et al, 2008), suggesting *Pax9* as a potential downstream target of Tbx1. Additionally, both Tbx1 and Pax9 are co-localized within the pharyngeal endoderm (Figure 3.5), and *Pax9* expression (about E8.5) starts after *Tbx1* expression (about 7.5) during embryogenesis. Therefore, we first hypothesized that Tbx1 directly regulates *Pax9* expression through binding to T-box binding elements (TBE) within the *Pax9* locus.

5.2 Binding of *Tbx1* within the *Pax9* locus

TBX1 is a T-box binding transcription factor that binds to T-box binding elements (TBE, also known as T-half sites) within the DNA. Therefore the *PAX9* locus was analysed using Mulan MultiTF tool (http://mulan.dcode.org) to identify potential T-box binding elements (TBE) within the *PAX9* gene.

The human *PAX9* sequence was aligned with other species including mouse (*Mus musculus*), rat (*Rattus novergicus*), monkey (*Macaca mulatta*), chicken (*Gallus gallus domesticus*), frog (*Xenopus laevis*) and zebrafish (*Danio rerio*) and analysed for conserved elements among these species.

The results from the MultiTF analysis revealed 10 highly conserved potential TBEs within the *PAX9* locus (Figure 5.1). Three TBEs (TBE-1, -2 and -3) are found within the *PAX9* promoter upstream of the first exon, one TBE (TBE-4) within the first intron, a fifth TBE (TBE-5) within the second intron, and 5 more TBEs (TBE-6 to -10) within the third intron.

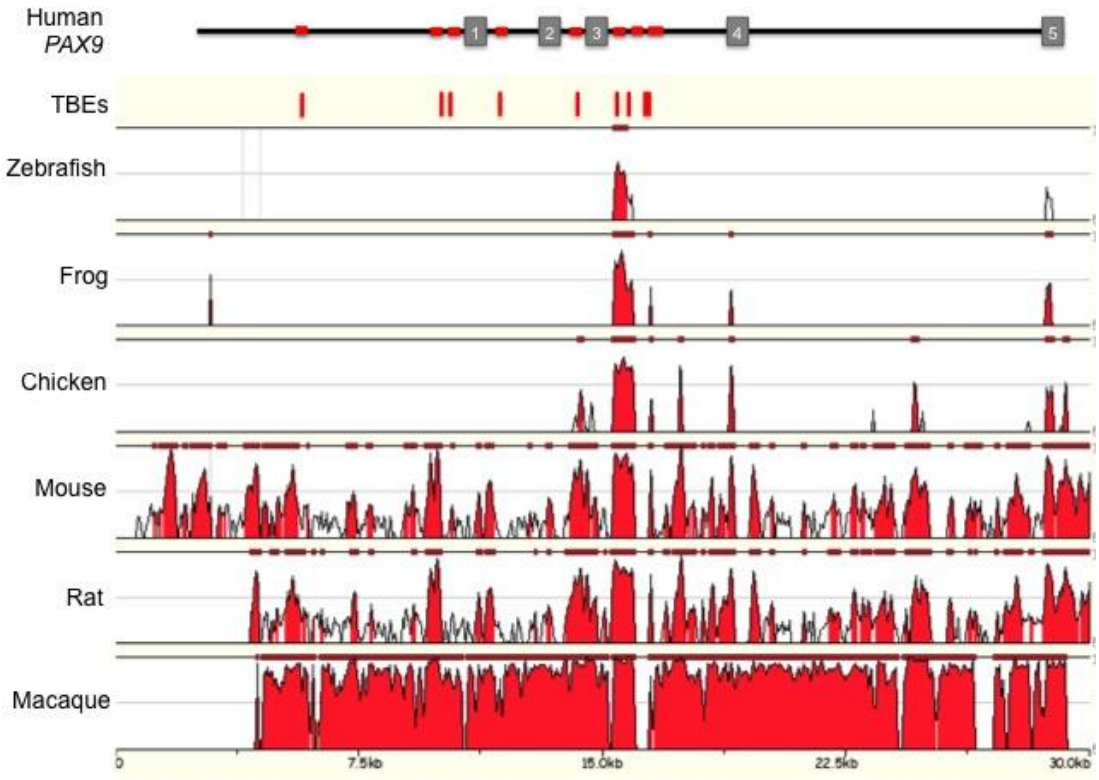

Figure 5.1. Alignment and identification of conserved potential TBEs within the *PAX9* locus.
Human *PAX9* locus was aligned with Macaque, Rat, Mouse, Chicken, Frog and Zebrafish *Pax9* using the Mulan online tool (http://mulan.dcode.org); the alignment was then used in MultiTF analysis tool to look for conserved potential T-box binding sites. Ten conserved potential T-box binding sites (TBEs) were identified within the *PAX9* locus. Three TBEs were found within the promoter upstream of the first exon (1), one TBE was found within the first intron, and another was found within the second intron. Five more TBEs were found within the third intron proximal to the 3rd exon (3).

To determine whether TBX1 binds to any of these potential TBEs, 500bp fragments containing each of the identified TBEs were generated by PCR and cloned into the Firefly luciferase expressing constructs pGL3-Basic or pGL3-promoter vectors (Figure 5.2a) as described in section 2.8.1. TBEs 6 and 7, and 8, 9 and 10 are found too close to each other, therefore, TBEs 6 and 7 were cloned together as one fragment, and 8, 9 and 10 were also cloned together as another fragment (Figure 5.2a).

The luciferase-expressing constructs containing each of the potential TBEs (Figure 5.2a) were then co-transfected into JEG3 cells as described in section 2.4.2, along with a *TBX1* cDNA expressing plasmid (cloned into pcDNA3.1) and a Renilla luciferase vector (pGL4.7) as a transfection control. A plasmid containing two synthetic T-box binding sites (2xTtkGL2; Zweier et al, 2007) was used as a positive control, whereas the same vector without the T-box sites (tkGL2) was used as a negative control. Cells were co-transfected with the corresponding plasmids and after 48 hours Renilla and Firefly luciferase were measured using the dual-luciferase assay (Promega) as described in section 2.9. Each group was performed in triplicate and each experiment was repeated at least three times.

As can be seen in Figure 5.2b, TBX1 (black bars) is able to bind to the 2xTtkGL2 construct that contains the two synthetic T-box binding sites, and activate luciferase in a robust way as expected, showing a significant 9-fold increase compared to the group co-transfected with an empty plasmid (pcDNA3.1, white bars). The vector lacking the T-box sites (tkGL2) does not show any activation of luciferase in the presence of TBX1 (black bars).

However, TBX1 does not seem to be able to activate luciferase expression in any of the TBE-containing constructs, with the exception of the construct containing TBEs 8, 9 and 10 (TBE-8+9+10), where TBX1 (Figure 5.2b, black bars) causes a significant 2-fold increase ($p<0.01$) compared to the group co-transfected with an empty plasmid (Figure 5.2b, white bars). The graph shown in Figure 5.2b is representative of 3 independent experiments showing the same trend of a significant increase in the TBE-8+9+10 construct.

To confirm this activation was due to actual binding of TBX1 and rule out an artefact of the experiment, one of the potential TBEs within the construct (TBE-8+9+10) was mutated using site-directed mutagenesis as described in section 2.8.4. TBE-9 was chosen because of its correspondence with the putative T-box binding sequence (AGGTGTGAAATT). The core sequence of TBE-9 (AAAGTGTGAG) was changed to AAAAAATGAG (Figure 5.2c), to completely abolish any potential TBX1 binding. As shown in Figure 5.2c, mutation of TBE-9 (TBE-8Δ9+10) abolishes binding of TBX1 and prevents activation of luciferase.

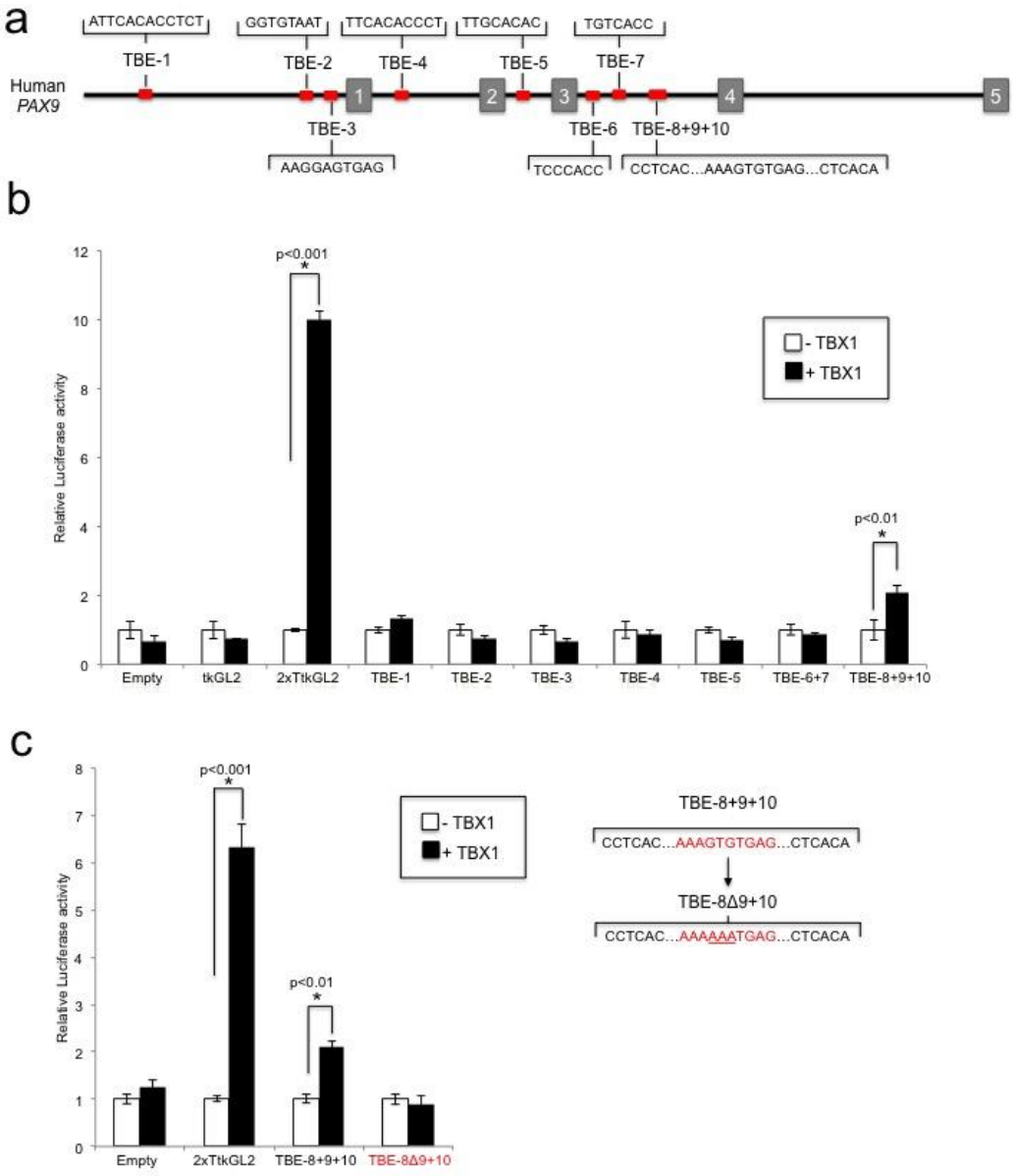

Figure 5.2. Luciferase assays on conserved TBEs within the *PAX9* locus.
(a) The potential TBEs found within the *PAX9* locus were cloned into luciferase expressing vectors, and luciferase assays were performed to assess for *TBX1* binding to any of the identified TBEs **(b)**. A construct containing 2 synthetic T-box binding sites (2xTtkGL2) was used as a positive control, whereas the same vector lacking the T-box elements was used as a negative control. **(b)** TBX1 (black bars) is able to robustly activate luciferase expression in the 2xTtkGL2 reporter causing a significant 9-fold increase ($p<0.001$) compared to the group transfected with the reporter in the absence of TBX1 (white bars). However, TBX1 does not seem to bind any of the identified TBEs as there is no luciferase activation in any of them, except for the last construct containing three TBEs (TBE-8+9+10), on which TBX1 presence caused a significant 2-fold increase in luciferase activity ($p<0.01$). To further validate binding to these TBEs, the middle element (TBE-9) was mutated using site directed mutagenesis to completely change its core sequence **(c)**, and the mutated construct (TBE-8Δ9+10) was then assayed for luciferase activation in the presence of TBX1. **(c)** Mutation of the core sequence of TBE-9 prevents luciferase activation by TBX1. Error bars represent SEM from triplicates of each group, and graphs are representative of three independent experiments. Statistical significance was calculated using a two-paired T-test.

The luciferase results (Figure 5.2) suggested that TBX1 binds to a conserved region within the 3rd intron of the *PAX9* gene. To confirm this *in vivo*, chromatin immunoprecipitation (ChIP) was performed.

Wild-type E9.5 embryos were collected and processed as described in section 2.11. Briefly, embryos were homogenized and fixed in 1% formaldehyde to preserve the DNA-protein interactions. Tissue was then lysed and the chromatin was sonicated into 200-500bp fragments. The sonicated chromatin was then incubated with protein A beads and antibodies raised against TBX1 and phospo-histone H3 (as a positive control) were used to immunoprecipitate the DNA-protein complexes. A rabbit immunoglobulin (IgG), and a sample without antibody and just the protein A beads, were used as negative controls. After immunoprecipitation, the cross-linking was reversed and the precipitated DNA was purified. A sample containing total chromatin (collected prior to immunoprecipitation) was used as the "input".

Immunoprecipitation of the target DNA sequences was assessed by end-point and qPCR (described in section 2.11) using primers (Table 2.7) targeting the previously identified TBEs. A set of primers targeting a random region within the same chromosome as *Pax9* (chromosome 12) but more than 1000 bp away from the *Pax9* gene was used as a negative control for the ChIP to show specificity of the precipitation and efficacy of the sonication.

The end-point PCR (Figure 5.3a) shows a PCR product in the positive controls (gDNA, INPUT and pHH3) as expected. However, amplification in the samples precipitated with a TBX1 antibody (Figure 5.3a, 4th lane) is not evident for most TBEs. Although TBE-1 and TBE-5 show amplification in the sample precipitated with TBX1, this is considered as unspecific amplification, as the IgG and no antibody (no AB) lanes also show amplification. Furthermore, contamination in these samples was ruled out since the water sample (H_2O) does not show any product, which suggests the amplification in the negative controls (IgG and no AB) is due to high background signal of the protein A beads themselves.

To accurately quantify the amount of specific immunoprecipitation and to potentially outstrip the background signal qPCR was performed. ChIP samples were amplified using SYBR green; the target samples were normalised with the INPUT sample and plotted as a percentage of the INPUT (total chromatin) as described in section 2.6. The qPCR results show that Tbx1 does not bind any of the potential TBEs as there is no specific amplification with any of them. Although TBE-5 and TBE-8+9+10 show a noticeable increase compared to the other TBEs, this amplification is not specific as it is similar to that seen in the IgG sample.

The ChIP experiment was repeated a second time with a different batch of embryos showing the same result, with no specific amplification of any of the TBEs and a high background signal of TBE-5 (Appendix B).

Chromatin immunoprecipitation requires large amounts of tissue to be able to obtain significant and detecTable amounts of chromatin after the precipitation, and typical ChIP protocols are designed to be performed from cells in culture.

To determine whether the high background signal seen in the previous ChIP experiments was due to insufficient starting tissue, a third ChIP experiment was performed from mouse embryonic fibroblast (MEFs) obtained from E13.5 embryos as described in section 2.7.2, using 5µg of chromatin (5 times more compared to embryonic tissue).

Chromatin immunoprecipitation from MEFs showed the same result as the previous experiments with no specific amplification of any of the TBEs and a high background signal of TBE-5 (Appendix B).

Three independent ChIP experiments show Tbx1 does not bind to any of the previously identified potential TBEs *in vivo*. Although the results from the luciferase assays and the ChIP are reproducible and consistent, both were targeted to specific regions of the *PAX9* locus based on the predicted TBEs.

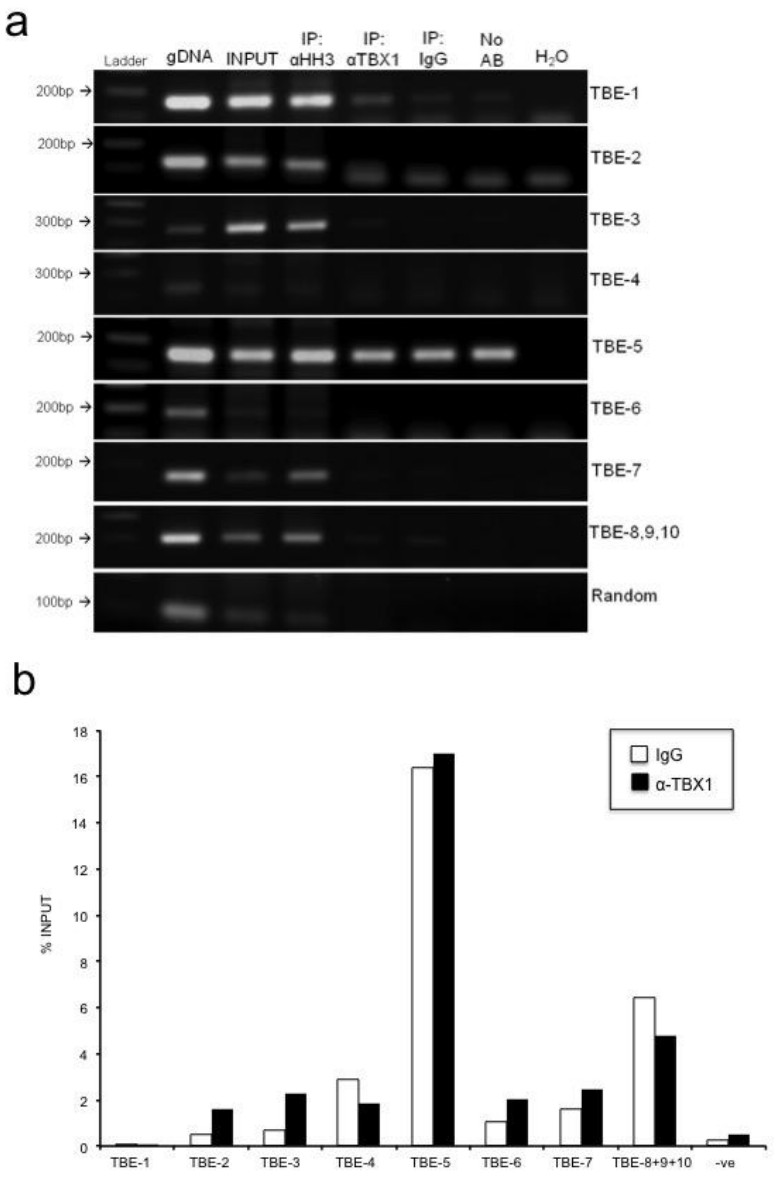

Figure 5.3. Chromatin immunoprecipitation of conserved TBEs within the *Pax9* locus.
Chromatin immunoprecipitation from E9.5 embryos was performed using an anti-TBX1 antibody and specific primers targeting the identified TBEs.
End-point PCR **(a)** and qPCR **(b)** were performed on immunoprecipitated samples. No binding was detected in any of the conserved TBEs; although TBE-5 appears to be amplified by end-point and qPCR, the IgG sample was also amplified, suggesting such amplification is not specific to Tbx1 immunoprecipitation. A sample immunoprecipitated with an anti-histone H3 antibody was used as a positive control for the immunoprecipitation procedure, whereas a sample incubated with an IgG and protein A/G beads only (no AB) were used as negative controls. Genomic DNA (gDNA) was used as positive control for the PCR, whereas a sample with no DNA and only water (H_2O) was used a negative control of the PCR. Primers targeting a random region within chromosome 12 distal to Pax9 gene were used as control for specificity of immunoprecipitation. For qPCR analysis, samples were run in triplicate and the average of each sample was calculated. TBX1 and IgG samples were then normalised with the INPUT and plotted as a percentage of INPUT.

To determine whether Tbx1 could potentially bind any other region of the *Pax9* locus, a 5kb fragment of the *Pax9* promoter, and the 2nd and 3rd introns of the *Pax9* gene were cloned into luciferase plasmids (Figure 5.4a). The promoter itself and the promoter plus the 2nd or 3rd intron were cloned into pGL3-basic, while the introns alone were cloned into pGL3-promoter downstream of luciferase (Figure 5.4a).

These constructs were co-transfected into JEG3 cells along with a Tbx1 expressing construct and a Renilla plasmid, and binding of Tbx1 to any of these constructs was assessed.

The luciferase assays on the constructs containing 5kb of the *Pax9* promoter and the 2nd and 3rd introns of the *Pax9* gene (Figure 5.4) show no activation of luciferase in any of the constructs suggesting that TBX1 does not bind anywhere within these regions of the promoter and the 2nd and 3rd introns (Figure 5.4).

The results from luciferase experiments with the promoter and intronic regions or the isolated predicted TBEs, together with the chromatin immunoprecipitation results indicate Tbx1 does not regulate *Pax9* expression by directly binding to elements within the *Pax9* locus.

Although *Pax9* expression is affected by loss of *Tbx1* (Ivins et al, 2005; Liao et al, 2008) the results show this regulation is not through direct binding of Tbx1 to the *Pax9* locus, suggesting Tbx1 may indirectly regulate *Pax9* expression through directly regulating expression of other genes upstream of *Pax9*.

However, the results presented in chapter 4 show a clear specific interaction between *Pax9* and *Tbx1* for the formation of the 4th PAAs and their derivatives.

Given that there is no direct interaction between Tbx1 and the *Pax9* gene as shown in this section, it was next hypothesised that Pax9 and Tbx1 interaction may occur at the protein level.

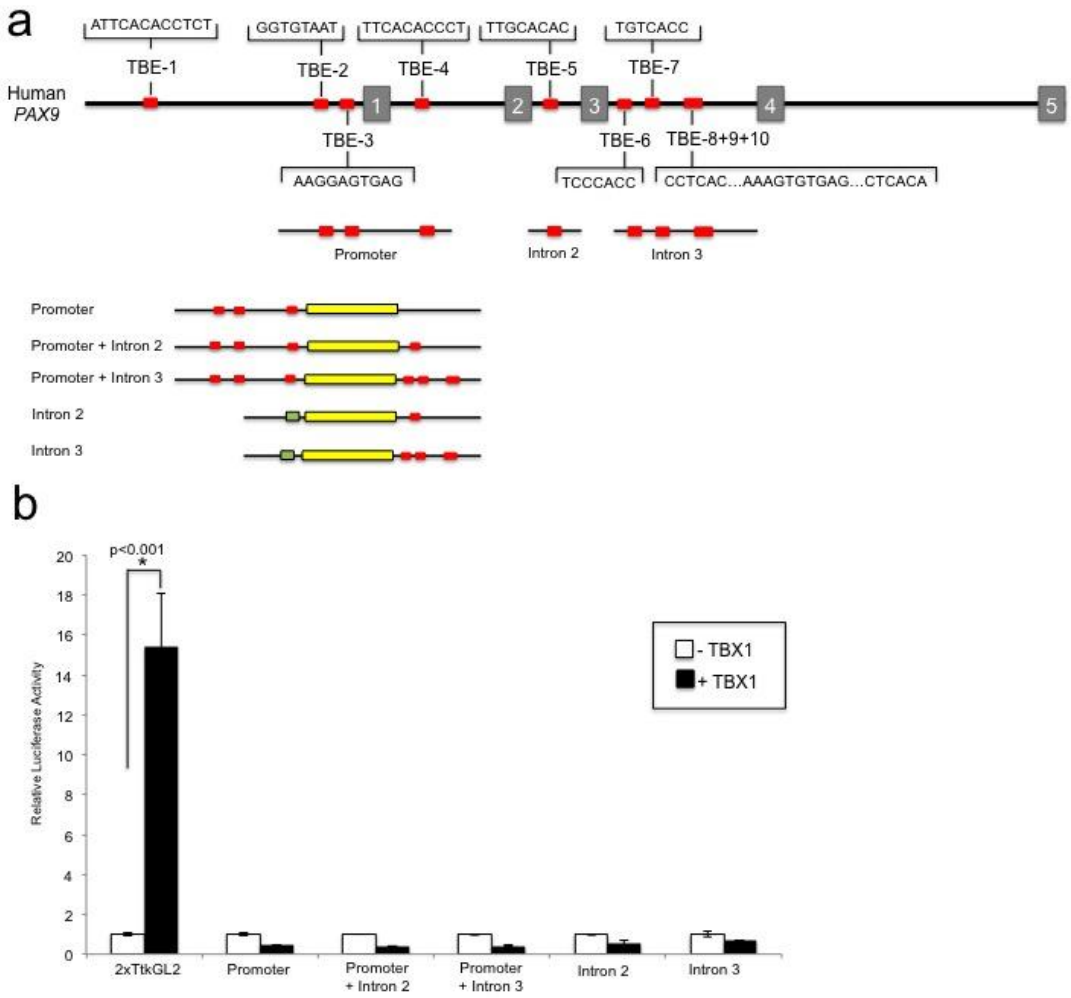

Figure 5.4. Luciferase assays on *Pax9* promoter and introns.
(a) A 5Kb region of the promoter and the 2nd and 3rd introns containing the conserved TBEs were cloned into luciferase expressing vectors. The promoter itself, or along with the 2nd or 3rd introns downstream of luciferase were generated to test for TBX1 binding to any of these constructs. Additionally, the introns without the promoter were also cloned downstream of luciferase as enhancers.
(b) Luciferase assays using these constructs was performed with (black bars) or without (white bars) TBX1. TBX1 is able to robustly activate luciferase expression in the 2xTtkGL2 reporter causing a significant 14-fold increase ($p<0.001$) compared to the group transfected without TBX1 (white bars). Luciferase activity was not detected in any of the constructs containing the promoter and introns. Error bars represent SEM from triplicates of each group, and the graph is representative of three independent experiments. Statistical significance was calculated using a two-paired T-test.

5.3 Investigating A Physical Interaction Between Tbx1 And Pax9 Proteins

As a second hypothesis for the interaction between *Tbx1* and *Pax9*, a physical interaction between Tbx1 and Pax9 proteins was proposed.

As a first approach to assess whether Pax9 affects Tbx1 transcriptional activity, Tbx1 was co-transfected with Pax9 in a luciferase assay, using the 2xTtkGL2 construct as a reporter for Tbx1 activity.

JEG3 cells were co-transfected with different concentrations (0, 0.01, 0.05, 0.1, 0.25, 0.5, and 1 µg) of a Pax9-expressing construct and 0.25 µg of a Tbx1-expressing plasmid. Each group was performed in triplicate and the experiment was repeated at least 3 times. Samples were normalised with the Renilla luciferase measurements as a transfection control, and plotted relative to the group transfected with Tbx1 alone, which was set as 100% of 2xTtkGL2 activation.

As seen in Figure 5.5a, Pax9 prevents Tbx1 luciferase activation in a dose-dependent manner, with the lowest dose of Pax9 (0.01µg) repressing about 40% of luciferase activation by Tbx1, while 0.1ug of Pax9 represses almost completely luciferase activation as it is not significantly different from the groups transfected with an empty plasmid (i.e. no Tbx1 or Pax9, only pcDNA3.1). To show specificity of Pax9 repression over Tbx1, one group was co-transfected with Tbx1 and AP2α; co-transfection with AP2α does not affect Tbx1 transcriptional activity (Figure 5.5a, grey bar).

To confirm that the observed repression of Tbx1 activity was an actual effect and not an artefact of the co-transfection, co-expression of both Pax9 and Tbx1 in the same cells was detected by immunocytochemistry (described in section 2.10) using antibodies against Pax9 and Tbx1. As shown in Figure 5.5b both Pax9 (green) and Tbx1 (red) are co-expressed within the same cells (Figure 5.5b).

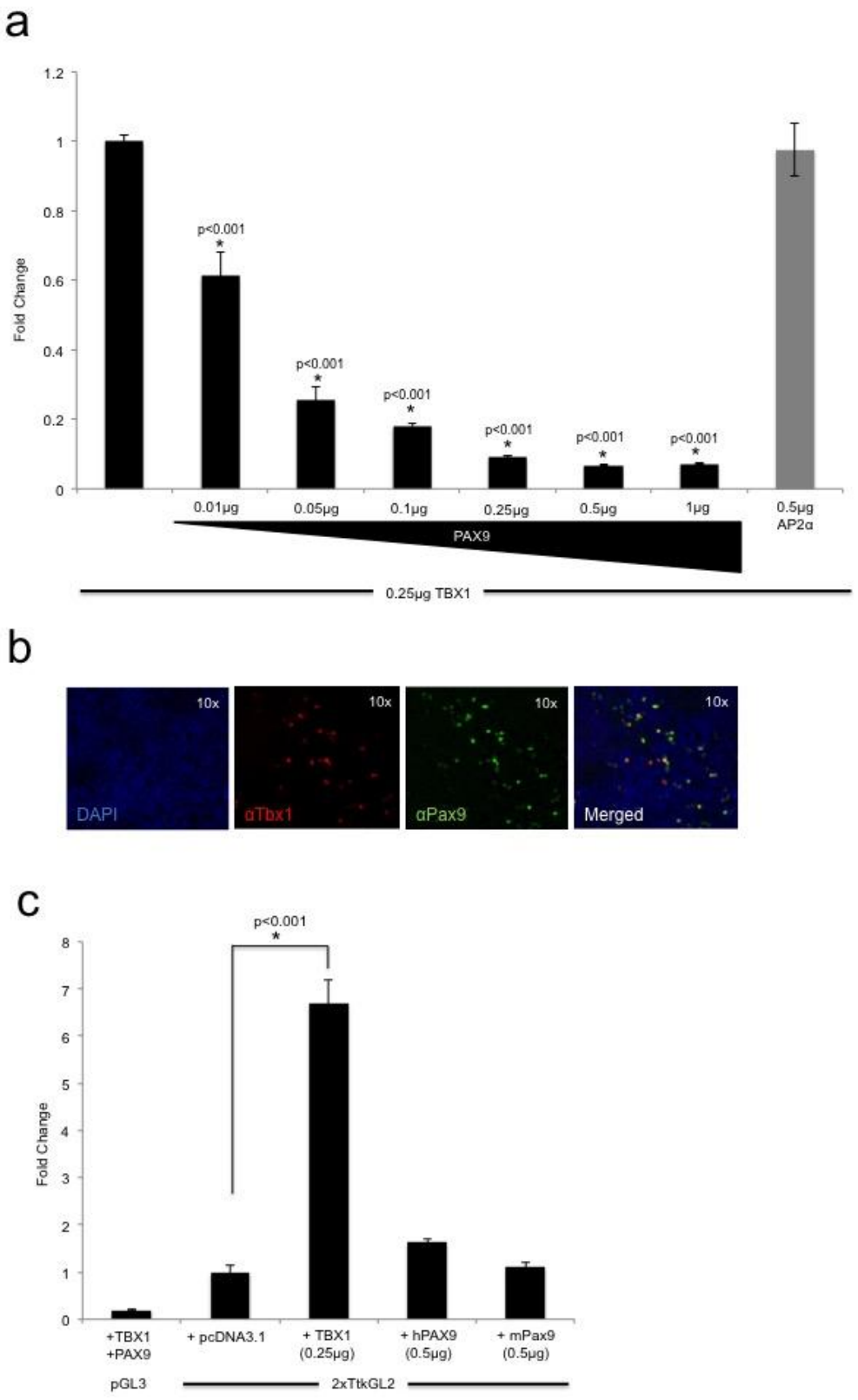

Figure 5.5. Co-transfection of PAX9 and TBX1 and Luciferase assays.
(a) To determine whether PAX9 affects TBX1 transcriptional activity, TBX1 was co-transfected with different concentrations (0.01, 0.05, 0.1, 0.25, 0.5 and 1µg) of PAX9 in a luciferase assay, using the 2xTtkGL2 construct as a reporter for TBX1 activity. DNA concentration in all samples was topped up to 2µg with the empty vector. Samples were normalised to the group transfected with TBX1 alone and plotted as the fold change over TBX1 activity. PAX9 prevents TBX1 luciferase activation in a dose-dependent manner, with the lowest dose of PAX9 (0.01µg)

significantly repressing about 40% of luciferase activation ($p<0.001$) compared to the group transfected with TBX1 only.
(b) co-expression of TBX1 and PAX9 within the same cells was detected by double immunocytochemistry of co-transfected cells with an anti-Tbx1 (red) and anti-Pax9 (green); merged image shows co-localization (yellow) of Tbx1 and Pax9 proteins within the same cells. **(c)** a luciferase assay from cells transfected only with human PAX9 (hPAX9) or mouse Pax9 (mPax9) shows Pax9 itself does not activate luciferase in the 2xTtkGL2 reporter construct. Error bars represent SEM from triplicates of each group, and the graphs are representative of three independent experiments. Statistical significance was calculated using a two-paired T-test.

Furthermore, Pax9 itself does not activate luciferase in the 2xTtkGL2 reporter construct (Figure 5.5c), indicating the transcriptional repression is due to an effect over Tbx1 activity and not due to competition over the 2xTtkGL2 binding sites. Additionally, Tbx1 and Pax9 are highly conserved between mouse and human, therefore both mouse and human plasmids have the same effects, with both human and mouse Tbx1 being able to robustly activate the 2xTtkGL2 reporter, and both human and mouse Pax9 having similar repressive activity over Tbx1 transcriptional function (Figure 5.5c).

These results suggest Pax9 interferes in some way with Tbx1 transcriptional activity. To determine whether Pax9 prevents Tbx1 binding to the DNA, chromatin immunoprecipitation was performed from JEG3 cells co-transfected with Tbx1 and increasing doses of Pax9 as assayed before in the luciferase assay.

Cells were co-transfected, fixed in 1% formaldehyde and lysed. Chromatin was then sonicated as described before and samples were incubated with an anti-TBX1 antibody, an IgG isotype control or protein A beads only. DNA was then purified and immunoprecipitation was assessed by end-point PCR using specific primers (Table 2.7) targeting the two T-box binding sites within the 2xTtkGL2 construct.

The result from the ChIP on the 2xTtkGL2 plasmid co-transfected with Tbx1 and increasing doses of the Pax9-expressing vector show that Pax9 does not affect Tbx1 binding to the 2xTtkGL2 construct (Figure 5.6) but instead just averts luciferase transcription.

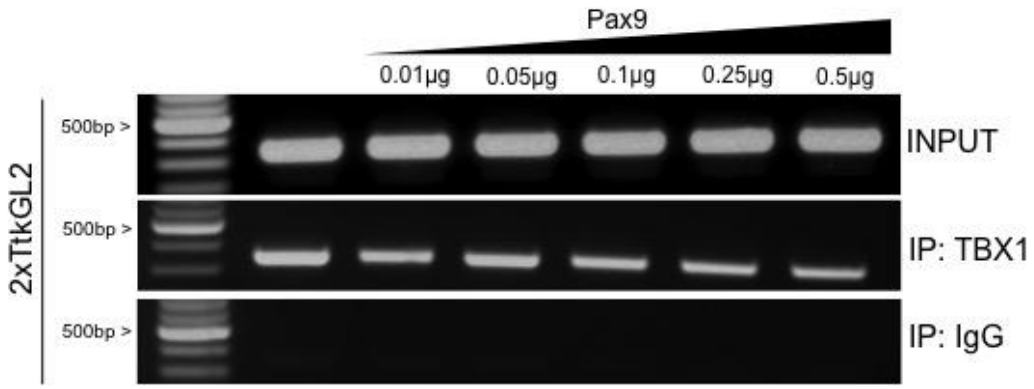

Figure 5.6. Chromatin immunoprecipitation of the 2xTtkGL2 construct from co-transfected cells.
To determine whether Pax9 prevents Tbx1 binding to the DNA, ChIP targeting the 2 synthetic T-box sites within the 2xTtkGL2 reported was performed from co-transfected cells with TBX1 and different concentrations (0.01, 0.05, 0.1, 0.25, 0.5µg) of PAX9. Immunoprecipitation of the DNA of interest was assessed by end-point PCR. PCR results show PAX9 does not interefere with DNA binding to the 2xTtkGL2 construct since an amplification product is detecTable in the samples immunoprecipitated with an anti-TBX1 antibody, whereas the IgG samples used as negative controls for the IP do not show any amplification product.

Pax9 has been previously reported to act as a repressor (Nornes et al, 1996; Tan et al, 2003). In this context, a conserved sequence within the Pax9 protein named the VP motif was found to directly interact with PLU-1 protein; this interaction has a repressive effect *in vitro*, whereas mutation or deletion of the VP motif completely disrupts this interaction and the repressive capacity *(*Nornes et al, 1996; Tan et al, 2003).

Therefore, to try to understand the repressive mechanism of Pax9 over Tbx1, a second approach was to prevent the repressive activity of Pax9.

The human PAX9 protein sequence was aligned with the mouse, rat, monkey, chicken, frog and zebrafish sequence to identify conserved residues within the VP motif. The PAX9 VP motif is highly conserved (Figure 5.7a) between human, mouse, rat and monkey, however, chicken pax9 presents one amino acid change, whereas frog and zebrafish have only 60% homology with human PAX9 (Figure 5.7a).

The amino acid changes in zebrafish pax9 modifiy the secondary structure according to the predicted structure (Figure 5.7b) using Geneious software (Biomatters).

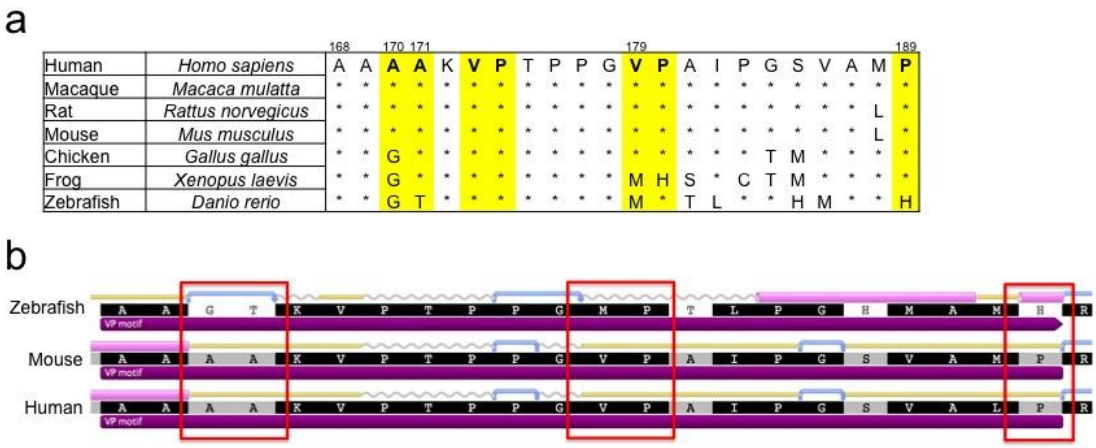

Figure 5.7. Alignment of the PAX9 protein sequence and conservation of the VP motif.
(a) Human PAX9 protein sequence was aligned with the mouse, rat, monkey, chicken, frog and zebrafish sequence to identify conservation of the VP motif. The PAX9 VP motif is highly conserved between human, mouse, rat and monkey. Chicken pax9 presents one amino acid change, whereas frog and zebrafish have only 60% homology with human PAX9.
(b) The secondary structure of human, mouse and zebrafish pax9 was predicted using Geneious software (Biomatters); the different residues in zebrafish pax9 present a different secondary structure compared to human and mouse (red boxes).

Given that precise protein folding and secondary structure are critical for protein-protein interactions, zebrafish pax9 was co-transfected with TBX1 in a luciferase assay to determine whether zebrafish pax9 can also repress TBX1 activity.

Zebrafish pax9 is also capable of repressing TBX1 activity (Figure 5.8a), suggesting the different residues and possible change in the secondary structure of the Pax9 protein do not affect Pax9 repressive activity.

To finally determine whether the VP motif is required for the repressive activity of Pax9 over Tbx1, the VP motif was completely deleted by mutagenesis using PCR as described in section 2.8.4. The repressive capacity of Pax9 without the VP motif was tested by luciferase assays. As seen in Figure 5.8b, the VP motif is not necessary for Pax9 repression over Tbx1, as Pax9 without the VP motif shows the same repression as wild-type Pax9 (Figure 5.8b). Additionally, to show specificity of this repression among other Pax family members, TBX1 was co-transfected with Pax1. As seen in Figure 5.8b, Pax1 does not significantly affect TBX1 activity, suggesting the repression is highly specific for PAX9.

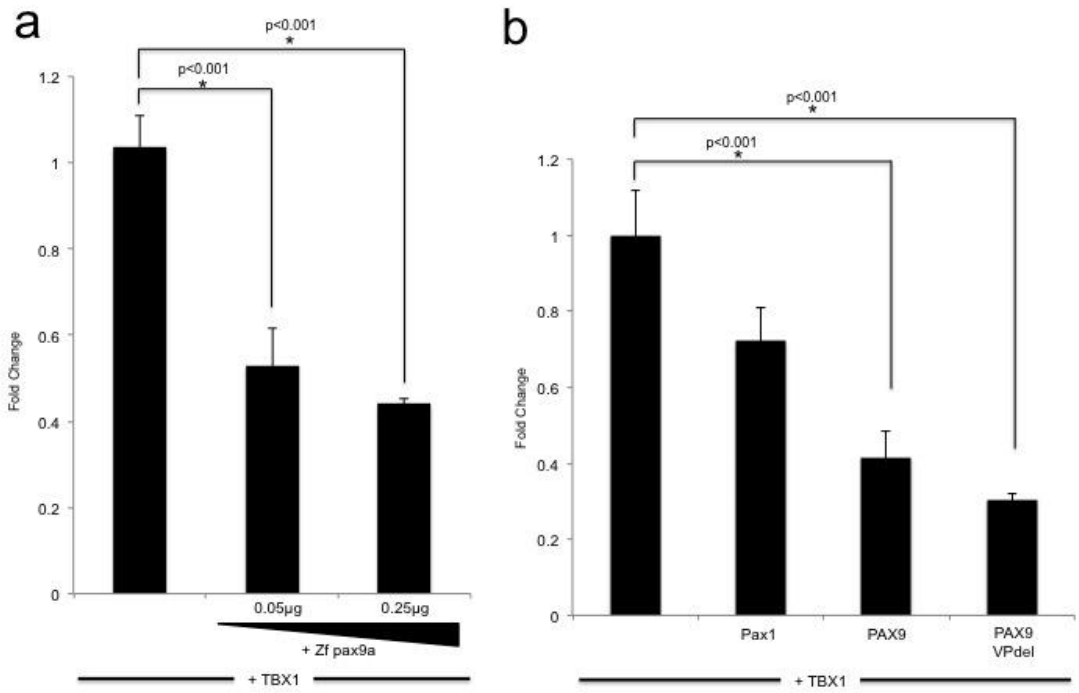

Figure 5.8. Luciferase assays of co-transfected cells with TBX1 and zebrafish pax9, and VP motif deletion.

(a) To determine whether the amino acid changes in zebrafish pax9 and possible change in the secondary structure, TBX1 was co-transfected with 0.05 and 0.25µg of zebrafish pax9 (Zf pax9a) in a luciferase assay. Zebrafish pax9 is able to repress TBX1 activity as luciferase activity was significantly reduced to 50% ($p<0.001$) in the presence of Zfpax9.

(b) The VP motif was deleted and Pax9 lacking the VP motif (PAX9-VPdel) was co-transfected with TBX1 in a luciferase assay. Deletion of the VP motif does not affect PAX9 repression over TBX1 as luciferase activity was significantly reduced to 30% ($p<0.001$) in the presence of PAX9-VPdel, similarly to wild-type PAX9. One group co-transfected with TBX1 and Pax1 was included showing Pax1 does not affect luciferase activation by TBX1. Error bars represent SEM from triplicates of each group, and the graphs are representative of three independent experiments. Statistical significance was calculated using a two-paired T-test.

Given that complete deletion of the VP motif does not affect Pax9 repressive capacity over Tbx1 transcriptional activity, a second approach to try to prevent this repression was to mutate Tbx1. This approach has a direct implication with human pathology as patients with cardiovascular malformations presenting mutations in *TBX1* have been previously reported (Zweier et al, 2007).

Four mutations in *TBX1* have been reported to cause 22q11DS-like phenotypes; three mutations (F148Y, H194Q, G310S) are located within the T-box domain and are known to cause a gain-of-function of TBX1, whereas the fourth, a cysteine deletion (1223delC) causes a complete loss of function of TBX1 due to deletion of a C-terminal nuclear localization signal (Zweier et al, 2007).

Furthermore, crystallography analysis of TBX1 structure revealed phenylalanine 148 (F148) to be exposed at the surface of the TBX1 protein and not at the DNA binding interface (El Omari et al, 2012). Additionally, given that hydrophobic residues are typically involved in protein-protein interactions it has been proposed F148 is required for interactions with other proteins. This therefore suggests that the F148Y mutation affects TBX1 interaction with other proteins (El Omari et al, 2012).

The *TBX1* mutated constructs (F148Y, H194Q, G310S, 1223delC) were used in a luciferase assay in the presence of PAX9 to determine whether any of these mutations prevents PAX9 repression of TBX1.

The F148Y, H194Q and G310S mutated versions of TBX1 can robustly promote luciferase expression, while F148Y and G310S constructs displayed a further significant increase in luciferase activity compared to wild-type TBX1, showing a gain-of-function due to mutation, whereas truncation mutation 1223delC showed complete loss of function (Figure 5.9, white bars) as previously reported by Zweier and colleagues (2007).

However, none of these mutations prevented the repression by PAX9 as they all showed a significant decrease in luciferase expression in the presence of PAX9 (black and grey bars, Figure 5.9).

These results suggest none of these residues are involved in any potential interaction with PAX9, as their mutations do not affect PAX9 repressive activity.

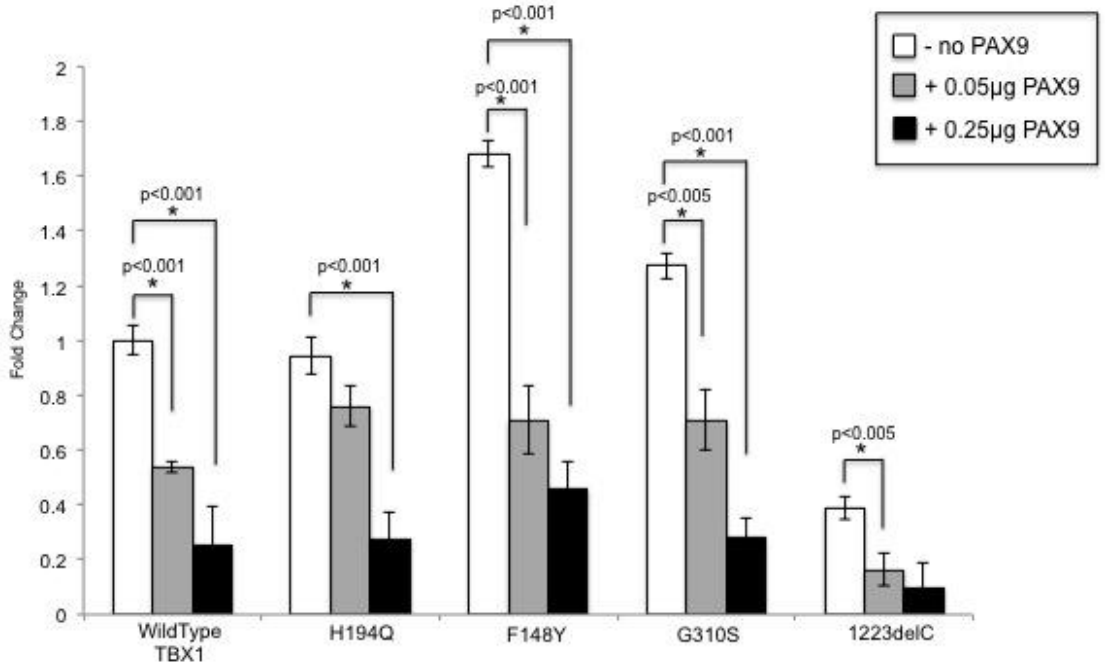

Figure 5.9. Luciferase assays on mutated TBX1.
Luciferase assays from cells co-transfected with 0.05 (grey bars) and 0.25µg (black bars) of PAX9 and human mutations of TBX1 shows F148Y, H194Q and G310S constructs can significantly promote luciferase expression (white bars), while F148Y and G310S constructs displayed a further significant increase compared to wild-type TBX1; whereas truncation mutation 1223delC showed complete loss of function with a 78% reduction in luciferase expression compared to wild-type TBX1. However, PAX9 can significantly repress this activity. Error bars represent SEM from triplicates of each group, and the graphs are representative of three independent experiments. Statistical significance was calculated using a two-paired T-test.

To this point, the interaction between Pax9 and Tbx1 at the functional level appears to be very robust with Pax9 showing a high capacity to repress Tbx1 activity *in vitro* in various luciferase assays. Therefore, to confirm this interaction between Tbx1 and Pax9, co-immunoprecipitation was performed (as described in section 2.12) *in vitro* and *in vivo.*

JEG3 cells co-transfected with Pax9 and Tbx1, and E9.5 mouse embryos, were immunoprecipitated using protein A/G beads and antibodies raised against TBX1 and PAX9. Following immunoprecipitation, Western blotting for both Tbx1 and Pax9 was performed for all samples.

Co-immunoprecipitation revealed that Tbx1 and Pax9 do not bind to each other as seen in Figure 5.10, where Pax9 is only detectable by western blot in the samples precipitated with a Pax9 antibody (Figure 5.7 lanes 3 and4) but not in samples precipitated with the Tbx1 antibody (Figure 5.7 lanes 1 and 2) in both JEG3 cells and E9.5 embryos. Similarly, Tbx1 is only detectable by western blot in the samples precipitated with the Tbx1 antibody but not in those precipitated with the Pax9 antibody.

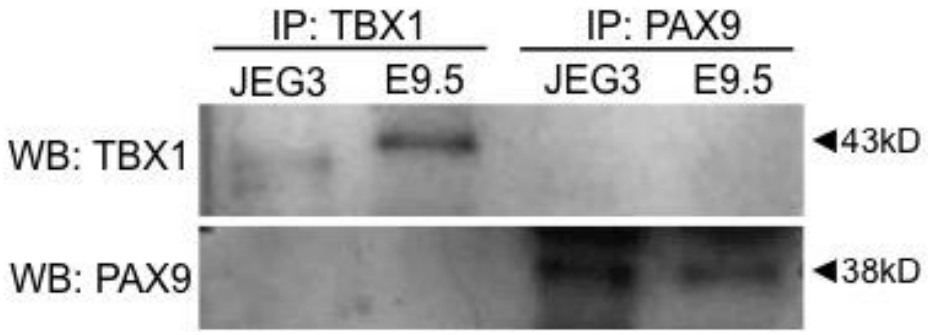

Figure 5.10. Co-immunoprecipitation of Tbx1 and Pax9.
To determine whether Tbx1 and Pax9 physically interact, co-IP was performed from wild-type E9.5 embryos (E9.5) and co-transfected JEG3 cells. Samples were immunoprecipitated with antibodies anti-TBX1 (lanes 1 and 2) or anti-PAX9 (lanes 3 and 4) and immunoblotted against both TBX1 (top panel) and PAX9 (bottom panel). Tbx1 can be detected by western blot in samples immunoprecipitated with an anti-TBX1 antibody, but not in those immunoprecipitated with anti-PAX9 antibody; whereas Pax9 is not detected in samples IP with anti-TBX1 antibody but is clearly detected after IP with an anti-PAX9 antibody. Tbx1 expected band was 43kDa, and Pax9 expected band was 38kDa.

Chromatin immunoprecipitation showed Tbx1 does not bind to the *Pax9* locus as a direct target (Figure 5.11a), while co-immunoprecipitation shows Tbx1 and Pax9 do not physically interact with each other (Figure 5.11b). However, Tbx1 transcriptional repression by Pax9 seen in luciferase assays is very robust, indicating some form of functional interaction, in addition to the genetic interaction discussed in chapter 4. Therefore, as a third hypothesis to explain the interaction between Tbx1 and Pax9, the possibility of both acting on a common downstream target (Figure 5.11c) was analysed.

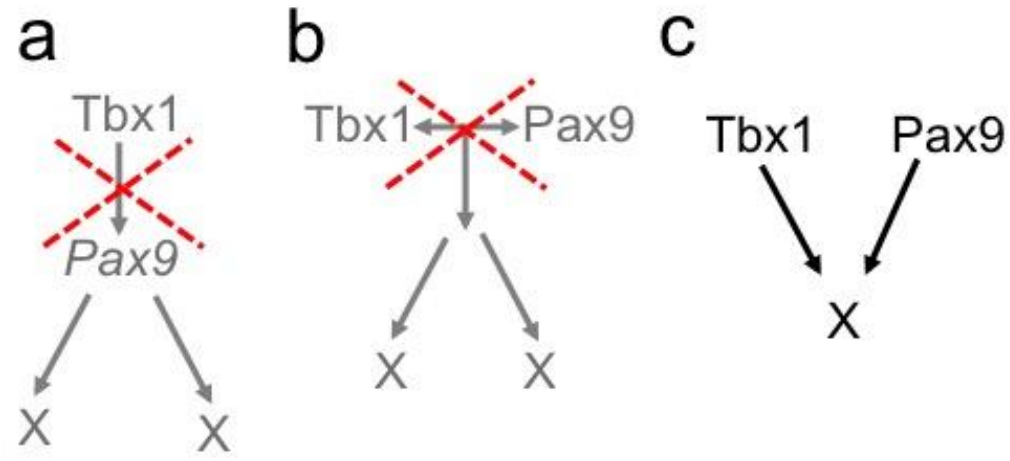

Figure 5.11. Proposed mechanism of interaction.
(a) Direct regulation of *Pax9* expression through direct binding of Tbx1 to potential T-box binding elements within the Pax9 locus was initially proposed but excluded based on the chromatin immunoprecipitation results in section 5.2.
(b) A physical interaction at the protein level between Pax9 and Tbx1 was proposed as a second hypothesis for the interaction, but has been excluded based on the co-immunoprecipitation experiments in section 5.3.
(c) The possibility of both Tbx1 and Pax9 acting on a common downstream target is proposed as a third hypothesis to explain the interaction

5.4 Exploring *Gbx2* As A Common Downstream Target Of Tbx1 And Pax9

Given that a direct interaction between Tbx1 and the Pax9 gene was ruled out by chromatin immunoprecipitation (section 5.2), and a physical interaction between Pax9 and Tbx1 proteins was also excluded (section 5.3), the potential of Tbx1 and Pax9 acting on a common downstream target was analysed.

Preliminary results in our group from a candidate gene analysis of 40 genes involved in cardiovascular development and/or expressed within the pharyngeal endoderm, revealed that *Gbx2*, *Ripply3* and *Gata5* were significantly downregulated in *Pax9*-null embryo pharyngeal arches. However, only *Gbx2* was also found to be downregulated in double heterozygous embryos (*Tbx1*$^{+/-}$;*Pax9*$^{+/-}$).

Gbx2 is downregulated about 30% in *Pax9*-null embryos and about 50% in double heterozygous embryos (*Tbx1*$^{+/-}$;*Pax9*$^{+/-}$) at E9.5 as analysed by qPCR (Figure 5.12; Simon Bamforth, unpublished data).

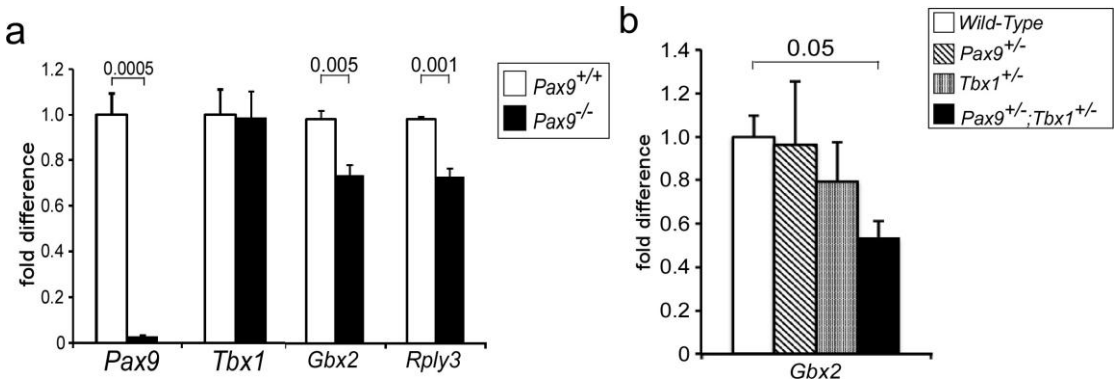

Figure 5.12. *Gbx2* mRNA levels are reduced in *Pax9*-null and double heterozygous embryos.
(a) qPCR from the dissected pharyngeal region of E9.5 *Pax9*-null embryos (black bars) revealed a significant 30% down-regulation of *Gbx2* ($p<0.005$) and Ripply3 ($p<0.001$) compared to wild-type embryos (white bars).
(b) qPCR from the dissected pharyngeal region of E9.5 double heterozygous embryos (*Pax9*$^{+/-}$;*Tbx1*$^{+/-}$) (black bars) shows a significant 55% down-regulation of *Gbx2* ($p<0.05$) compared to wild-type embryos (white bars); while *Gbx2* mRNA levels were not different in *Pax9*$^{+/-}$ or *Tbx1*$^{+/-}$ embryos. Error bars represent SEM from triplicates of each group. Statistical significance was calculated using a two-paired T-test. (Simon Bamforth, unpublished data).

Gastrulation brain homeobox 2 gene (*Gbx2*) encodes a homeobox transcription factor known to be required for the specification of the mid/hindbrain regions (Wassarman et al, 1997; Martinez, 2001). *Gbx2* is expressed in the region caudal to the midbrain (Wassarman et al, 1997; Martinez, 2001) as well as within the pharyngeal arches between E8.5 and E10.5 (Wassarman et al, 1997; Waters et al, 2003).

Gbx2-null mice die soon after birth with forebrain and cerebellar defects (Wassarman et al, 1997) and these defects are mainly due to a significant reduction in proliferation and survival of anterior hindbrain precursors (Wassarman et al, 1997). Furthermore, homozygous loss of *Gbx2* also affects neural crest cell (NCC) migration leading to a reduced number of NCC within the caudal pharyngeal arches, consequently affecting the development of the PA-derived structures including cranial nerves, the middle ear bones and the 4th PAAs (Byrd and Meyers, 2005).

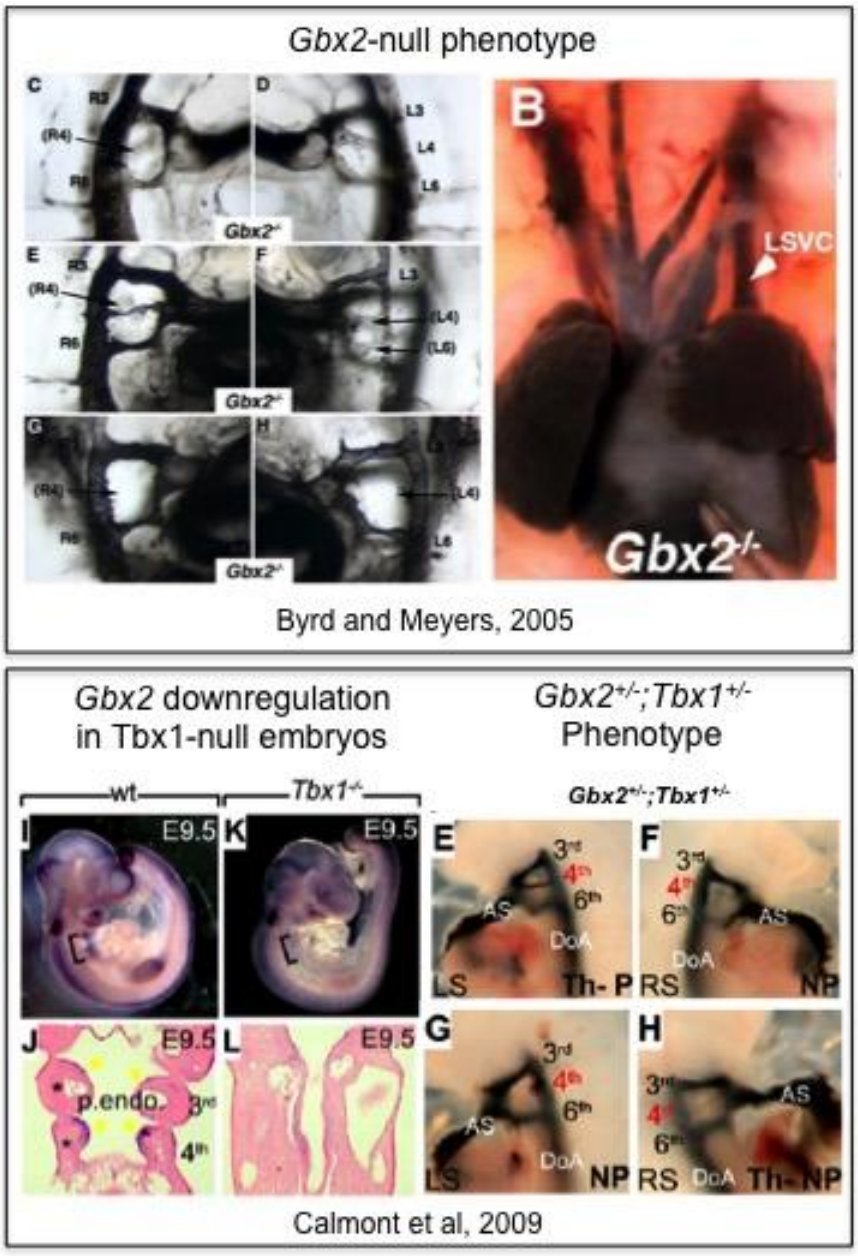

Figure 5.13. *Gbx2*-null and *Gbx2*$^{+/-}$;*Tbx1*$^{+/-}$ phenotypes.
Gbx2-null and double heterozygous embryos (*Gbx2*$^{+/-}$;*Tbx1*$^{+/-}$) present with 4th PAA defects, such as hypoplastic or non-patent vessels unilateral or bilaterally. Additionally, *Gbx2* mRNA levels are visibly decreased in *Tbx1*$^{-/-}$ embryos.
(Adapted from Byrd and Meyers, 2005 and Calmont et al, 2009)

Gbx2-null embryos present with similar cardiovascular defects as those seen in *Tbx1*$^{+/-}$;*Pax9*$^{+/-}$ embryos including IAA and ARSA derived from abnormal formation of the 4th PAAs (Figure 5.13a, Byrd and Meyers, 2005). Furthermore, *Gbx2* was also found to genetically interact with *Tbx1* as double heterozygous embryos (*Tbx1*$^{+/-}$;*Gbx2*$^{+/-}$) show a significant increase in penetrance of 4th PAAs defects (Figure 5.13b, Calmont et al, 2009).

The 4th PAAs defects seen in *Gbx2*-null and *Tbx1*$^{+/-}$;*Gbx2*$^{+/-}$ embryos are due to defective migration of NCC towards the PAs as previously mentioned. This abnormal migration is due to loss of Slit/Robo signalling in NCC, which is critical for their migration (Calmont et al, 2009), although neither *Tbx1* nor *Gbx2* are expressed in NCC.

The similarity between *Gbx2*-null, *Tbx1*$^{+/-}$;*Gbx2*$^{+/-}$ and *Tbx1*$^{+/-}$;*Pax9*$^{+/-}$ embryos specifically affecting the development of the 4th PAA suggest *Gbx2* could potentially be within the same genetic network as *Tbx1* and *Pax9*.

Byrd and Meyers (2005) previously suggested that *Gbx2* expression was regulated indirectly by Tbx1 through Fgf8, however, Caprio and Baldini (2014) have recently shown that *Gbx2* is a direct target of Tbx1, where Tbx1 directly binds to a T-box binding element found downstream of the 2nd exon of the *Gbx2* gene (Caprio and Baldini, 2014).

Therefore, as a third hypothesis to explain the genetic interaction between *Tbx1* and *Pax9*, Gbx2 was proposed as a common downstream target of both Tbx1 and Pax9.

To test this hypothesis, the downregulation of *Gbx2* in double heterozygous embryos (*Tbx1*$^{+/-}$;*Pax9*$^{+/-}$) was confirmed by *in situ* hybridisation in E9.5 embryos (3 embryos per genotype). As seen in Figure 5.14d, *Gbx2* expression is notably reduced in double heterozygous embryos (*Tbx1*$^{+/-}$;*Pax9*$^{+/-}$) and not significantly affected in *Pax9* nor *Tbx1* heterozygotes (Figure 5.14b, c), corroborating the downregulation of *Gbx2* identified previously by qPCR (Figure 5.12).

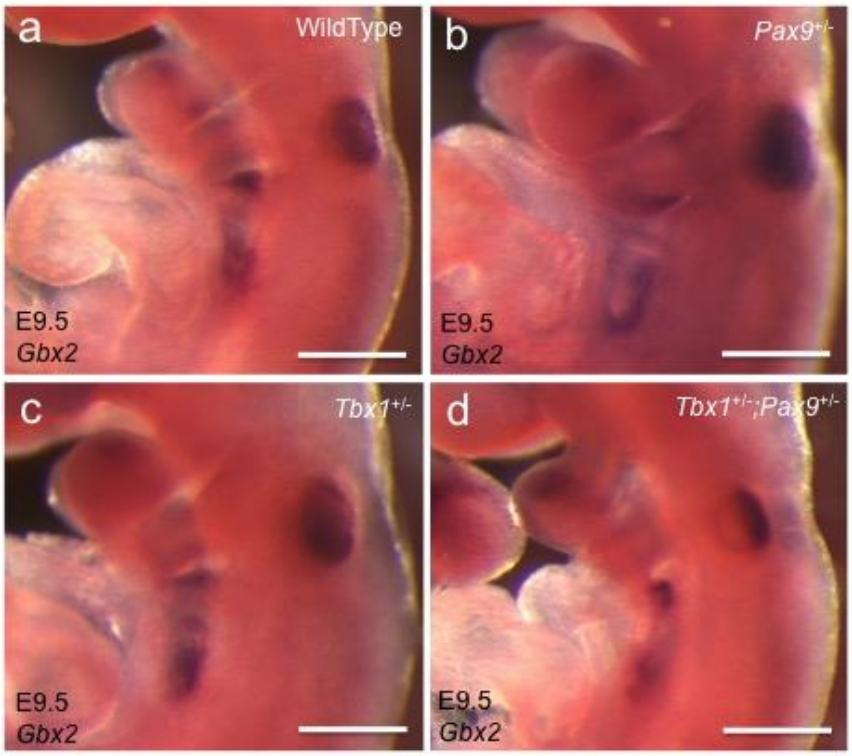

Figure 5.14. *Gbx2* mRNA levels are visibly reduced in E9.5 double heterozygous embryos. Whole-mount in situ hybridisation using a *Gbx2* riboprobe was performed to further confirm *Gbx2* down-regulation in double heterozygous embryos. *Gbx2* mRNA levels appear visibly reduced within the pharyngeal region of double heterozygous embryos **(d)** compared to wild-type **(a)**, *Pax9*$^{+/-}$ **(b)** and *Tbx1*$^{+/-}$ **(c)** embryos at E9.5 (n=3 per genotype). Scale bar, 500μm.

Knowing that Gbx2 is significantly downregulated in double heterozygotes, to determine whether both Tbx1 and Pax9 directly regulate *Gbx2* expression, the *Gbx2* locus was analysed using MultiTF software as previously described to search for potential T-box binding elements (TBE) and Pax-binding sites.

MultiTF analysis revealed two putative Pax-binding sites (Pax) within a 490bp region found 2.5kb downstream of the 2nd exon of *Gbx2* (Figure 5.15a); interestingly this region is highly conserved between human and mouse with 99% homology. Within this region, one T-box binding site (TBE) was also found (Figure 5.15a), corresponding to the one previously identified by Caprio and Baldini (2014).

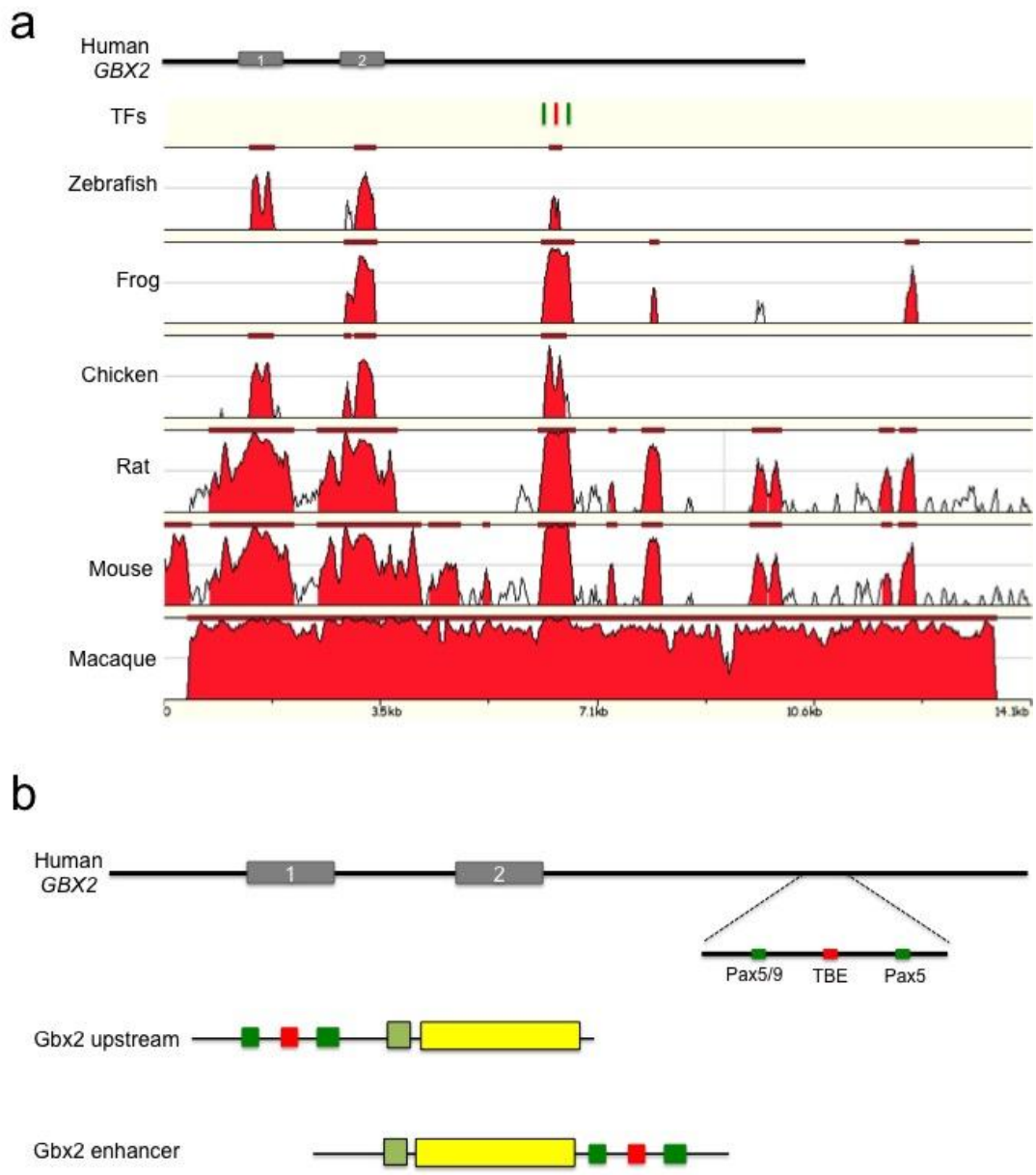

Figure 5.15. Alignment and identification of conserved potential TBEs and Pax-binding sites within the *GBX2* locus.

(a) Human *GBX2* locus was aligned with Macaque, Rat, Mouse, Chicken, Frog and Zebrafish *Gbx2* using the Mulan online tool (http://mulan.dcode.org); the alignment was then used in MultiTF analysis tool to look for conserved potential T-box binding sites and Pax-binding sites. Two putative Pax-binding sites (green lines) were identified within a 490bp highly conserved region found 2.5kb downstream of exon 2 of *Gbx2* gene; within this region, one T-box binding site (red line) was also found.

(b) The 490bp conserved region containing the two Pax-binding sites and one TBE was cloned into luciferase expressing vectors with a minimal promoter (pGL3-promoter) upstream as a promoter, and down-stream of luciferase as an enhancer.

Therefore, to test whether Tbx1 and/or Pax9 bind within this region of the *Gbx2* gene, the 490bp region was cloned into a luciferase-expressing vector (pGL3-promoter) both upstream of the promoter and downstream of luciferase as an enhancer (Figure 5.1b). These constructs were co-transfected along with different doses of TBX1, PAX9, or both, and the Renilla construct, into JEG3 cells, and luciferase expression was measured as previously described.

Interestingly, TBX1 seems to significantly down-regulate luciferase expression to 50% ($p<0.005$) of the *Gbx2* enhancer (Figure 5.16a) at a concentration of 0.5µg, compared to the group transfected with an empty plasmid (pcDNA). However, PAX9 is able to significantly promote luciferase expression in the 3 tested doses (Figure 5.16a). Moreover, co-transfection of both TBX1 and PAX9 shows no significant change in luciferase expression, suggesting luciferase activation by PAX9 is prevented by the presence of TBX1 (Figure 5.16b).

Taken together these results suggest that PAX9 is able to promote luciferase expression *in vitro* of this region of *GBX2.* Furthermore, TBX1 presence is able to repress PAX9-driven luciferase expression and even to down-regulate the activity of the minimal promoter within the pGL3-promoter construct.

Although in an opposite way, this latter result resembles the repression by Pax9 over Tbx1 discussed previously in section 5.3; altogether supporting a strong interaction between Tbx1 and Pax9 at the functional level. However, this interaction over the *Gbx2* gene needs to be further validated *in vivo* using chromatin precipitation.

In this context, chromatin immunoprecipitation was performed from E8.5, E9.5 and E10.5 embryos. Samples were immunoprecipitated using an anti-TBX1 or anti-PAX9 antibody and chromatin precipitation was assessed by end-point PCR (Figure 5.17) using primers (Table 2.7) targeting the TBEs and Pax-binding sites found within the identified conserved region downstream of exon 3, and TBEs previously predicted within the *Gbx2* promoter (Ivins et al, 2005; Caprio and Baldini, 2014).

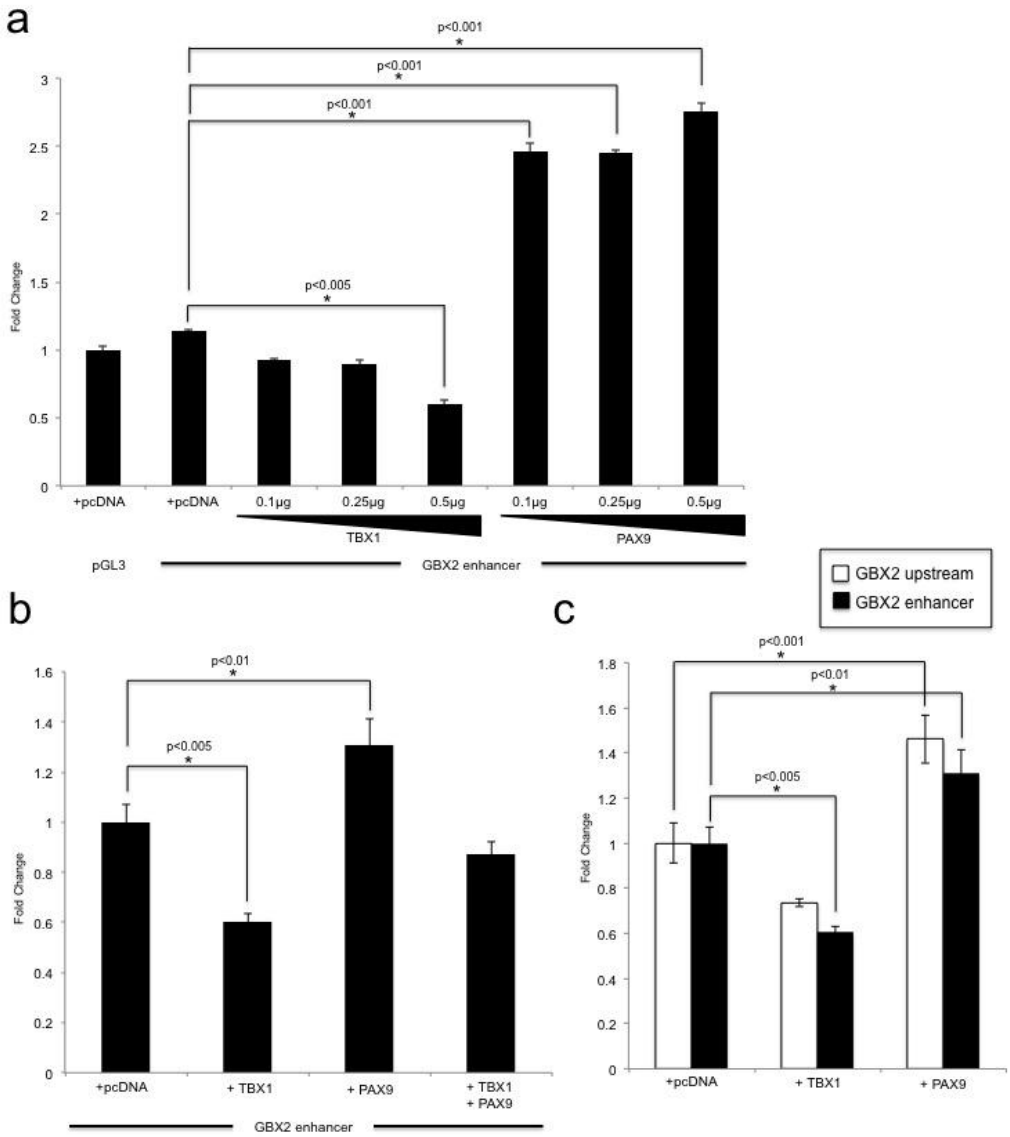

Figure 5.16. Luciferase assays on the *GBX2* conserved region.
Luciferase assays from cells co-transfected with the cloned *GBX2* conserved region and *TBX1* and *PAX9* alone or together were performed to determine potential binding to this region. **(a)** Cells were co-transfected with the cloned *GBX2* region as an enhancer and with different doses (0.1, 0.25, 0.5µg) of TBX1 or PAX9 in a luciferase assay. *A* significant 0.5-fold reduction in luciferase activity was observed with 0.5µg of *TBX1* ($p<0.005$) compared to the *GBX2* construct co-transfected with an empty vector (pcDNA). *PAX9* can promote luciferase expression of the Gbx2 construct, showing a significant 1.5-fold increase in luciferase expression ($p<0.001$).
(b) The *GBX2* construct was co-transfected with both TBX1 and PAX9 in a luciferase assay; co-transfection with both PAX9 and TBX1 does not show any significant changes in luciferase expression compared to the empty vector. **(c)** Both constructs of the *GBX2* conserved region cloned upstream as a promoter (white bars), and down-stream of luciferase as an enhancer (black bars) were co-transfected with TBX1 or PAX9 in a luciferase experiment. TBX1 causes a significant 0.5-fold reduction in luciferase expression ($p<0.005$) compared to the groups co-transfected with an empty vector (pcDNA) in both constructs. PAX9 is able to significantly promote a 0.4-fold increase in luciferase expression ($p<0.001$) compared to the empty vector in both constructs. Error bars represent SEM from triplicates of each group, and graphs are representative from three independent experiments. Statistical significance was calculated using a two-paired T-test.

However, this ChIP experiment was not successful as the negative controls (IgG and no antibody) showed noticeable amplification in all samples (Figure 5.17), indicating a high level of background caused just by the protein A/G beads, since the 'no antibody' (no AB) samples present high amplification (Figure 5.17). Possible contamination of the samples was excluded, as PCR samples with only water (H_2O) do not show amplification.

Additionally, from the previous ChIP experiment, aliquots of all samples after immunoprecipitation and before reversing the cross-linking were collected, and ChIP-western blot was performed (described in section 2.11 and 2.13; Caprio and Baldini, 2014).

Briefly, samples from the 3 stages (E8.5, E9.5, E10.5) were collected after immunoprecipitation with TBX1 and PAX9 and were then subjected to typical western blot against TBX1 and PAX9. This approach allows for the detection of protein co-occupancy within a region of DNA, but it is not possible to know specifically which genomic region is being targeted.

However, from this approach Tbx1 and Pax9 co-occupancy was not identified (Figure 5.18), as Tbx1 was only detected in samples immunoprecipitated with an anti-TBX1 antibody (Figure 5.18), whilst similarly Pax9 was only detected in samples precipitated with an anti-PAX9 antibody (Figure 5.18).

Although the results from ChIP and ChIP-Western blot did not show an interaction *in vivo*, the luciferase assays show a robust and reproducible effect of both Tbx1 and Pax9 over the *Gbx2* enhancer region, suggesting both could work together on regulating *Gbx2* expression through acting on a down-stream conserved regulatory region.

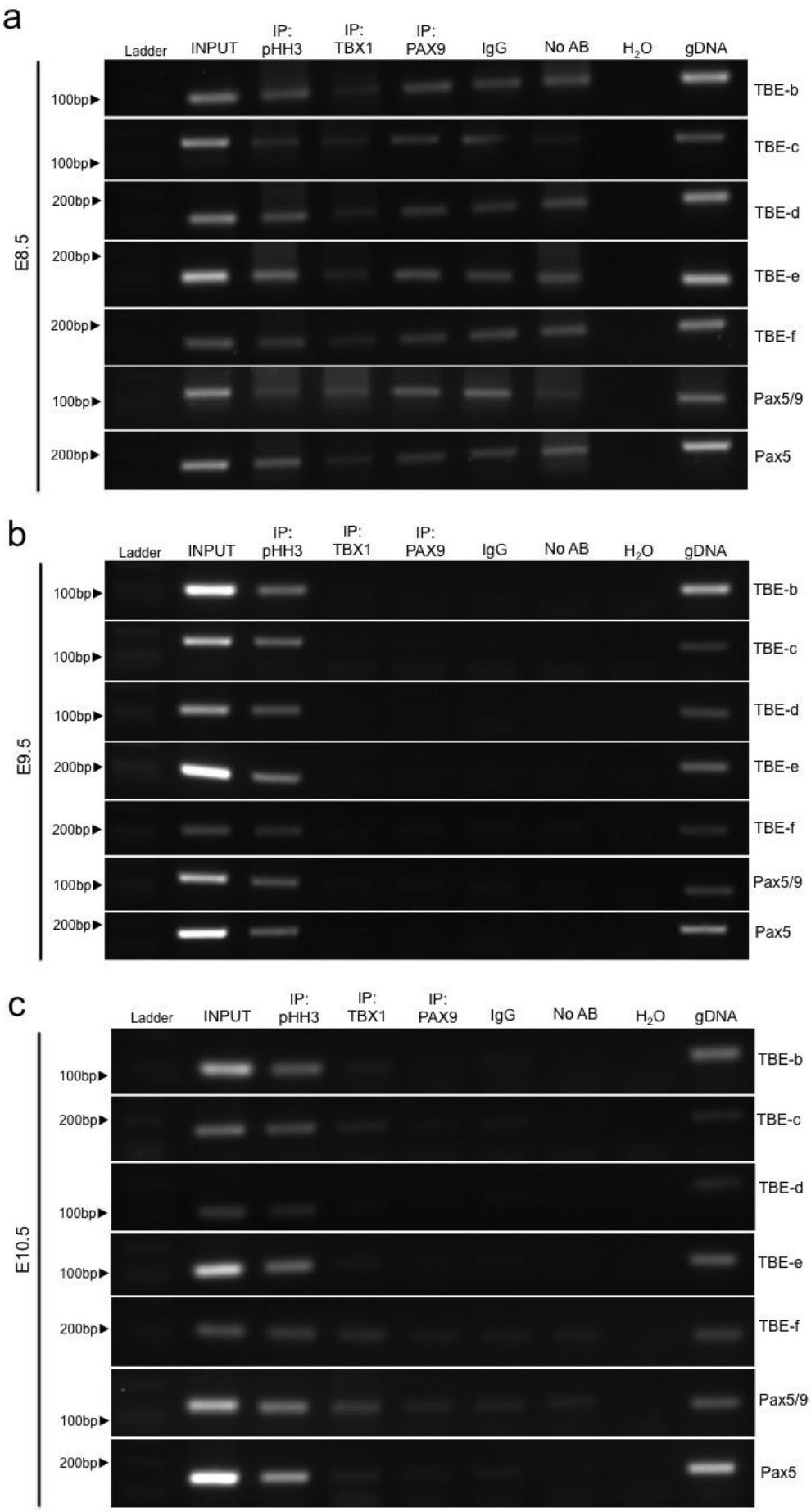
a
Ladder
INPUT
IP: pHH3
IP: TBX1
IP: PAX9
IgG
No AB
H_2O
gDNA
E8.5
100bp
100bp
200bp
200bp
200bp
100bp
200bp
TBE-b
TBE-c
TBE-d
TBE-e
TBE-f
Pax5/9
Pax5
b
Ladder
INPUT
IP: pHH3
IP: TBX1
IP: PAX9
IgG
No AB
H_2O
gDNA
E9.5
100bp
100bp
100bp
200bp
200bp
100bp
200bp
TBE-b
TBE-c
TBE-d
TBE-e
TBE-f
Pax5/9
Pax5
c
Ladder
INPUT
IP: pHH3
IP: TBX1
IP: PAX9
IgG
No AB
H_2O
gDNA
E10.5
100bp
200bp
100bp
100bp
200bp
100bp
200bp
TBE-b
TBE-c
TBE-d
TBE-e
TBE-f
Pax5/9
Pax5

Figure 5.17. Chromatin immunoprecipitation of TBEs and Pax-binding sites within the *GBX2* locus.

Chromatin immunoprecipitation from E8.5 **(a)**, E9.5 **(b)** and E10.5 **(c)** embryos was performed using an anti-TBX1 antibody and anti-PAX9 antibody, and specific primers targeting the identified TBEs and Pax-binding sites; end-point PCR was performed on immunoprecipitated samples.

(a) ChIP from E8.5 embryos resulted unreliable since the negative controls (IgG and no AB) show unspecific amplification of all identified TBEs and Pax-binding sites.

(b) No binding was detected in any of the TBEs or Pax-binding sites from ChIP of E9.5 embryos, with only the positive controls (INPUT and pHH3) showing positive amplification.

(c) No specific binding was detected at E10.5 in any of the TBEs or Pax-binding sites, although amplification is detected in some of the target sites, such amplification does not seem to be specific since the negative controls (IgG and noAB) also show amplification.

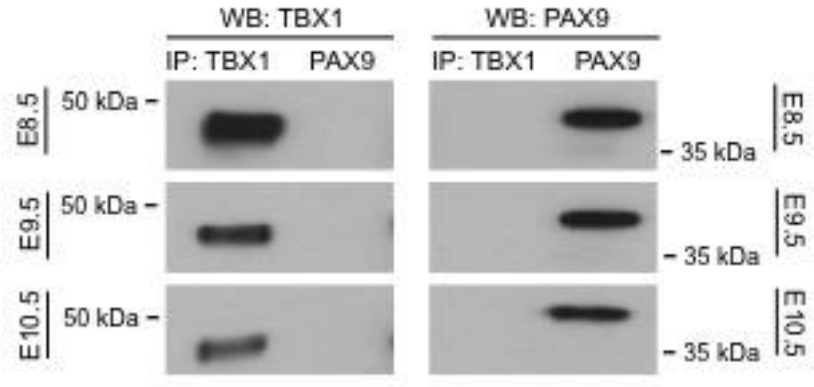

Figure 5.18. ChIP-western blot

To detect co-ocupancy of Tbx1 and Pax9 proteins within a region in the DNA, aliquots of samples from the 3 stages (E8.5, E9.5, E10.5) were collected after immunoprecipitation with TBX1 or PAX9 and before reversing the cross-linking; samples were then subjected to western blot with an anti-TBX1 and anti-PAX9 antibodies. Tbx1 and Pax9 co-occupancy was not identified as Tbx1 is only detected in samples immunoprecipitated with an anti-TBX1 antibody, whilst similarly Pax9 is only detected in samples precipitated with an anti-PAX9 antibody in all three stages.

5.5 Discussion

The first aim of this chapter was to determine whether Tbx1 directly binds to the *Pax9* locus to regulate its expression, however, the ChIP results show Tbx1 does not bind to the *Pax9* locus. Although the qPCR results show some enrichment in the TBE-5 region, this amplification seems to be unspecific given that the IgG control group also showed similar enrichment.

The IgG used as a negative control has no antigen immunoreactivity and therefore should not bind to any protein, thus the high background signal seen in the IgG and no antibody samples suggest potential DNA secondary structures within this region, or other proteins bound to the DNA could be interacting with the protein A beads and/or the IgG, consequently causing unspecific precipitation.

However, no significant enrichment was seen in any of the analysed TBEs, indicating Tbx1 does not bind directly to the *Pax9* locus *in vivo*, and suggesting *Pax9* expression may be regulated indirectly by Tbx1. To address this, the *Pax9* gene can be analysed using MultiTF software to search for other transcription factor binding sites, particularly focusing on transcription factors known to be affected by loss of Tbx1.

In this context*, Pax9* expression is induced by ectodermal Fgf8 (Neubüser et al, 1995), which is a known direct target of Tbx1 (Vitelli et al, 2002; Hu et al, 2004), suggesting this could be one pathway through which Tbx1 regulates *Pax9* expression. Moreover, Bmp4 signalling represses *Pax9* expression (Neubüser et al, 1995), whilst Tbx1 is able to inhibit Bmp4 signalling by directly interacting with Smad1 (Fulcoli et al., 2009), suggesting another way for Tbx1 to regulate *Pax9* expression.

Moreover, a functional interaction between Pax9 and Tbx1 was found *in vitro* using luciferase assays where Pax9 is able to repress Tbx1 transcriptional activity in a dose-dependent manner and prevent luciferase expression of a T-box reporter construct (2xTtkGL2). However, Pax9 does not affect Tbx1 binding to DNA, but only its transcriptional activity.

Although this repression does not seem to be through direct interaction between Pax9 and Tbx1 proteins, it is possible other co-factors commonly interact with Pax9 and Tbx1, thus the repression seen in the luciferase assays is an off-target effect over a co-factor required for Tbx1 transcriptional activity.

Additionally, Pax9 was able to drive luciferase expression of a cloned conserved region down-stream of the *Gbx2* gene, whilst co-transfection with Tbx1 prevented this Pax9-mediated luciferase expression, further demonstrating a functional interaction between Tbx1 and Pax9 *in vitro*.

As mentioned before, a physical interaction between Pax9 and Tbx1 was not detected by co-immunoprecipitation, nor a co-occupancy of both proteins within the *Gbx2* cloned region. Therefore, the precise nature of this functional interaction *in vivo* remains to be clarified.

Many technical difficulties for the analysis of this interaction *in vivo* have been identified and are being addressed in order to further investigate and corroborate these results.

For instance, the lack of detection of co-occupancy in the latter experiment could be due to insufficient tissue to be able to detect the interaction; if Pax9 and Tbx1 interact either physically with each other in a protein-protein fashion, or by co-occupying a region of DNA within the *Gbx2* gene to regulate its expression, this interaction only occurs within the pharyngeal endoderm, where *Pax9* is exclusively expressed; additionally, not all cells within the pharyngeal endoderm co-express Pax9 and Tbx1 at the same time, consequently making the interaction difficult to detect either by chromatin immunoprecipitation and co-immunoprecipitation.

To address this issue, many more embryos need to be collected for each experiment in order to have sufficient starting tissue to be able to detect the interaction after the subsequent steps of each technique.

Nonetheless, the robustness and reproducibility of the *in vitro* results are proof of concept of a functional interaction between Pax9 and Tbx1. In this context, the effect of Pax9 and Tbx1 over the *Gbx2* enhancer region suggest both Pax9 and Tbx1 could work together to regulate *Gbx2* expression; although it is not possible to conclude from this experiment whether they act as promoters or repressors of *Gbx2* and their precise role *in vivo* on *Gbx2* remains to be elucidated.

Gbx2 is a good common downstream target candidate of Pax9 and Tbx1 given that both *Gbx2*-null and *Pax9*$^{+/-}$;*Tbx1*$^{+/-}$ present defects specifically affecting the development of the 4th PAAs. Additionally, it was recently shown Tbx1 and p53 bind to the same *Gbx2* enhancer region identified in this chapter (Caprio and Baldini, 2014). In this context, p53 binds to this 490bp down-stream region and negatively regulates *Gbx2* expression through recruiting the polycomb repressive complex to methylate and silence *Gbx2* expression (Caprio and Baldini, 2014).

Interestingly, it was also recently reported that Pax9 plays a key role for maintenance of heterochromatin, where Pax9 knockdown leads to a decrease in H3K9me3 regions within heterochromatin, suggesting Pax9 may be involved in DNA methylation (Bulut-Karslioglu et al, 2012).

Moreover, other Pax proteins are known to interact with methylation complexes, such as Pax2, which interacts with PAXIP1 (Lechner et al, 2000), an essential cofactor for H3K4me3 (Patel et al, 2007; Cho et al, 2007) and such interaction is associated with active chromatin states (Stein et al, 2011). Moreover, PAXIP1 also binds p53-binding protein 1 (p53BP1) to control gene expression (Jowsey et al, 2004), whereas Pax2 and Pax5 can inhibit *p53* expression and p53-mediated gene expression (Stuart et al, 1995).

Considering these reports, it is possible that Pax9 is also part of the Tbx1-p53 system that regulates *Gbx2* expression, either as a repressor promoting methylation and silencing *Gbx2* expression, or as a promoter acting over the *Gbx2* enhancer.

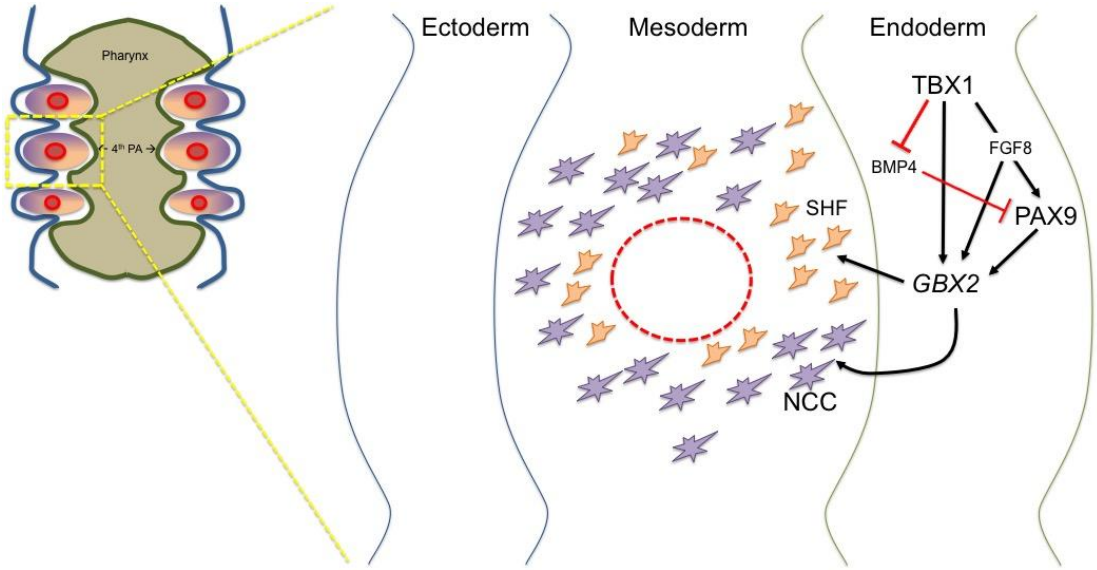

Figure 5.19. Proposed pathway.
Based on the results from this dissertation and previous reports, it is proposed that TBX1 indirectly regulates PAX9 expression, perhaps through FGF8 signalling, while TBX1 and PAX9 act on GBX2 to regulate its expression and promote second heart field cells proliferation and proper neural crest cell migration to control formation of the 4th PAAs.

Chapter 6. Final Discussion

6.1. *Pax9* in cardiovascular development as a genetic modifier of 22q11DS phenotype

A novel role for *Pax9* in cardiovascular development was identified in this project, specifically showing Pax9 requirement for correct development of the pharyngeal arch arteries. Furthermore, a strong genetic interaction between *Pax9* and *Tbx1* was found, where *Pax9* and *Tbx1* double haploinsufficiency leads to a significant increase in the prevalence of 4th PAA defects, and a significant increase in the incidence of IAA-B.

The fact that double haploinsufficiency affects specifically the 4th PAAs (typical of *Tbx1* heterozygosity), but not the 1st, 2nd and 3rd PAAs as occurs in *Pax9*-null embryos, suggest *Pax9* haploinsufficiency exacerbates the Tbx1 heterozygous phenotype increasing the incidence of bilateral 4th PAA defects in a synergistic interaction.

To this date, *TBX1* and *PAX9* mutations have not been associated in human patients with CCVM, however, the results shown in this dissertation position *PAX9* as a potential modifier of 22q11 deletion syndrome. Although mutations on *PAX9* directly affecting its function may define the 22q11DS phenotype, mutations affecting other components of the proposed TBX1-PAX9-GBX2 pathway could determine the presentation of the phenotype but be more difficult to detect.

In this context, mutations on *GBX2*, as the proposed downstream common target of TBX1 and PAX9 could result in a double heterozygous-like phenotype. Similarly, mutations affecting intermediate elements downstream of TBX1 and required for correct PAX9 expression could disrupt the pathway by altering PAX9 expression levels to a heterozygous-like level, which in the context of 22q11 deletion may result in a double heterozygous-like phenotype.

6.2. *Gbx2* as a common downstream target of Tbx1 and Pax9

The third aim of this project was to determine the molecular mechanism by which Tbx1 and Pax9 interact. As part of this objective, *Gbx2* mRNA levels were found significantly reduced in double heterozygous embryos, which led to the hypothesis of *Gbx2* as a down-stream target of Tbx1 and Pax9.

In vitro assays revealed both Tbx1 and Pax9 interact with a conserved region of the *Gbx2* gene suggesting Tbx1 and Pax9 act on *Gbx2* as a common downstream target to control in part cardiovascular development.

Moreover, *Gbx2*-null mice present with similar 4th PAA defects as those seen in double heterozygous embryos, as a phenocopy of *Tbx1*;*Pax9* double haploinsufficiency phenotype, further supporting the idea of Gbx2 being within the same genetic pathway and downstream of Tbx1 and Pax9.

In this context, it has been shown Tbx1 directly binds to the conserved regulatory region of *Gbx2* to promote its expression, whereas p53 negatively regulates *Gbx2* expression by mediating methylation of the *Gbx2* locus. Interestingly, it was recently suggested that Pax9 is necessary for epigenetic control of heterochromatin by modulating DNA methylation.

Altogether, these evidences suggest Pax9 could be part of the Tbx1-p53 complex that regulates *Gbx2* expression, binding to this conserved regulatory region downstream of the *Gbx2* gene.

6.3. Future work

Although the effect of *Pax9* homozygous deletion and *Pax9*;*Tbx1* double haploinsufficiency clearly affects the development of the pharyngeal arch arteries, the cellular mechanism causing abnormal remodelling of the cranial PAAs and lack of formation of the 4th PAAs still remains to be elucidated.

In this context, it remains to be determined whether abnormal development of the pharyngeal arch arteries is a consequence of increased apoptosis, insufficient endothelial differentiation, or deficient neural crest cell migration into the pharyngeal arches.

This can be determined by immunostaining of sectioned pharyngeal arches of *Pax9*-null and double heterozygous embryos using specific markers for apoptosis (caspase 3), proliferation (phospho-histone H3, Ki-67), endothelial differentiation (CD-31), smooth muscle differentiation (α-SMA), neural crest cells (Wnt1, Sox10).

Moreover, the precise role of Tbx1 and Pax9 regulating *Gbx2* expression *in vivo* needs to be further analysed to precisely determine how Pax9 and Tbx1 control *Gbx2* expression. To achieve this, the pharyngeal arch region of wildtype embryos will be collected and chromatin immunoprecipitation will be performed, targeting the conserved region containing the identified putative Pax-binding sites and TBEs.

As mentioned before, many technical difficulties have been identified and will be addressed, including the amount of starting tissue, and extra considerations to prevent unspecific binding of the IgG and protein A/G beads such as additional blocking and washing steps.

Furthermore, it would be interesting to generate *Pax9*;*Gbx2* double heterozygous and *Tbx1*;*Pax9*;*Gbx2* triple heterozygotes, to analyse the incidence of 4th PAA defects and determine whether triple heterozygosity increases the penetrance of IAA-B up to 100%.

Additionally, to further understand the role of Pax9 and Tbx1 *in vivo*, would be interesting to modify the conserved genomic region downstream of *Gbx2* where Pax9 and Tbx1 presumably bind, using gene-editing tools such as the CRISPR/Cas9 system, to prevent Tbx1/Pax9 binding and determine whether this mutation recapitulates the *Tbx1*;*Pax9* double heterozygous phenotype; this approach would provide with a more clinically relevant insight into the mechanism regulating *Gbx2* to control cardiovascular development, as mutations within this region could occur in 22q11DS patients consequently modifying the phenotype.

Similarly, it should be interesting to generate $Pax9^{-/-}$;$p53^{+/-}$ embryos and determine whether *p53* heterozygosity can rescue the *Pax9*-null phenotype as it occurs in the *Tbx1*;*p53* double heterozygous embryos (Caprio and Baldini, 2014).

Moreover, it remains to be investigated which genes and signalling pathways are disrupted as a consequence of *Pax9* loss. This is being approached by using whole transcriptome sequencing (RNA-seq) of *Pax9*-null embryos, to determine which transcripts are dysregulated; targets identified by this approach will be further validated by qPCR and in situ hybridisation, and potentially analysed in vivo using mouse models. This same approach could be later applied to *Tbx1*;*Pax9* double heterozygous embryos.

Finally, in a translational perspective, gene sequencing of *PAX9* and *GBX2* (or other affected genes identified by RNA-seq) in patients with 22q11 deletion would help in understanding the genetic aetiology of the phenotype. This would need to be approached by whole genome sequencing, as mutations within regulatory regions outside exons such as the one proposed downstream of *GBX2* could be responsible for dysregulation of gene expression.

6.4. Conclusions

The data presented in this thesis demonstrates *Pax9* is required for cardiovascular development, particularly for correct development of the pharyngeal arch arteries.

The results also demonstrate that *Pax9* genetically interacts with *Tbx1* for the formation of the 4th pharyngeal arch arteries, and further support the possibility of *PAX9* being a genetic modifier of 22q11DS phenotype.

The results also demonstrate that Tbx1 does not regulate *Pax9* expression directly binding to the *Pax9* locus, nor Tbx1 and Pax9 physically interact with each other.

Finally, the results support the hypothesis that Tbx1 and Pax9 act over *Gbx2* as a common target to regulate, at least in part, cardiovascular development.

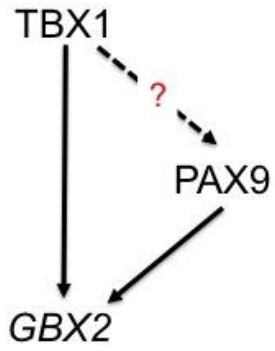

Appendix A. Optimization of Luciferase Assays

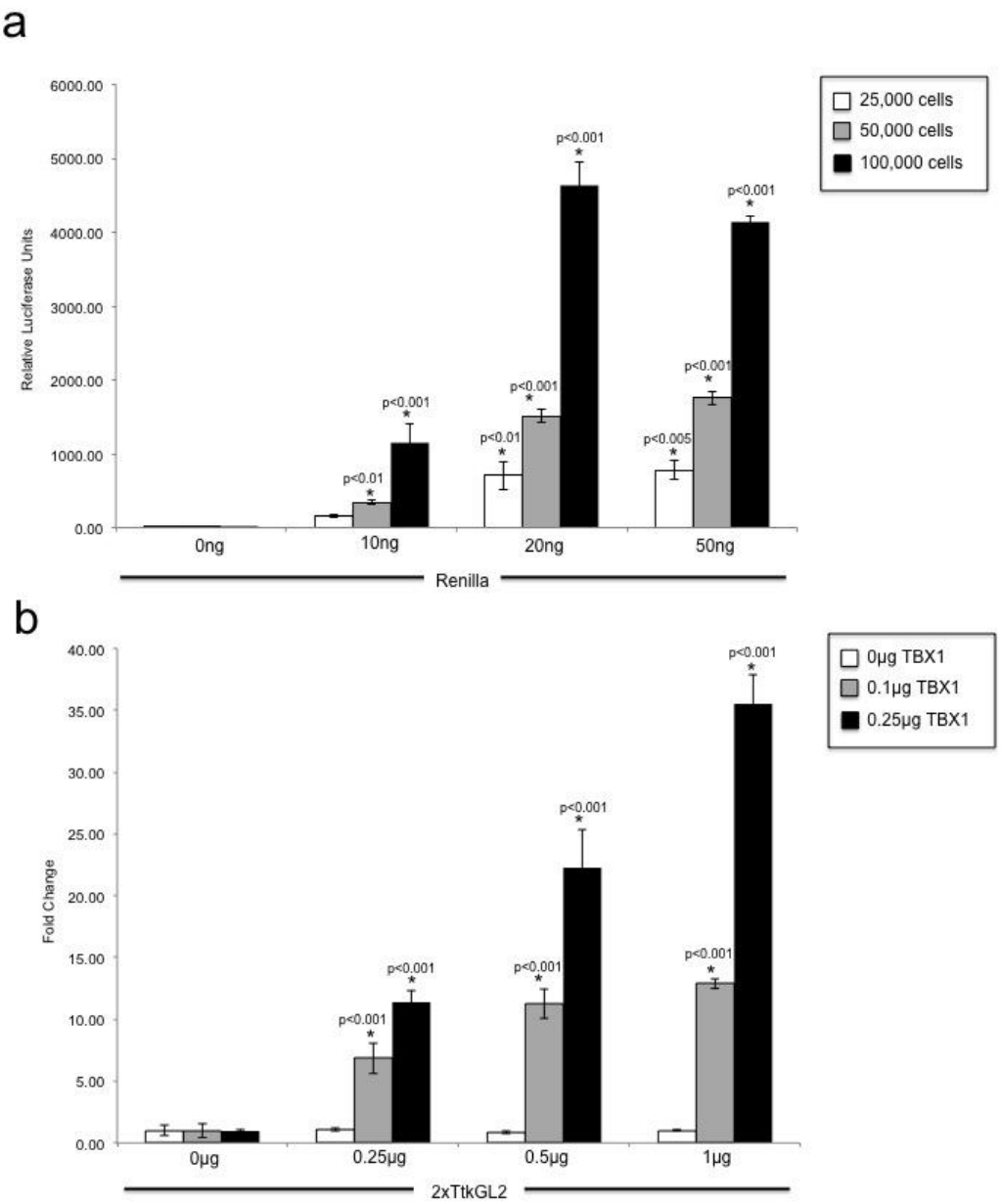

Appendix A. Optimization of luciferase assays.

(a) Increasing number of JEG3 cells (25,000, 50,000 and 100,000) were seeded and transfected with different doses (0, 10, 20, 50ng) of a Renilla luciferase expressing vector (pGL4.7) to determine the optimal number of cells and concentration of renilla.

(b) JEG3 cells were co-transfected with different doses of the 2xTtkGL2 reporter (x axis), and increasing concentrations of a TBX1 expressing plasmid to determine the optimal concentration of TBX1 to activate the 2xTtkGL2 reporter.

Appendix B. Chromatin immunoprecipitation of TBEs within the *Pax9* locus

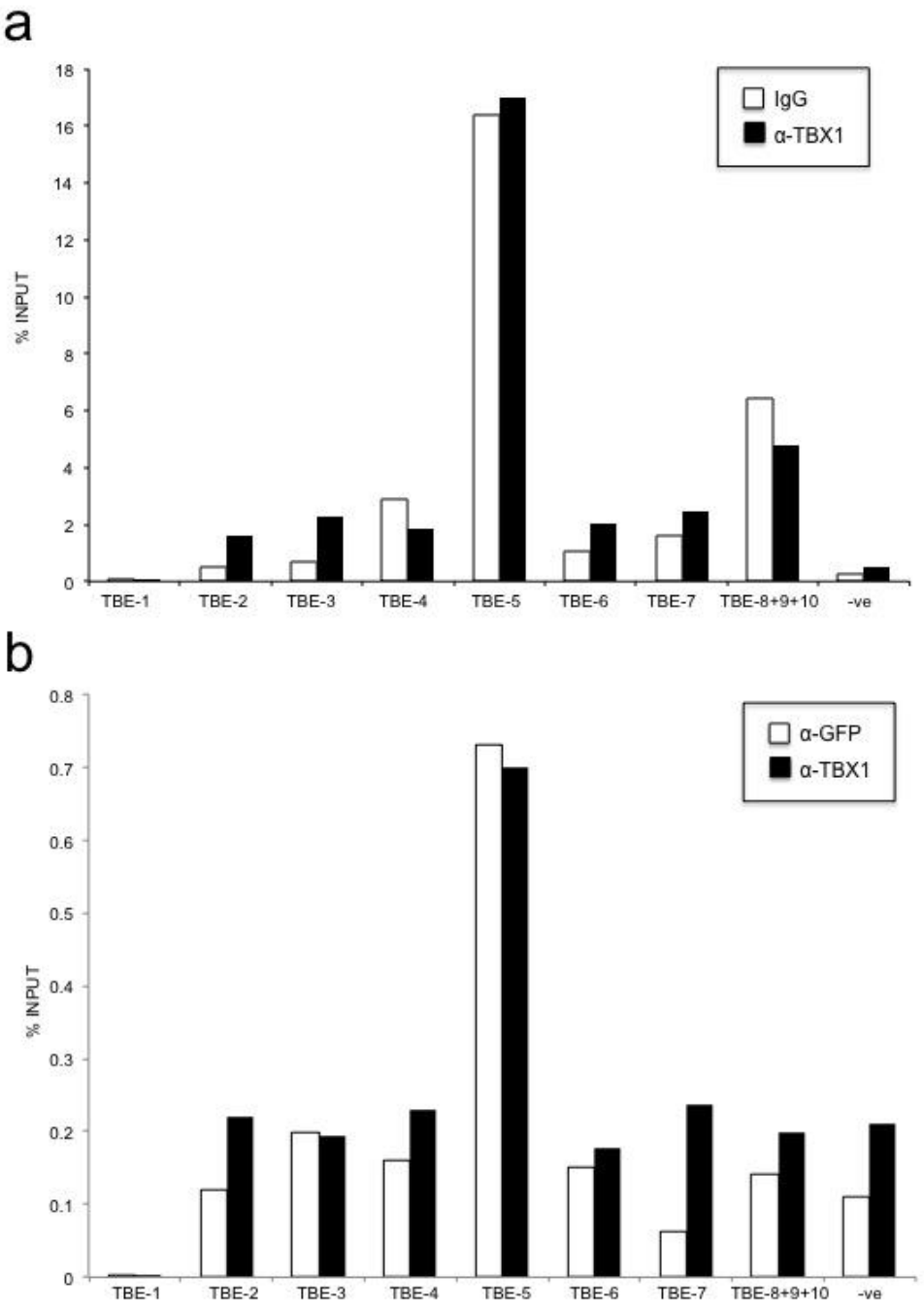

Appendix B. Chromatin immunoprecipitation of TBEs within the Pax9 locus on MEFs
(a) ChIP from MEFs (b) ChIP from E9.5 wild-type embryos using an anti-GFP as isotype control antibody

References

Abu-Issa, R., Smyth, G., Smoak, I., Yamamura, K. and Meyers, E.N. (2002) Fgf8 is required for pharyngeal arch and cardiovascular development in the mouse, Development, 129(19), pp. 4613-25.

Aggarwal, V.S., Morrow, B.E., (2008). Genetic modifiers of the physical malformations in velo-cardio-facial syndrome/DiGeorge syndrome. Dev Disabil Res Rev 14, 19-25.

Andersen, T., Troelsen, K. & Larsen, L. (2013) Of mice and men: molecular genetics of congenital heart disease. Cellular and Molecular Life Sciences. 71 (8), 1327–1352.

Anderson, R.H., Webb, S., Brown, N.A., Lamers, W., Moorman, A., 2003. Development of the heart: Septation of the atriums and ventricles. Heart 89, 949-958.

Anderson, M.J., Pham, V.N., Vogel, A.M., Weinstein, B.M., et al. (2008) Loss of unc45a precipitates arteriovenous shunting in the aortic arches. Developmental biology. 318 (2), 258–267.

Arcuri C, Zito I, Santini F, Muzzi F, Panetta V, Squitti R. (2011). Understanding the implications of the PAX9 gene in tooth development. Eur J Paediatr Dent. 2011 Dec;12(4):245-8.

Arnold, J.S., Werling, U., Braunstein, E.M., Liao, J., Nowotschin, S., Edelmann, W., Hebert, J.M. and Morrow, B.E. (2006) Inactivation of Tbx1 in the pharyngeal endoderm results in 22q11DS malformations, Development, 133(5), pp. 977-87.

Begemann, G., Schilling, T.F., Rauch, G.J., Geisler, R., et al. (2001) The zebrafish neckless mutation reveals a requirement for raldh2 in mesodermal signals that pattern the hindbrain. Development (Cambridge, England). 128 (16), 3081–3094.

Bajolle, F., Zaffran, S., Kelly, R.G., Hadchouel, J., Bonnet, D., Brown, N.A., Buckingham, M.E., 2006. Rotation of the myocardial wall of the outflow tract is implicated in the normal positioning of the great arteries. Circ Res 98, 421-428.

Bamforth, S.D., Chaudhry, B., Bennett, M., Wilson, R., Mohun, T.J., Van Mierop, L.H., Henderson, D.J. and Anderson, R.H. (2013) Clarification of the identity of the mammalian fifth pharyngeal arch artery, Clin Anat.

Bamforth, S.D., Schneider, J.E. and Bhattacharya, S. (2012) High-throughput analysis of mouse embryos by magnetic resonance imaging, Cold Spring Harb Protoc, 2012(1), pp. 93-101.

Bergwerff, M., DeRuiter, M.C., Hall, S., Poelmann, R.E., et al. (1999) Unique vascular morphology of the fourth aortic arches: possible implications for pathogenesis of type-B aortic arch interruption and anomalous right subclavian artery. Cardiovascular research. 44 (1), 185–196.

Bollag, R.J., Siegfried, Z., Cebra-Thomas, J.A., Garvey, N., et al. (1994) An ancient family of embryonically expressed mouse genes sharing a conserved protein motif with the T locus. Nature genetics. 7 (3), 383–389.

Botta A, Lindsay EA, Jurecic V, Baldini A (1997) Comparative mapping of the DiGeorge syndrome region in mouse shows inconsistent gene order and differential degree of gene conservation. Mammalian Genome 8, 12: 890-895

Brade, T. et al. (2013). Embryonic Heart Progenitors and Cardiogenesis.Cold Spring Harbor Perspectives in Medicine, 3(10), p.a013847a013847.

Bruneau, B.G. (2008) The developmental genetics of congenital heart disease, Nature, 451(7181), pp. 943-8.

Burn, J., Goodship, J., (2002). Congenital heart disease, in: Rimoin, D.L., Connor, J.M., Pyeritz, R.E., Korf, B.R. (Eds.), Principles and Practice of Medical Genetics. Churchill Livingstone, London.

Buckingham, M., Meilhac, S. and Zaffran, S. (2005). Building the mammalian heart from two sources of myocardial cells. Nature Reviews Genetics, 6(11), pp.826–837.

Byrd, N.A. and Meyers, E.N. (2005) Loss of Gbx2 results in neural crest cell patterning and pharyngeal arch artery defects in the mouse embryo, Dev Biol, 284(1), pp. 233-45.

Cai, C.L., Liang, X., Shi, Y., Chu, P.H., Pfaff, S.L., Chen, J. and Evans, S. (2003) Isl1 identifies a cardiac progenitor population that proliferates prior to differentiation and contributes a majority of cells to the heart, Dev Cell, 5(6), pp. 877-89.

Calmont, A., Ivins, S., Van Bueren, K.L., Papangeli, I., Kyriakopoulou, V., Andrews, W.D., Martin, J.F., Moon, A.M., Illingworth, E.A., Basson, M.A. and Scambler, P.J. (2009) Tbx1 controls cardiac neural crest cell migration during arch artery development by regulating Gbx2 expression in the pharyngeal ectoderm, Development, 136(18), pp. 3173-83.

Castellanos, R., Xie, Q., Zheng, D., Cvekl, A., et al. (2014) Mammalian TBX1 preferentially binds and regulates downstream targets via a tandem T-site repeat. PloS one. 9 (5), e95151.

Caprio, C. and Baldini, A. (2014). p53 suppression partially rescues the mutant phenotype in mouse models of DiGeorge syndrome. Proceedings of the National Academy of Sciences, 111(37), p.1338513390.

Chalepakis G1, Fritsch R, Fickenscher H, Deutsch U, Goulding M, Gruss P. (1991) The molecular basis of the undulated/Pax-1 mutation. Cell. 6;66(5):873-84.

Chalepakis, G. & Gruss, P. (1995) Identification of DNA recognition sequences for the Pax3 paired domain. Gene. 162 (2), 267–270.

Chapman, D.L., Garvey, N., Hancock, S., Alexiou, M., Agulnik, S.I., Gibson-Brown, J.J., Cebra-Thomas, J., Bollag, R.J., Silver, L.M., Papaioannou, V.E., 1996. Expression of the T-box family genes, Tbx1-Tbx5, during early mouse development. Dev Dyn 206, 379-390.

Chen, L., Fulcoli, F.G., Ferrentino, R., Martucciello, S., Illingworth, E.A., Baldini, A., 2012. Transcriptional Control in Cardiac Progenitors: Tbx1 Interacts with the BAF Chromatin Remodeling Complex and Regulates Wnt5a. PLoS Genet 8, e1002571.

Chen, H., Shi, S., Acosta, L., Li, W., Lu, J., Bao, S., Chen, Z., Yang, Z., Schneider, M.D., Chien, K.R., Conway, S.J., Yoder, M.C., Haneline, L.S., Franco, D. and Shou, W. (2004) BMP10 is essential for maintaining cardiac growth during murine cardiogenesis, Development, 131(9), pp. 2219-31.

Chen, C.P., Lee, C.C., Chen, L.F., Chuang, C.Y., et al. (1997) Prenatal diagnosis of de novo proximal interstitial deletion of 14q associated with cebocephaly. Journal of medical genetics. 34 (9), 777–778.

Chi, N. & Epstein, J.A. (2002) Getting your Pax straight: Pax proteins in development and disease.Trends in genetics : TIG. 18 (1), 41–47.

Christoffels, V., Habets, P., Franco, D., Campione, M., et al. (2000) Chamber formation and morphogenesis in the developing mammalian heart. Developmental biology. 223 (2) p.266–278

Christoffels, V., Hoogaars, W., Tessari, A., Clout, D., et al. (2004) T-box transcription factor Tbx2 represses differentiation and formation of the cardiac chambers. Developmental dynamics : an official publication of the American Association of Anatomists. 229 (4) p.763–770

Congdon, E.D., 1922. Transformation of the aortic arch system during the development of the human embryo. Contrib Embryol 68, 49-110.

Conlon, F.L., Fairclough, L., Price, B.M., Casey, E.S., et al. (2001) Determinants of T box protein specificity. Development (Cambridge, England). 128 (19), 3749–3758.

Couly, G. and Le Douarin, N.M. (1990). Head morphogenesis in embryonic avian chimeras: evidence for a segmental pattern in the ectoderm corresponding to the neuromeres. *Development (Cambridge, England)*, 108(4), pp.543–58.

Cordier A.C., Haumont S. M. (1980) Development of thymus, parathyroids and tulrimo-brachial bodies in NMRI and nude mice. The American journal of anatomy 157: 227-263

Couly, G.F., Coltey, P.M. & Le Douarin, N.M. (1992) The developmental fate of the cephalic mesoderm in quail-chick chimeras. Development (Cambridge, England). 114 (1), 1–15.

Cudney SM1, Vieira AR. (2012) Molecular factors resulting in tooth agenesis and contemporary approaches for regeneration: a review. Eur Arch Paediatr Dent.;13(6):297-304.

Danielian, P.S., Muccino, D., Rowitch, D.H., Michael, S.K. and McMahon, A.P. (1998) Modification of gene activity in mouse embryos in utero by a tamoxifen-inducible form of Cre recombinase, Curr Biol, 8(24), pp. 1323-6.

D'Amico-Martel A. Noden D.M. (1983) . Contributions of placodal and neural crest cells to avian cranial peripheral ganglia. American Journal of anatomy, 166, 4: 445-468

De Coster PJ, Marks LA, Martens LC, Huysseybe A (2009) Dental agenesis: genetic and clinical perspectives. J Oral Pathology and medicine

DeRuiter, M.C., Gittenberger-de Groot, A.C., Poelmann, R.E., VanIperen, L., et al. (1993) Development of the pharyngeal arch system related to the pulmonary and bronchial vessels in the avian embryo. With a concept on systemic-pulmonary collateral artery formation. Circulation. 87 (4), 1306–1319.

Devriendt K1, Swillen A, Fryns JP. (1998) Deletion in chromosome region 22q11 in a child with CHARGE association. Clin Genet. 53(5):408-10.

Dyer, Laura A., & Kirby, Margaret L. (2009). The role of secondary heart field in cardiac development. Developmental Biology, 336(2), 137-144.

Eisenberg, C.A. and Eisenberg, L.M. (1999). WNT11 promotes cardiac tissue formation of early mesoderm. Developmental dynamics : an official publication of the American Association of Anatomists, 216(1), pp.45–58.

Embleton, N.D., Wyllie, J.P., Wright, M.J., Burn, J., et al. (1996) Natural history of trisomy 18. Archives of disease in childhood. Fetal and neonatal edition. 75 (1), F38–41.

Engleka, K.A., Manderfield, L.J., Brust, R.D., Li, L., Cohen, A., Dymecki, S.M. and Epstein, J.A. (2012) Islet1 derivatives in the heart are of both neural crest and second heart field origin, Circ Res, 110(7), pp. 922-6.

Epstein, J., Cai, J., Glaser, T., Jepeal, L., et al. (1994) Identification of a Pax paired domain recognition sequence and evidence for DNA-dependent conformational changes. The Journal of biological chemistry. 269 (11), 8355–8361.

Erami, C., Charaf-Eddine, A., Aggarwal, A., Rivard, A.L., Giles, H.W. and Nowicki, M.J. (2013) Dysphagia lusoria in an infant, J Pediatr, 162(6), pp. 1289-90.

Ewart, A.K., Morris, C.A., Ensing, G.J., Loker, J., et al. (1993) A human vascular disorder, supravalvular aortic stenosis, maps to chromosome 7. Proceedings of the National Academy of Sciences of the United States of America. 90 (8), 3226–3230.

Freeman, S.B., Bean, L.H., Allen, E.G., Tinker, S.W., et al. (2008) Ethnicity, sex, and the incidence of congenital heart defects: a report from the National Down Syndrome Project. Genetics in medicine : official journal of the American College of Medical Genetics. 10 (3), 173–180.

Fulcoli, F.G., Huynh, T., Scambler, P.J., Baldini, A., 2009. Tbx1 regulates the BMP-Smad1 pathway in a transcription independent manner. PLoS One 4, e6049.

Galili, N., Baldwin, H.S., Lund, J., Reeves, R., et al. (1997) A region of mouse chromosome 16 is syntenic to the DiGeorge, velocardiofacial syndrome minimal critical region. Genome research. 7 (1), 17–26.

Garg, V., Yamagishi, C., Hu, T., Kathiriya, I.S., Yamagishi, H., Srivastava, D., 2001. Tbx1, a DiGeorge syndrome candidate gene, is regulated by sonic hedgehog during pharyngeal arch development. Dev Biol 235, 62-73.

Garcia-Martinez, V. & Schoenwolf, G. (1993) Primitive-streak origin of the cardiovascular system in avian embryos. Developmental biology. 159 (2) p.706–719

Gordon, J., Bennett, A.R., Blackburn, C.C. & Manley, N.R. (2001) Gcm2 and Foxn1 mark early parathyroid- and thymus-specific domains in the developing third pharyngeal pouch. Mechanisms of development. 103 (1-2), 141–143.

Gordon, J.W., Scangos, G.A., Plotkin, D.J., Barbosa, J.A., et al. (1980) Genetic transformation of mouse embryos by microinjection of purified DNA. Proceedings of the National Academy of Sciences of the United States of America. 77 (12), 7380–7384.

Goulding, M.D., Chalepakis, G., Deutsch, U., Erselius, J.R., et al. (1991) Pax-3, a novel murine DNA binding protein expressed during early neurogenesis. The EMBO journal. 10 (5), 1135–1147.

Gong, W., Gottlieb, S., Collins, J., Blescia, A., Dietz, H., Goldmuntz, E., McDonald-McGinn, D.M., Zackai, E.H., Emanuel, B.S., Driscoll, D.A., Budarf, M.L., 2001. Mutation analysis of TBX1 in non-deleted patients with features of DGS/VCFS or isolated cardiovascular defects. J Med Genet 38, E45.

Graham, A., Smith, A., 2001. Patterning the pharyngeal arches. Bioessays 23, 54-61.

Grammatopoulos, G.A., Bell, E., Toole, L., Lumsden, A., et al. (2000) Homeotic transformation of branchial arch identity after Hoxa2 overexpression. Development (Cambridge, England). 127 (24), 5355–5365.

Grego-Bessa, J. et al. (2007). Notch signaling is essential for ventricular chamber development.Developmental cell, 12(3), pp.415–29.

Greulich, F., Rudat, C., and Kispert, A. (2011). Mechanisms of T-box gene function in the developing heart. Cardiovascular Research 91, 212-222.

Grevellec, A. and Tucker, A.S. (2010) The pharyngeal pouches and clefts: Development, evolution, structure and derivatives, Semin Cell Dev Biol, 21(3), pp. 325-32.

Guo C, Sun Y, Zhou B, Adam RM, Li X, Pu WT, Morrow BE, Moon A, Li X.(2011). A Tbx1-Six1/Eya1-Fgf8 genetic pathway controls mammalian cardiovascular and craniofacial morphogenesis. J Clin Invest, 121, 1585-95

Guris DL, Fantes J, Tara D, Druker BJ, Imamoto A.(2001). Mice lacking the homologue of the human 22q11.2 gene CRKL phenocopy neurocristopathies of DiGeorge syndrome. Nat Genet. Mar;27(3):293-8.

Guris, D.L., Duester, G., Papaioannou, V.E., Imamoto, A., 2006. Dose-dependent interaction of Tbx1 and Crkl and locally aberrant RA signaling in a model of del22q11 syndrome. Dev Cell 10, 81-92.

Günther T; Z F Chen; J Kim; M Priemel; J M Rueger; M Amling; J M Moseley; T J Martin; D J Anderson; G Karsenty (2000) Genetic ablation of parathyroid glands reveals another source of parathyroid hormone. Nature 406, 199-203

Hetzer-Egger, C., Schorpp, M., Haas-Assenbaum, A., Balling, R., et al. (2002) Thymopoiesis requires Pax9 function in thymic epithelial cells. European journal of immunology. 32 (4), 1175–1181.

High, F.A. and Epstein, J.A. (2008) The multifaceted role of Notch in cardiac development and disease, Nat Rev Genet, 9(1), pp. 49-61.

Hilfer SR, Brown JW. (1984). The development of pharyngeal endocrine organs in mouse and chick embryos. Scan Electron Microsc. (Pt 4):2009-22.

Hiruma T, Hirakow R. (1995) Formation of the pharyngeal arch arteries in the chick embryo. Observations of corrosion casts by scanning electron microscopy Anat Embryol (Berl). May;191(5):415-23.

Hiruma, T., Nakajima, Y. and Nakamura, H. (2002) Development of pharyngeal arch arteries in early mouse embryo, J Anat, 201(1), pp. 15-29.

Hisato Yagi MS,Yoshiyuki Furutani PhD,Hiromichi Hamada MD,Takashi Sasaki MSD,Shuichi Asakawa PhD,Shinsei Minoshima PhD,Fukiko Ichida MD,Kunitaka Joo MD,Misa Kimura MS,Shin-ichiro Imamura DVM,Naoyuki Kamatani MD,Kazuo Momma MD,Atsuyoshi Takao MD,Makoto Nakazawa MD,Nobuyoshi Shimizu PhD,Dr Rumiko Matsuoka MD (2003) Role of TBX1 in human del22q11.2 syndrome. The Lancet Vol. 362, Issue 9393, Pages 1366-1373

Van den Hoff, M.J. et al. (1999). Myocardialization of the cardiac outflow tract. Developmental biology, 212(2), pp.477–90

Hoffman, J.I. (1995) Incidence of congenital heart disease: I. Postnatal incidence, Pediatr Cardiol, 16(3), pp. 103-13.

Hoffman, J.I.E., Kaplan, S., (2002). The incidence of congenital heart disease. Journal of the American College of Cardiology 39, 1890-1900.

Hoffman, J.I., Kaplan, S. and Liberthson, R.R. (2004) Prevalence of congenital heart disease, Am Heart J, 147(3), pp. 425-39.

Hu, T., Yamagishi, H., Maeda, J., McAnally, J., Yamagishi, C., Srivastava, D., 2004. Tbx1 regulates fibroblast growth factors in the anterior heart field through a reinforcing autoregulatory loop involving forkhead transcription factors. Development 131, 5491-5502.

Hunt P; M Gulisano; M Cook; M H Sham; A Faiella; D Wilkinson; E Boncinelli; R Krumlauf. (1991) A distinct Hox code for the branchial region of the vertebrate head. Nature 353, 861 - 864

Hutson, M.R. and Kirby, M.L. (2003) Neural crest and cardiovascular development: a 20-year perspective, Birth Defects Res C Embryo Today, 69(1), pp. 2-13.

Ivins, S., Lammerts van Beuren, K., Roberts, C., James, C., Lindsay, E., Baldini, A., Ataliotis, P., Scambler, P.J., 2005. Microarray analysis detects differentially expressed genes in the pharyngeal region of mice lacking Tbx1. Dev Biol 285, 554-569.

Jerome, L.A., Papaioannou, V.E., (2001). DiGeorge syndrome phenotype in mice mutant for the T-box gene, Tbx1. Nat Genet 27, 286-291.

Kameda, Y., 2009. Hoxa3 and signaling molecules involved in aortic arch patterning and remodeling. Cell Tissue Res 336, 165-178.

Kardong, K., 2008. Vertebrates: Comparative Anatomy, Function, Evolution. McGraw-Hill Higher Education.

Kameda, Y. et al. (2004). The role of Hoxa3 gene in parathyroid gland organogenesis of the mouse.The journal of histochemistry and cytochemistry : official journal of the Histochemistry Society, 52(5), pp.641–51.

Kamnasaran, D., O'Brien, P.C.M., Schuffenhauer, S., Quarrell, O., Lupski, J.R., Grammatico, P., Ferguson-Smith, M.A., Cox, D.W., (2001). Defining the breakpoints of proximal chromosome 14q rearrangements in nine patients using flow-sorted chromosomes. American Journal of Medical Genetics 102, 173-182.

Kamnasaran D, Chen CP, Devriendt K, Mehta L, Cox DW. (2005). Defining a holoprosencephaly locus on human chromosome 14q13 and characterization of potential candidate genes. Genomics.;85(5):608-21.

Kardong K. 2008. Vertebrates: Comparative Anatomy, Function, Evolution. Boston: McGraw-Hill Higher Education.

Kellenberger, C.J. (2010). Aortic arch malformations. Pediatric Radiology 40, 876-884.

Kelly, R., Brown, N. & Buckingham, M. (2001) The arterial pole of the mouse heart forms from Fgf10-expressing cells in pharyngeal mesoderm. Developmental cell. 1 (3) p.435–440

Kirby M.L. (2007). Cardiac Development (ISBN-13: 978-0-19-517819-7)

Kirby, M.L., Hunt, P., Wallis, K., Thorogood, P., 1997. Abnormal patterning of the aortic arch arteries does not evoke cardiac malformations. Dev Dyn 208, 34-47.

Kirby, M.L. (1993) Cellular and molecular contributions of the cardiac neural crest to cardiovascular development, Trends Cardiovasc Med, 3(1), pp. 18-23.

Kirby, M.L., Waldo, K.L., (1995). Neural crest and cardiovascular patterning. Circ Res 77, 211-215.

Kirby, M.L. and Waldo, K.L. (1990) Role of neural crest in congenital heart disease, Circulation, 82(2), pp. 332-40.

Kist R, Watson M, Wang X, Cairns P, Miles C, Reid DJ, Peters H. (2005). Reduction of Pax9 gene dosage in an allelic series of mouse mutants causes hypodontia and oligodontia. Hum Mol Genet. 2005 Dec 1;14(23):3605-17.

Kist R, Greally E, Peters H. (2007) Derivation of a mouse model for conditional inactivation of Pax9. Genesis. 2007 Jul;45(7):460-4

Kutsche, L.M. and Van Mierop, L.H. (1984) Cervical origin of the right subclavian artery in aortic arch interruption: pathogenesis and significance, Am J Cardiol, 53(7), pp. 892-5.

Lazaridis, E. and Saunders, J.C. (2008). Can you hear me now? A genetic model of otitis media with effusion. The Journal of clinical investigation, 118(2), pp.471–4.

Le Douarin, N.M. & Jotereau, F.V. (1975) Tracing of cells of the avian thymus through embryonic life in interspecific chimeras. The Journal of experimental medicine. 142 (1), 17–40.

Le Douarin N.M., Kalcheim C., editors (1999). The neural crest. Cambridge, UK:Cambridge University Press

Leong, C.R., Solaimanzadeh, I., Rosca, M., Siegel, D., et al. (2012) Embolization of an Aberrant Right Subclavian Artery Aneurysm with Amplatzer Vascular Plug without Bypass. The International journal of angiology : official publication of the International College of Angiology, Inc. 21 (4), 237–240.

Li, P., Pashmforoush, M. and Sucov, H.M. (2012) Mesodermal retinoic acid signaling regulates endothelial cell coalescence in caudal pharyngeal arch artery vasculogenesis, Dev Biol, 361(1), pp. 116-24.

Liao, J., Aggarwal, V.S., Nowotschin, S., Bondarev, A., Lipner, S., Morrow, B.E., 2008. Identification of downstream genetic pathways of Tbx1 in the second heart field. Developmental Biology 316, 524-537.

Liao, J., Kochilas, L., Nowotschin, S., Arnold, J.S., Aggarwal, V.S., Epstein, J.A., Brown, M.C., Adams, J., Morrow, B.E., 2004. Full spectrum of malformations in velo-cardio-facial syndrome/DiGeorge syndrome mouse models by altering Tbx1 dosage. Hum Mol Genet 13, 1577-1585.

Liu, Z., Yu, S. & Manley, N.R. (2007) Gcm2 is required for the differentiation and survival of parathyroid precursor cells in the parathyroid/thymus primordia. Developmental biology. 305 (1), 333–346.

Lindsay, E.A. (2001) Chromosomal microdeletions: dissecting del22q11 syndrome, Nat Rev Genet, 2(11), pp. 858-68.

Lindsay, E.A. and Baldini, A. (2001) Recovery from arterial growth delay reduces penetrance of cardiovascular defects in mice deleted for the DiGeorge syndrome region, Hum Mol Genet, 10(9), pp. 997-1002.

Lindsay, E.A., Vitelli, F., Su, H., Morishima, M., Huynh, T., Pramparo, T., Jurecic, V., Ogunrinu, G., Sutherland, H.F., Scambler, P.J., Bradley, A. and Baldini, A. (2001) Tbx1 haploinsufficieny in the DiGeorge syndrome region causes aortic arch defects in mice, Nature, 410(6824), pp. 97-101.

Lindsay, E.A., Botta, A., Jurecic, V., Carattini-Rivera, S., Cheah, Y.C., Rosenblatt, H.M., Bradley, A. and Baldini, A. (1999) Congenital heart disease in mice deficient for the DiGeorge syndrome region, Nature, 401(6751), pp. 379-83.

Lomonico, M.P., Moore, G.W., Hutchins, G.M., 1986. Rotation of the junction of the outflow tract and great arteries in the embryonic human heart. Anat Rec 216, 544-549.

Maas, N.M., Van Buggenhout, G., Hannes, F., Thienpont, B., et al. (2008) Genotype-phenotype correlation in 21 patients with Wolf-Hirschhorn syndrome using high resolution array comparative genome hybridisation (CGH). Journal of medical genetics. 45 (2), 71–80.

Mallo, M. (2001). Formation of the middle ear: recent progress on the developmental and molecular mechanisms. Developmental biology, 231(2), pp.410–9.

Meilhac, S.M. et al. (2004). Oriented clonal cell growth in the developing mouse myocardium underlies cardiac morphogenesis. The Journal of cell biology, 164(1), pp.97–109.

Meilhac, S.M. et al. (2004). The clonal origin of myocardial cells in different regions of the embryonic mouse heart. Developmental cell, 6(5), pp.685–98.

Manley, N.R. and Capecchi, M.R. (1998). Hox group 3 paralogs regulate the development and migration of the thymus, thyroid, and parathyroid glands. Developmental biology, 195(1), pp.1–15.

Merscher, S., Funke, B., Epstein, J.A., Heyer, J., Puech, A., Lu, M.M., Xavier, R.J., Demay, M.B., Russell, R.G., Factor, S., Tokooya, K., Jore, B.S., Lopez, M., Pandita, R.K., Lia, M., Carrion, D., Xu, H., Schorle, H., Kobler, J.B., Scambler, P., Wynshaw-Boris, A., Skoultchi, A.I., Morrow, B.E., Kucherlapati, R., 2001. TBX1 is responsible for cardiovascular defects in velo-cardio-facial/DiGeorge syndrome. Cell 104, 619-629.

Mazzanti L1, Cacciari E. (1998) Congenital heart disease in patients with Turner's syndrome. Italian Study Group for Turner Syndrome (ISGTS). J Pediatr. 133(5):688-92.

Meberg A; Hals J; Thaulow E (2007) Congenital heart defects--chromosomal anomalies, syndromes and extracardiac malformations. Acta paediatrica 96, 8: 1142-1145

Mesbah, K., Rana, M.S., Francou, A., van Duijvenboden, K., Papaioannou, V.E., Moorman, A.F., Kelly, R.G., and Christoffels, V.M. (2011). Identification of a Tbx1/Tbx2/Tbx3 genetic pathway governing pharyngeal and arterial pole morphogenesis. Human Molecular Genetics 21, 1217-1229.

Mikawa, T. and Gourdie, R.G. (1996). Pericardial mesoderm generates a population of coronary smooth muscle cells migrating into the heart along with ingrowth of the epicardial organ. Developmental biology, 174(2), pp.221–32.

Mjaatvedt, C., Nakaoka, T., Moreno-Rodriguez, R., Norris, R., et al.(2001) The outflow tract of the heart is recruited from a novel heart-forming field. Developmental biology. 238 (1) p.97–109

Mulder G B; N Manley; L Maggio-Price. (1998). Retinoic acid-induced thymic abnormalities in the mouse are associated with altered pharyngeal morphology, thymocyte maturation defects, and altered expression of Hoxa3 and Pax1. Teratology 58 6: 263-275

Muzumdar, M.D., Tasic, B., Miyamichi, K., Li, L., Luo, L., (2007). A global double-fluorescent Cre reporter mouse. Genesis 45, 593-605.
Neubüser, A., Koseki, H., Balling, R., 1995. Characterization and Developmental Expression of Pax9, a Paired-Box-Containing Gene Related to Pax1. Developmental Biology 170, 701-716.

Nemer M. (2008). Genetic insights into normal and abnormal heart development. Cardiovascular pathology 17, 48-54

Nie X, Brown CB, Wang Q, Jiao K. (2011). Inactivation of Bmp4 from the Tbx1 expression domain causes abnormal pharyngeal arch artery and cardiac outflow tract remodeling. Cells Tissues Organs, 193, 393-403

Niederreither, K., Vermot, J., Schuhbaur, B., Chambon, P., et al. (2000) Retinoic acid synthesis and hindbrain patterning in the mouse embryo.Development (Cambridge, England). 127 (1), 75–85.

Noden DM. 1998. Interactions and fates of avian craniofacial mesenchyme. Development.103 Suppl:121-40.

Nowotschin, S., Liao, J., Gage, P.J., Epstein, J.A., Campione, M., Morrow, B.E., 2006. Tbx1 affects asymmetric cardiac morphogenesis by regulating Pitx2 in the secondary heart field. Development 133, 1565-1573.

Obler, D., Juraszek, A.L., Smoot, L.B. & Natowicz, M.R. (2008) Double outlet right ventricle: aetiologies and associations. Journal of medical genetics. 45 (8), 481–497.

Okubo, T., Kawamura, A., Takahashi, J., Yagi, H., Morishima, M., Matsuoka, R. and Takada, S. (2011) Ripply3, a Tbx1 repressor, is required for development of the pharyngeal apparatus and its derivatives in mice, Development, 138(2), pp. 339-48.

Papangeli, I., Scambler, P., 2012. Tbx1 Genetically Interacts With the TGFβ/BMP Inhibitor Smad7 During Great Vessel Remodeling. Circulation Research.

Pane, L. S., Zhang, Z., Ferrentino, R., Huynh, T., Cutillo, L., & Baldini, A. (2012). Tbx1 is a negative modulator of Mef2c. Human Molecular Genetics, 21(11), 2485-2496.

Parisot, P., Mesbah, K., Théveniau-Ruissy, M., and Kelly, R.G. (2011). Tbx1, subpulmonary myocardium and conotruncal congenital heart defects. Birth Defects Research Part A: Clinical and Molecular Teratology 91, 477-484.

Del Pasqua Alessia, Gabriele Rinelli, Alessandra Toscano, Roberta Iacobelli, Cristina Digilio, Bruno Marino, Claudia Saffirio, Sergio Mondillo, Luciano Pasquini, Stephen Pruett Sanders and Andrea de Zorzi (2009). New Findings concerning Cardiovascular Manifestations emerging from Long-term Follow-up

of 150 patients with the Williams-Beuren-Beuren syndrome. Cardiology in the Young, 19, pp 563-567.

Pasqualetti, M., Ori, M., Nardi, I. & Rijli, F.M. (2000) Ectopic Hoxa2 induction after neural crest migration results in homeosis of jaw elements in Xenopus. Development (Cambridge, England). 127 (24), 5367–5378.

Paylor R, Glaser B, Mupo A, Ataliotis P, Spencer C, Sobotka A, Sparks C, Choi CH, Oghalai J, Curran S, Murphy KC, Monks S, Williams N, ODonovan MC, Owen MJ, Scambler PJ, Lindsay E. (2006). Tbx1 haploinsufficiency is linked to behavioral disorders in mice and humans: implications for 22q11 deletion syndrome. PNAS 103, 7729-34

Pennacchio L.A. (2003). Insights from human/mouse genome comparisons. Mammalian genome, 14, 7: 429-436

Pérez Jurado, L.A., Peoples, R., Kaplan, P., Hamel, B.C., et al. (1996) Molecular definition of the chromosome 7 deletion in Williams syndrome and parent-of-origin effects on growth. American journal of human genetics. 59 (4), 781–792.

Peters H, Neubüser A, Kratochwil K, Balling R. (1998). Pax9-deficient mice lack pharyngeal pouch derivatives and teeth and exhibit craniofacial and limb abnormalities. Genes and Development 17, 2735-47

Peters, H., Wilm, B., Sakai, N., Imai, K., Maas, R., Balling, R., 1999. Pax1 and Pax9 synergistically regulate vertebral column development. Development 126, 5399-5408.

Pexieder T. 1978. Development of the outflow tract of the embryonic heart. Birth Defects Orig Artic Ser. 14(7):29-68.

Piotrowski, T., Ahn, D.G., Schilling, T.F., Nair, S., Ruvinsky, I., Geisler, R., Rauch, G.J., Haffter, P., Zon, L.I., Zhou, Y., Foott, H., Dawid, I.B., Ho, R.K., 2003. The zebrafish van gogh mutation disrupts tbx1, which is involved in the DiGeorge deletion syndrome in humans. Development 130, 5043-5052.

Piotrowski, T., Nusslein-Volhard, C., 2000. The endoderm plays an important role in patterning the segmented pharyngeal region in zebrafish (Danio rerio). Dev Biol 225, 339-356.

Puech, A., Saint-Jore, B., Funke, B., Gilbert, D.J., et al. (1997) Comparative mapping of the human 22q11 chromosomal region and the orthologous region in mice reveals complex changes in gene organization. Proceedings of the National Academy of Sciences of the United States of America. 94 (26), 14608–14613.

Quinlan, R., Gale, E., Maden, M. & Graham, A. (2002) Deficits in the posterior pharyngeal endoderm in the absence of retinoids. Developmental dynamics : an official publication of the American Association of Anatomists. 225 (1), 54–60.

Randall, V., McCue, K., Roberts, C., Kyriakopoulou, V., Beddow, S., Barrett, A.N., Vitelli, F., Prescott, K., Shaw-Smith, C., Devriendt, K., Bosman, E., Steffes, G., Steel, K.P., Simrick, S., Basson, M.A., Illingworth, E. and Scambler, P.J. (2009) Great vessel development requires biallelic expression of Chd7 and Tbx1 in pharyngeal ectoderm in mice, J Clin Invest, 119(11), pp. 3301-10.

Rauch, R., Rauch, A., Koch, A., Kumpf, M., Dufke, A., Singer, H. and Hofbeck, M. (2002) Cervical origin of the subclavian artery as a specific marker for monosomy 22q11, Am J Cardiol, 89(4), pp. 481-4.

Rawles ME. 1943. The heart forming areas of the early chick blastoderm. Physiol Zool 16:22–42.

Rijli FM, Mark M, Lakkaraju S, Dierich A, Dollé P, Chambon P. (1993) A homeotic transformation is generated in the rostral branchial region of the head by disruption of Hoxa-2, which acts as a selector gene. Cell. 1993 Dec 31;75(7):1333-49.

Roberts, L.K., Gerald, B., 1978. Absence of both common carotid arteries. American Journal of Roentgenology 130, 981-982.

Rogers, L. (1929). The Thyroid Arteries Considered in Relation to their Surgical Importance. Journal of anatomy, 64(Pt 1), pp.50–61.

Rosenquist, G. (1970) Location and movements of cardiogenic cells in the chick embryo: the heart-forming portion of the primitive streak. Developmental biology. 22 (3) p.461–475

Ryan, A.K., Goodship, J.A., Wilson, D.I., Philip, N., et al. (1997) Spectrum of clinical features associated with interstitial chromosome 22q11 deletions: a European collaborative study. Journal of medical genetics. 34 (10), 798–804.

Ryckebusch, L., Bertrand, N., Mesbah, K., Bajolle, F., Niederreither, K., Kelly, R.G., Zaffran, S., 2010. Decreased Levels of Embryonic Retinoic Acid Synthesis Accelerate Recovery From Arterial Growth Delay in a Mouse Model of DiGeorge Syndrome. Circ Res 106, 686-694.

Saitta, S.C., Harris, S.E., Gaeth, A.P., Driscoll, D.A., et al. (2004) Aberrant interchromosomal exchanges are the predominant cause of the 22q11.2 deletion. Human molecular genetics. 13 (4), 417–428.

Santen, G.W.E., Sun, Y., Gijsbers, A.C.J., Carré, A., Holvoet, M., Haeringen, A.v., Lesnik Oberstein, S.A.J., Tomoda, A., Mabe, H., Polak, M., Devriendt, K., Ruivenkamp, C.A.L., Bijlsma, E.K., 2012. Further delineation of the phenotype of chromosome 14q13 deletions: (positional) involvement of FOXG1 appears the main determinant of phenotype severity, with no evidence for a holoprosencephaly locus. Journal of Medical Genetics 49, 366-372.

Sato, A., Scholl, A.M., Kuhn, E.B., Stadt, H.A., Decker, J.R., Pegram, K., Hutson, M.R. and Kirby, M.L. (2011) FGF8 signaling is chemotactic for cardiac neural crest cells, Dev Biol, 354(1), pp. 18-30.

Sedmera D, Pexieder T, Vuillemin M, Thompson RP, Anderson RH.(2000). Developmental patterning of the myocardium. Anat Rec 258, 319-37

Scambler, P.J., 2000. The 22q11 deletion syndromes. Hum. Mol. Genet. 9, 2421-2426.

Scambler, P.J. (2010) 22q11 deletion syndrome: a role for TBX1 in pharyngeal and cardiovascular development, Pediatr Cardiol, 31(3), pp. 378-90.

Shaikh, T.H., Kurahashi, H. & Emanuel, B.S. (2001) Evolutionarily conserved low copy repeats (LCRs) in 22q11 mediate deletions, duplications, translocations, and genomic instability: an update and literature review. Genetics in medicine : official journal of the American College of Medical Genetics. 3 (1), 6–13.

Shaikh, T.H., Kurahashi, H., Saitta, S.C., O'Hare, A.M., et al. (2000) Chromosome 22-specific low copy repeats and the 22q11.2 deletion syndrome: genomic organization and deletion endpoint analysis. Human molecular genetics. 9 (4), 489–501.

Shprintzen, R.J. (2008) Velo-cardio-facial syndrome: 30 Years of study. Developmental disabilities research reviews. 14 (1), 3–10.

Schellberg R, Schwanitz G, Lutz Grävinghoff, Rolf Kallenberg, Detlef Trost, Ruth Raff and Walter Wiebe (2004). New trends in chromosomal investigation in children with cardiovascular malformations. Cardiology in the Young, 14, pp 622-629.

Schmittgen, T.D. and Livak, K.J. (2008) Analyzing real-time PCR data by the comparative C(T) method, Nat Protoc, 3(6), pp. 1101-8.

Simrick, Subreena, Szumska, Dorota, Gardiner, Jennifer R., Jones, Kieran, Sagar, Karun, Morrow, Bernice, Basson, M. Albert. (2012). Biallelic expression of Tbx1 protects the embryo from developmental defects caused by increased

receptor tyrosine kinase signaling. Developmental Dynamics, 241(8), 1310-1324.

Schuffenhauer, S., Leifheit, H.-J., Lichtner, P., Peters, H., Murken, J., Emmerich, P., 1999. De novo deletion (14)(q11.2q13) including PAX9: clinical and molecular findings. J Med Genet 36, 233-236.

Shapira, S.K., Anderson, K.L., Orr-Urtregar, A., Craigen, W.J., Lupski, J.R., Shaffer, L.G., 1994. De novo proximal interstitial deletions of 14q: cytogenetic and molecular investigations. Am J Med Genet 52, 44-50.

Sinha S1, Abraham S, Gronostajski RM, Campbell CE. (2000) Differential DNA binding and transcription modulation by three T-box proteins, T, TBX1 and TBX2. Gene. 27;258(1-2):15-29.

Stalmans, I., Lambrechts, D., De Smet, F., Jansen, S., Wang, J., Maity, S., Kneer, P., von der Ohe, M., Swillen, A., Maes, C., Gewillig, M., Molin, D.G., Hellings, P., Boetel, T., Haardt, M., Compernolle, V., Dewerchin, M., Plaisance, S., Vlietinck, R., Emanuel, B., Gittenberger-de Groot, A.C., Scambler, P., Morrow, B., Driscol, D.A., Moons, L., Esguerra, C.V., Carmeliet, G., Behn-Krappa, A., Devriendt, K., Collen, D., Conway, S.J. and Carmeliet, P. (2003) VEGF: a modifier of the del22q11 (DiGeorge) syndrome?, Nat Med, 9(2), pp. 173-82.

Stalsberg, H. & DeHaan, R. (1969) The precardiac areas and formation of the tubular heart in the chick embryo. Developmental biology. 19 (2) p.128–159

Spiteri, E., Babcock, M., Kashork, C.D., Wakui, K., et al. (2003) Frequent translocations occur between low copy repeats on chromosome 22q11.2 (LCR22s) and telomeric bands of partner chromosomes. Human molecular genetics. 12 (15), 1823–1837.

Su, D., Ellis, S., Napier, A., Lee, K., et al. (2001) Hoxa3 and pax1 regulate epithelial cell death and proliferation during thymus and parathyroid organogenesis. Developmental biology. 236 (2), 316–329.

Sutherland HF1, Kim UJ, Scambler PJ. (1998) Cloning and comparative mapping of the DiGeorge syndrome critical region in the mouse. Genomics. 15;52(1):37-43.

Taddei, I., Morishima, M., Huynh, T. and Lindsay, E.A. (2001) Genetic factors are major determinants of phenotypic variability in a mouse model of the DiGeorge/del22q11 syndromes, Proc Natl Acad Sci U S A, 98(20), pp. 11428-31.

Tadros, T.M., Klein, M.D. and Shapira, O.M. (2009) Ascending aortic dilatation associated with bicuspid aortic valve: pathophysiology, molecular biology, and clinical implications, Circulation, 119(6), pp. 880-90.

Tam, P., Parameswaran, M., Kinder, S. & Weinberger, R. (1997) The allocation of epiblast cells to the embryonic heart and other mesodermal lineages: the role of ingression and tissue movement during gastrulation. Development (Cambridge, England). 124 (9) p.1631–1642

Timmerman, L.A. et al. (2004). Notch promotes epithelial-mesenchymal transition during cardiac development and oncogenic transformation. Genes & development, 18(1), pp.99–115.

Thom, T., Haase, N., Rosamond, W., Howard, V.J., et al. (2006) Heart disease and stroke statistics--2006 update: a report from the American Heart Association Statistics Committee and Stroke Statistics Subcommittee. Circulation. 113 (6), e85–151.

Thomas K.R., Capecchi M.R. (1987). Site-directed mutagenesis by gene targeting in mouse embryo-derived stem cells. Cell, 6, 51: 503-512

Trainor, P.A., Tan, S.S. & Tam, P.P. (1994) Cranial paraxial mesoderm: regionalisation of cell fate and impact on craniofacial development in mouse embryos. Development (Cambridge, England). 120 (9), 2397–2408.

Van Mierop LH.1979. Embryology of the univentricular heart. Herz. Apr;4(2):78-85.

Vincent, S.D., Mayeuf-Louchart, A., Watanabe, Y., Brzezinski, J.A.t., Miyagawa-Tomita, S., Kelly, R.G., Buckingham, M., 2014. Prdm1 functions in the mesoderm of the second heart field, where it interacts genetically with Tbx1, during outflow tract morphogenesis in the mouse embryo. Hum Mol Genet 23, 5087-5101.

Vitelli, F., Morishima, M., Taddei, I., Lindsay, E.A., Baldini, A., 2002a. Tbx1 mutation causes multiple cardiovascular defects and disrupts neural crest and cranial nerve migratory pathways. Hum Mol Genet 11, 915-922.

Vitelli, F., Taddei, I., Morishima, M., Meyers, E.N., Lindsay, E.A. and Baldini, A. (2002) A genetic link between Tbx1 and fibroblast growth factor signaling, Development, 129(19), pp. 4605-11.

Vitelli, F., Zhang, Z., Huynh, T., Sobotka, A., Mupo, A., and Baldini, A. (2006). Fgf8 expression in the Tbx1 domain causes skeletal abnormalities and modifies the aortic arch but not the outflow tract phenotype of Tbx1 mutants. Developmental Biology 295, 559-570.

Voss, Anne K., Vanyai, Hannah K., Collin, C., Dixon, Mathew P., McLennan, Tamara J., Sheikh, Bilal N., Scambler, P., Thomas, T., 2012. MOZ Regulates the Tbx1 Locus, and Moz Mutation Partially Phenocopies DiGeorge Syndrome. Developmental Cell 23, 652-663.

Waldo, K., Miyagawa-Tomita, S., Kumiski, D. and Kirby, M.L. (1998) Cardiac neural crest cells provide new insight into septation of the cardiac outflow tract: aortic sac to ventricular septal closure, Dev Biol, 196(2), pp. 129-44.

Waldo, K.L., Kumiski, D. and Kirby, M.L. (1996) Cardiac neural crest is essential for the persistence rather than the formation of an arch artery, Dev Dyn, 205(3), pp. 281-92.

Wallin, J., Eibel, H., Neubüser, A., Wilting, J., et al. (1996) Pax1 is expressed during development of the thymus epithelium and is required for normal T-cell maturation. Development (Cambridge, England). 122 (1), 23–30.

Wagner M and Siddiqui M. A. Q.. (2007). Signal Transduction in Early Heart Development (II): Ventricular Chamber Specification, Trabeculation, and Heart Valve Formation. Exp Biol Med (Maywood) 232: 866-880

Wendling, O., Chambon, P. & Mark, M. (1999) Retinoid X receptors are essential for early mouse development and placentogenesis. Proceedings of the National Academy of Sciences. 96 (2), 547–551.

Weninger, W.J., Mohun, T.J., 2007. Three-dimensional analysis of molecular signals with episcopic imaging techniques. Methods Mol Biol 411, 35-46.
Yagi, H., Furutani, Y., Hamada, H., Sasaki, T., Asakawa, S., Minoshima, S., Ichida, F., Joo, K., Kimura, M., Imamura, S., Kamatani, N., Momma, K., Takao, A., Nakazawa, M., Shimizu, N., Matsuoka, R., 2003. Role of TBX1 in human del22q11.2 syndrome. Lancet 362, 1366-1373.

Xu, H., Cerrato, F. and Baldini, A. (2005) Timed mutation and cell-fate mapping reveal reiterated roles of Tbx1 during embryogenesis, and a crucial function during segmentation of the pharyngeal system via regulation of endoderm expansion, Development, 132(19), pp. 4387-95.

Xu, H., Morishima, M., Wylie, J.N., Schwartz, R.J., Bruneau, B.G., Lindsay, E.A. and Baldini, A. (2004) Tbx1 has a dual role in the morphogenesis of the cardiac outflow tract, Development, 131(13), pp. 3217-27.

Xu, P.-X.X., Zheng, W., Laclef, C., Maire, P., et al. (2002) Eya1 is required for the morphogenesis of mammalian thymus, parathyroid and thyroid. Development (Cambridge, England). 129 (13), 3033–3044.

Yamagishi, H., Maeda, J., Hu, T., McAnally, J., Conway, S.J., Kume, T., Meyers, E.N., Yamagishi, C., Srivastava, D., 2003. Tbx1 is regulated by tissue-

specific forkhead proteins through a common Sonic hedgehog-responsive enhancer. Genes Dev 17, 269-281.

Yashiro, K., Shiratori, H. and Hamada, H. (2007) Haemodynamics determined by a genetic programme govern asymmetric development of the aortic arch, Nature, 450(7167), pp. 285-8.

Zaffran, S. et al. (2004). Right ventricular myocardium derives from the anterior heart field.Circulation research, 95(3), pp.261–8.

Zhang, Z., Cerrato, F., Xu, H., Vitelli, F., Morishima, M., Vincentz, J., Furuta, Y., Ma, L., Martin, J.F., Baldini, A. and Lindsay, E. (2005) Tbx1 expression in pharyngeal epithelia is necessary for pharyngeal arch artery development, Development, 132(23), pp. 5307-15.

Zhang, Z., Huynh, T. and Baldini, A. (2006) Mesodermal expression of Tbx1 is necessary and sufficient for pharyngeal arch and cardiac outflow tract development, Development, 133(18), pp. 3587-95.

Zhang, Z., Baldini, A., 2008. In vivo response to high-resolution variation of Tbx1 mRNA dosage. Hum Mol Genet 17, 150-157.

Zou, Dan, Silvius, Derek, Davenport, Julie, Grifone, Raphaelle, Maire, Pascal, & Xu, Pin-Xian. (2006). Patterning of the third pharyngeal pouch into thymus/parathyroid by Six and Eya1. Developmental Biology, 293(2), 499-512.

Zweier C, Sticht H, Aydin-Yaylagül I, Campbell CE, Rauch A. (2007). Human TBX1 missense mutations cause gain of function resulting in the same phenotype as 22q11.2 deletions. American Journal of human genetics 80, 510-7.